

Forschungszentrum Karlsruhe
Technik und Umwelt

Wissenschaftliche Berichte
FZKA 5657

**Aspects of Similitude
Theory in Solid Mechanics
Part I: Deformation Behavior**

T. Malmberg

Institut für Reaktorsicherheit
Projekt Nukleare Sicherheitsforschung

Dezember 1995

Forschungszentrum Karlsruhe
Technik und Umwelt

Wissenschaftliche Berichte

FZKA 5657

Aspects of Similitude Theory in Solid Mechanics
Part I: Deformation Behavior

Thilo Malmberg

Institut für Reaktorsicherheit

Projekt Nukleare Sicherheitsforschung

Forschungszentrum Karlsruhe GmbH, Karlsruhe

1995

Als Manuskript gedruckt
Für diesen Bericht behalten wir uns alle Rechte vor

Forschungszentrum Karlsruhe GmbH
Postfach 3640, 76021 Karlsruhe

ISSN 0947-8620

Abstract

The core melt down and the subsequent steam explosion in a Light Water Reactor is an accident scenario under discussion. Here the resulting impact loading of the vessel head and its integrity is of primary concern. It was reasoned that an experimental approach (BERDA experiment), using a scaled down model (scale 1:10) which simulates this impact scenario with an alternative energy source, is required. Appropriate similarity laws should be used to design the small scale model and to transfer the experimental results to the actual (1:1)-configuration.

This impact scenario involves the motion, the elastic-plastic deformation and the failure of various solid structures at elevated temperatures and the motion and deformation of a viscous fluid as well as their interaction.

In the present two-part report the emphasis is on aspects of similitude theory for solid continua and structures in general. In part I the analysis is restricted to the *deformation behavior*. Using the "method of differential equations", similarity laws are derived and size effects are discussed for two important phenomena:

- Motion and deformation of an elastic-viscoplastic continuum with isotropic hardening;
- motion and deformation of an elastic-time independent plastic continuum with isotropic hardening.

The presence of gravitational forces is discussed. They are expected to be of minor importance and they are therefore excluded from the further analysis. The derived similarity conditions are interpreted and the limitations are analyzed if different or the same materials are used for the model and the prototype. In particular, if the material response is viscoplastic and if the same material is used for the model and the prototype, a size effect occurs. Using a simple impact problem, this is quantitatively assessed for stainless steel AISI 304 at room temperature. It is shown that this size effect is enhanced if the structure is undergoing strain softening.

The quality of the derived similarity laws and the conclusions obtained depend, among others, upon the assumed scale invariance of the basic material data; a provisional discussion of some experimental results and preliminary theoretical models is presented. Further, the scale factors are listed. Finally, several aspects, which need more attention, are indicated.

In part II of this report, which is still in preparation, similarity laws and size effects in case of failure and fracture are studied.

Aspekte der Ähnlichkeitstheorie in der Festkörpermechanik

Teil I: Deformationsverhalten

Zusammenfassung

Der Kernschmelzunfall und die in der Folge auftretende Dampfexplosion in einem Leichtwasserreaktor sind ein zur Zeit diskutiertes Unfallszenario. Dabei ist die Impaktbelastung des Druckbehälterdeckels und seine Integrität von besonderem Interesse. Ein experimentelles Vorgehen (BERDA-Experiment), bei dem in einem verkleinerten Modell (Maßstab 1:10) das Impaktszenario mit einer alternativen Energiequelle simuliert wird, wird als erforderlich angesehen. Entsprechende Ähnlichkeitsgesetze sollten den Entwurf des Modells erlauben und die Übertragung der experimentellen Ergebnisse auf die aktuelle (1:1)-Konfiguration ermöglichen.

Dieses Impaktszenario beinhaltet die Bewegung, die elastisch-plastische Deformation und das Versagen verschiedener Festkörperstrukturen bei erhöhten Temperaturen und die Bewegung und Deformation einer viskosen Flüssigkeit sowie ihre Wechselwirkungen.

In dem vorliegenden, zweiteiligen Bericht liegt die Betonung auf mehr allgemeinen Aspekten der Ähnlichkeitstheorie für Festkörperkontinua und Strukturen. Im 1. Teil beschränkt sich die Analyse auf das *Deformationsverhalten*. Mittels der "Methode der Differentialgleichungen" werden für zwei wichtige Phänomene Ähnlichkeitsgesetze abgeleitet und Größeneffekte diskutiert:

- Bewegung und Deformation eines elastisch-viskoplastischen Kontinuums mit isotroper Verfestigung;
- Bewegung und Deformation eines elastisch-zeitunabhängig plastischen Kontinuums mit isotroper Verfestigung.

Die Bedeutung von Gewichtskräften wird diskutiert. Es wird erwartet, daß sie von untergeordneter Wichtigkeit sind, und sie werden deshalb bei der weiteren Analyse vernachlässigt. Die abgeleiteten Ähnlichkeitsbedingungen werden interpretiert und die Einschränkungen werden analysiert, wenn dasselbe Material für Modell und Prototyp verwendet wird. Ein Größeneffekt tritt insbesondere dann auf, wenn das Materialverhalten viskoplastisch ist und wenn dasselbe Material im Modell und Prototyp Anwendung findet. Dies wird quantitativ überprüft für den rostfreien Stahl AISI 304 bei Raumtemperatur anhand eines einfachen Impaktpro-

blems. Es wird gezeigt, daß der Größeneffekt verstärkt wird, wenn die Struktur eine Erweichung mit der Deformation erfährt.

Die Qualität der abgeleiteten Ähnlichkeitsgesetze und Schlußfolgerungen hängt unter anderem von der angenommenen Skaleninvarianz der Basismaterialdaten ab; eine vorläufige Diskussion einiger experimenteller Resultate und erster theoretischer Modelle wird vorgestellt. Weiterhin werden die Maßstabsfaktoren angegeben. Schließlich werden einige Aspekte berührt, die weiterer Aufmerksamkeit bedürfen.

Im 2. Teil dieses Berichtes, der noch in Vorbereitung ist, werden Ähnlichkeitsgesetze und Größeneffekte für Versagens- und Bruchphänomene studiert.

Aspects of Similitude Theory in Solid Mechanics,

Part I : Deformation Behavior

1. Introduction	1
2. Basic Equations for Two Simple Constitutive Models Characterizing Elastic-Plastic and Elastic-Viscoplastic Deformation Behavior	6
3. Similarity Laws for the Deformation Behavior	17
3.1 Derivation of Similarity Laws	17
3.2 Interpretations and Discussions	28
3.2.1 Modeling Similarity of Gravitational Forces	28
3.2.2 Modeling the Density Distribution	30
3.2.3 Modeling the Constitutive Response	30
3.2.4 Size Effect for Viscoplastic Material Response	40
3.2.4.1 Constant Flow Stress Assumption	40
3.2.4.2 Varying Viscous Stress	48
3.2.4.3 Enhancement of the Strain Rate Effect Due to Strain- or Deformation-Softening	60
3.2.5 Scale Invariance of Material Data	66
3.3 Scale Factors	86
3.4 Summary and Conclusions	90
References	98

1. Introduction

Within the frame of the safety analysis of Light Water Reactors a core melt down and a subsequent steam explosion is an accident scenario under discussion [1]. After melt down the steam explosion is assumed to take place in the lower part of the reactor pressure vessel. Large masses of molten core material (80 t are envisaged) will be accelerated upward and will force its way through the upper internal structures (grid plate, guide tubes and support columns, support grid) deforming and crushing them, and will finally impact on the head of the pressure vessel. There are other mechanical consequences in the lower part of the vessel but here the loading of the head is of primary concern. Of course, the crucial question is the integrity of the the vessel head and its bolting since a failure would endanger the containment.

A reliable theoretical treatment of this problem requires modeling of complex interactions between the molten core material and the deforming in-vessel structures and the vessel head. It was reasoned [1, 2] that an experimental approach, using a scaled down model experiment (scale 1:10) which simulates this scenario with an alternative energy source, is preferable and that appropriate similarity laws should allow the transfer of the results to the actual 1:1 configuration. Some preliminary scaling factors were put down in ref. [2].

If such an approach should be successful, then it is of utmost importance to understand and quantify the governing physical phenomena. If the appropriate balance equations and constitutive relations have been set up, the similarity laws can be found by transforming the governing equations in a dimensionless form which automatically yields a set of dimensionless characteristic numbers or functions. Similarity of model and prototype response means that the dimensionless solutions for displacement, strain, velocity, stress etc. of model and prototype equations are identical. This implies the equality of the corresponding characteristic numbers or functions; these requirements represent *the similarity laws*. This approach is called the "method of differential equations" [3, 4], or simply the "method of equations", and will be used in this study. There are other approaches like

- the method of ratios of forces, energies etc.
- or dimensional analysis and application of the Buckingham-II-Theorem.

However, the "method of differential equations" allows a deeper insight into the laws of similarity and has also a wider applicability, particularly if laws of similarity for distorted models are sought [3].

It may be argued that, if the differential equations are known, it would be straight forward to solve these by numerical methods rather than to obtain a solution experimentally using a small scale model and similarity laws. Here the important point is that the development of an analytical or numerical solution may be extremely difficult, if not impossible; on the other hand solutions which are obtainable are subject to various simplifications and their reliability is hardly to assess. However, the model experiment and the transfer of its results to the prototype situation with the similarity laws is not necessarily more reliable. It is evident that the derived similarity laws are valid only as far as the underlying physical theory is valid and appropriate. Therefore the identification of the relevant physical processes and their mathematical characterization is most important whereas the derivation of the similarity laws from this theoretical basis is mathematically a simple matter.

Experience with similarity analysis in general, as published in the literature, shows that some of the similarity laws cannot be satisfied at all and others can be satisfied only approximately. If small scale model experiments are done under these circumstances, size-effects occur, i.e. the dimensionless solutions for the model and the prototype are not identical but depend on the scale. Thus, ignoring the inadequacy of the similarity, a prediction of the prototype behavior from the model experiment causes misleading conclusions.

Therefore, besides the derivation of the similarity laws and a discussion of their realization, a qualitative and quantitative analysis of size effects is indispensable for a reliable similarity theory of model tests. This can be done theoretically to some extent but ultimately systematic model experiments at various scales are necessary.

The above sketched impact szenario involves the motion, the elastic-plastic deformation and the failure of various *solid structures* at elevated temperatures and the motion and deformation of a viscous *fluid* as well as the interaction of the structures and the fluid. Similarity laws have been developed extensively in the field of fluid mechanics but have received far less attention in the mechanics of solid continua or structures. This is reflected in relevant text books on similitude theory (e.g. [3 - 12]); there a detailed treatment of elastic-plastic or even

elastic-viscoplastic continua or structures under the aspect of similarity is practically not existing. Murphy [10] made use of dimensional analysis to derive similitude rules for simple perfect and distorted elastic structures; plasticity was but only briefly mentioned. Langhaar [3] applied dimensional analysis to different elastic and some plastic structures on an elementary level. Baker et al. [6] gave a very limited treatment of elastic-plastic deformations but valuable experimental data of similarity experiments of simple structures under blast loading were presented. Some more in-depth studies were published by Jones [13 - 15]. Educational articles have been published by Goodier [53], Soper [55] and Young [56], and Murphy [57] gave a literature survey. Nevertheless, scaling laws related to structural mechanics have been applied in a variety of engineering applications, mostly based on dimensional analysis and the Buckingham- Π -Theorem, e.g. [58 - 66]. However, thorough analyses of similarity laws for elastic-plastic and elastic-viscoplastic material deformation behaviour under a threedimensional state of stress and for failure or fracture rules have found very limited attention; although some scaling laws for static fracture of linear or non-linear elastic structures with geometrically scaled cracks have been derived (e.g. [67]). More comprehensive studies are wanting. This situation prompted the present effort.

In a previous unpublished report [16] similarity laws have been derived for several theoretical models, describing some of the phenomena involved in the above impact szenario; this included also the coupling of fluid and structure. However, the main aspect of that study was the constitutive modeling of a class of inelastic materials.

In the present two-part report the emphasis is on aspects of similitude theory for solid continua and structures. In part I the analysis is restricted to the *deformation behavior* of structural materials; it is assumed that progressive damage processes or fracture do not affect the deformation behavior. In part II *failure and fracture* are studied.

Similarity laws are derived and size effects are discussed for two important phenomena:

- Motion and deformation of an elastic-viscoplastic continuum with isotropic hardening; this constitutive model allows to describe the strain-rate dependent yielding in dynamic plasticity.
- Motion and deformation of an elastic-time independent plastic continuum with isotropic hardening.

These constitutive models belong to the simplest models and allow to describe the multiaxial response under monotonous radial loading. Of course, more advanced models exist which allow to encompass also kinematic hardening and other phenomena. Naturally, they would require different and more similarity conditions. However, presently it appears to be advisable to restrict oneself to the simplest theoretical basis.

This development will be based on the assumption of infinitesimal strains and rotations such that the kinematics is linear, density changes need not to be considered and the undeformed reference and the current configuration of the solid body need not to be distinguished. These assumptions are certainly not correct in the described accident szenario since it is expected that the upper internal structures are likely to buckle and crush up; this is a structural stability problem and its theoretical treatment requires at least the allowance for large rotations, i.e., a nonlinear kinematic. However, this has no consequences for the similarity laws, provided the buckling and crushing can be described with the same constitutive equations but supplemented with nonlinear kinematic relations and properly chosen objective time rates in the evolution equations. If, however, very large strains occur, it is expected that progressive damaging will occur which is presently not included in the theory. Nevertheless, if a size effect is present in small scale modeling, its theoretical estimate will be certainly affected whether or not the nonlinear kinematics is accounted for.

Part I is organized as follows. In section 2 the well known balance equations and constitutive relations for an elastic-viscoplastic and an elastic-time independent plastic material as well as boundary and initial conditions are listed. A theoretical discussion of these models is not included (see e.g. [16]). Some illustrative experimental data characterizing the viscoplastic response are contained.

In section 3 the similarity laws are derived and discussed for these two models and equivalent alternative similarity parameters are introduced. The presence of gravitational forces is discussed. Principially they impose severe restrictions but fortunately they are expected to be of no importance for the described impact szenario and they are therefore excluded from the further analysis. Then the derived similarity conditions are interpreted and conclusions are drawn with respect to the similarity of basic material tests which are required to identify the material parameters of the constitutive model. Further the limitations are analyzed if different or the same materials (at the same temperature) are used for the model and the prototype. Especially, if the material response is viscoplastic and if the

same material is used, a size effect occurs. Using a simple impact model this is quantitatively assessed for stainless steel type 304 at room temperature. It is also demonstrated that this size effect is enhanced if the structure is subject to strain- or deformation softening.

The quality of the derived similarity laws and the conclusions obtained from them depends, among others, upon the assumed *scale invariance* of the basic material data, e.g. Young's modulus, yield stress, hardening stress, viscosity parameters and others. A rudimentary discussion of some experimental results taken from the open literature and of preliminary theoretical models is presented. Finally, the scale factors associated with the two constitutive models are listed. Section 3 closes with a summary and conclusions of the most important theoretical findings.

2. Basic Equations for Two Simple Constitutive Models Characterizing Elastic-Plastic and Elastic-Viscoplastic Deformation Behavior

In the following the complete set of equations consisting of the balance equations, constitutive relations as well as initial and boundary conditions are formulated to describe two relatively simple models for the *elastic-time independent plastic* behavior and the *elastic-viscoplastic* behavior, both involving isotropic hardening. These models can be set up within a thermodynamic frame to assure consistence with thermodynamic principles [16, 17]. This is not enclosed in this study. In most engineering applications of plasticity, and also in this report, it is tacitly assumed that processes are isothermal; thus the energy balance and the coupling with the temperature field are ignored. Therefore, only purely mechanical theories are considered. It is also noted that only small deformations and rotations are considered. Then the governing equations are as follows.

Cauchy's first law of motion reads

$$\frac{\partial \sigma_{kl}}{\partial x_k} + \rho \left(f_l - \frac{\partial^2 u_l}{\partial t^2} \right) = 0, \quad l = 1, 2, 3, \quad (2.1)$$

where

- $\sigma_{kl} = \sigma_{lk}$: symmetric stress tensor
- u_l : displacement vector
- f_l : body force density
- x_k : cartesian coordinates
- t : time
- $\rho = \rho_0 = \text{const}$: density (small deformation assumption) .

In the gravitational field the body force density f_l derives from a potential U

$$f_k = - \frac{\partial U}{\partial x_k}, \quad k = 1, 2, 3 \quad (2.2)$$

$$U = g \left(a'_1 x_1 + a'_2 x_2 + a'_3 x_3 \right)$$

- g : gravitational acceleration
- a'_k : direction cosinus between constant body force field and cartesian coordinate system (dimensionless)

The relations between strains ε_{kl} and displacements u_k

$$\varepsilon_{kl} = \frac{1}{2} \left(\frac{\partial u_k}{\partial x_l} + \frac{\partial u_l}{\partial x_k} \right) \quad (2.3)$$

are linearized in the displacement derivatives because of the small-strain assumption.

For both plasticity models we assume that the total strain is additively composed of an elastic and a plastic or viscoplastic strain, i.e.

$$\varepsilon_{kl} = \underbrace{\varepsilon_{kl}^e}_{\text{elastic strain}} + \underbrace{\varepsilon_{kl}^p}_{\text{plastic strain}} \quad (2.4)$$

The elastic strain is assumed to be related to the stresses via Hooke's law

$$\varepsilon_{kl}^e = \frac{1+\nu}{E} \sigma_{kl} - \frac{\nu}{E} \sigma_{mm} \delta_{kl} \quad (2.5)$$

implying isotropic behavior; here the two material parameters

E: Young's modulus

ν : Poissons number

are involved. Clearly, the relations (2.1) to (2.5) apply to both plasticity models.

The time-independent plastic response is assumed to be characterized by a yield surface for isotropic hardening

$$f(\sigma_{mn}, p) = 0 \quad (2.6)$$

and an associated flow law. The yield function f is given by

$$f(\sigma_{mn}, p) = \sigma_{equ} - (\sigma_y + \hat{R}(p)) \quad (2.7)$$

where

$$\sigma_{\text{equ}} = \left(\frac{3}{2} \sigma_{o,mn} \sigma_{o,mn} \right)^{\frac{1}{2}} \quad ; \text{ v. Mises equivalent stress} \quad (2.8)$$

$$\sigma_{o,mn} = \sigma_{mn} - \frac{1}{3} \sigma_{kk} \delta_{mn} \quad ; \text{ deviatoric stress} \quad (2.9)$$

$$p = \int_0^t \left(\frac{2}{3} \dot{\varepsilon}_{mn}^p \dot{\varepsilon}_{mn}^p \right)^{\frac{1}{2}} dt \quad ; \text{ accumulated plastic strain} \quad (2.10)$$

σ_y : initial uniaxial yield stress

$\hat{R}(p) \geq 0$: yield stress increase due to isotropic strain hardening .

The associated flow law which describes the evolution of the plastic strain of a "time-indepernt" plastic material is given by

$$\dot{\varepsilon}_{kl}^p = \begin{cases} \frac{1}{d\hat{R}/dp} \left(\frac{\partial f}{\partial \sigma_{mn}} \dot{\sigma}_{mn} \right) \frac{\partial f}{\partial \sigma_{kl}} ; & f = 0 \cap \frac{\partial f}{\partial \sigma_{mn}} \dot{\sigma}_{mn} > 0 \\ 0 & ; f < 0 \text{ or} \\ & f = 0 \cap \frac{\partial f}{\partial \sigma_{mn}} \dot{\sigma}_{mn} \leq 0 \end{cases} \quad (2.11)$$

with

$$\frac{\partial f}{\partial \sigma_{kl}} = \frac{1}{\sigma_{\text{equ}}} \frac{3}{2} \sigma_{o,kl} \quad (2.12)$$

This relation is homogeneous of degree one in the time scale and therefore, the time scale does not affect the stress-strain response, excluding inertia effects.

The switch conditions correspond to the following situations

$$\begin{aligned} f = 0 \cap \frac{\partial f}{\partial \sigma_{mn}} \dot{\sigma}_{mn} > 0 & \quad \text{plastic loading} \\ f < 0 & \quad \text{elastic response} \\ f = 0 \cap \frac{\partial f}{\partial \sigma_{mn}} \dot{\sigma}_{mn} < 0 & \quad \text{elastic response due to unloading} \\ f = 0 \cap \frac{\partial f}{\partial \sigma_{mn}} \dot{\sigma}_{mn} = 0 & \quad \text{elastic response due to neutral loading .} \end{aligned}$$

It is noted that the yield surface (2.6) can be visualized in the two-dimensional stress space as shown in Fig. 1: The v. Mises ellipse shows an affine expansion due to the isotropic hardening.

In the uniaxial state of stress the yield condition reads

$$\begin{aligned}\sigma_{\text{equ}} &= \sigma_{11} = \sigma_y + \hat{R}(p) \\ p &= \varepsilon_{11}^p\end{aligned}\tag{2.13}$$

which simply represents the uniaxial stress-plastic strain curve (Fig. 2a).

Aside from the elastic constants E and ν , the quantities

$$\sigma_y \text{ and } R = \hat{R}(p) ,$$

obtainable from a tensile test, completely define the response of this simple time-independent plasticity model.

The viscoplastic material law is also assumed to follow an isotropic hardening mode. The evolution law is taken to be [16, 18]

$$\varepsilon_{kl}^p = \begin{cases} A \phi(f) \frac{\partial f}{\partial \sigma_{kl}} ; f > 0 \\ 0 ; f \leq 0 \end{cases}\tag{2.14}$$

where f is given by (2.7). As before an explicit temperature dependence is not considered. Here A is a relaxation parameter with the dimension (Time)⁻¹; the function ϕ is dimensionless. For $f > 0$ and with (2.10) squaring of both sides of (2.14) gives

$$\dot{p} = A \phi(f) .\tag{2.15}$$

Inversion yields

$$f - \phi^{-1} \left(\frac{\dot{p}}{A} \right) = 0 .\tag{2.16}$$

According to Perzyna [18], this is called the "dynamic yield condition" for a viscoplastic isotropic strain hardening material; it describes the "dependence of the yield condition on the strain rate". However, for the model discussed here, this description is misleading since the equation (2.16) does not represent a surface in the stress space which separates the elastic from the plastic response; this is done solely by the condition $f = 0$.

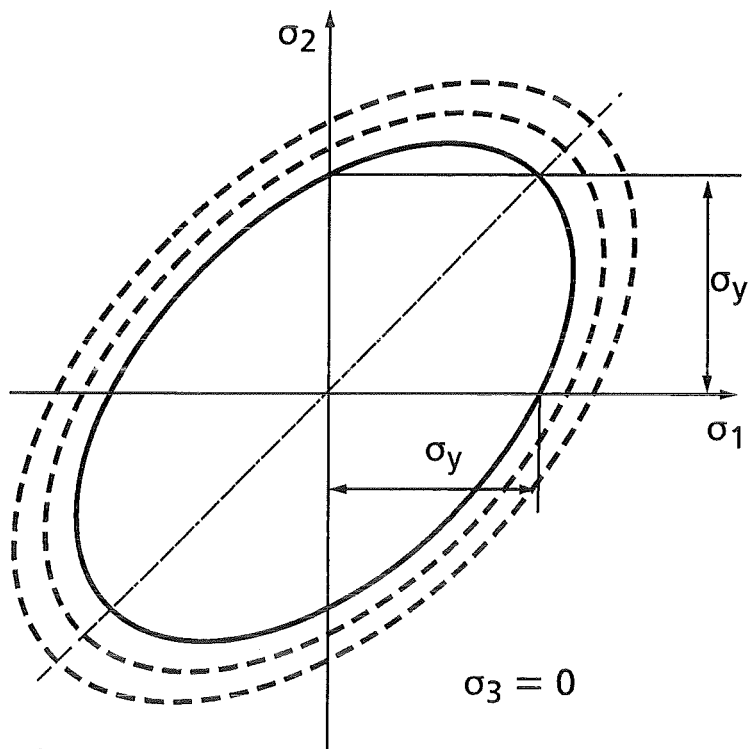
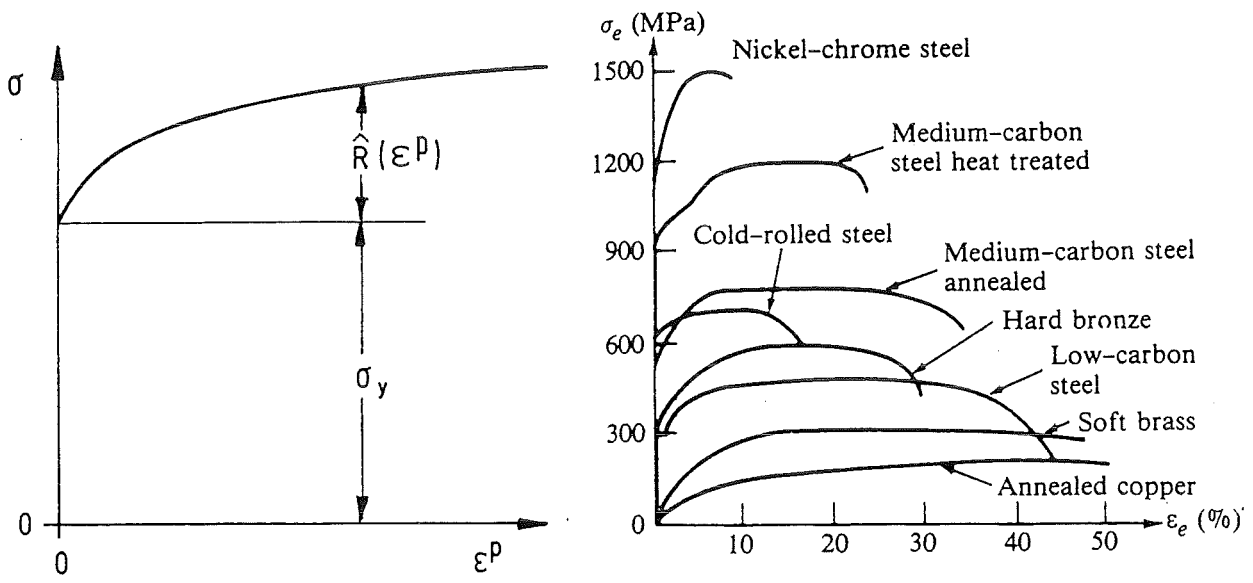


Fig. 1: v. Mises Ellipse and Isotropic Expansion



(a) Schematic Stress-Plastic Strain Curve (Moderately Large Strains)

(b) Engineering Stress-Strain Curves Including Necking and Fracture, from [68]

Fig. 2: Uniaxial Stress-Strain Curves

With (2.7) equation (2.16) yields

$$\sigma_{\text{equ}} = \sigma_y + \hat{R}(\rho) + \phi^{-1} \left(\frac{\dot{\rho}}{A} \right) . \quad (2.17)$$

The right hand side consists of three parts: A constant term σ_y equivalent to the *initial yield stress*, a nonlinear *strain hardening term* $\hat{R}(\rho)$ and a *nonlinear viscous stress* $\phi^{-1}(\dot{\rho}/A)$. In fact, this represents the multiaxial equivalent of the "dynamic stress strain curve" for constant $\dot{\rho}^*$.

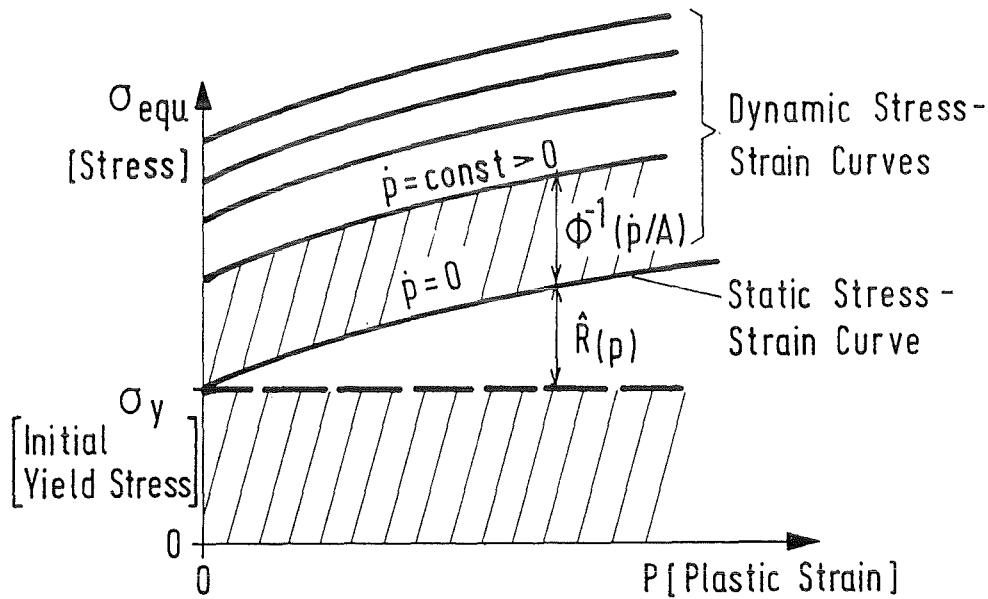


Fig. 3: Static and Dynamic Stress-Plastic Strain Curves (Schematic)

Fig. 3 illustrates that a change of the viscoplastic strain rate produces a parallel shift of the "static stress - plastic strain curve" defined by

$$\sigma_s := \sigma_y + \hat{R}(\rho) . \quad (2.18)$$

With σ_{equ} being the applied stress, the difference $\sigma_{\text{equ}} - \sigma_s$ is called the "overstress".

In the following a power function is assumed for ϕ

$$\phi = \left(\frac{f}{\sigma_N} \right)^n , \quad n \geq 1 ; \quad (2.19)$$

* Note that $\dot{\rho}$ is the rate of the accumulated *viscoplastic* strain.

σ_N is not a material parameter but some normalizing stress. Then the "dynamic stress strain curve" takes the form

$$\sigma_{\text{equ}} = \sigma_y + \hat{R}_{(p)} + \sigma_N \left(\frac{\dot{p}}{A} \right)^{\frac{1}{n}} . \quad (2.20)$$

For a uniaxial state of stress σ_{equ} and p have to be replaced by the uniaxial stress σ and the plastic strain ε^p .

Putting

$$\sigma_N = \sigma_y \quad \text{and} \quad A = A_y , \quad (2.21)$$

(2.20) takes - in the uniaxial case - the convenient form

$$\sigma = \sigma_y + \hat{R}_{\left(\varepsilon^p\right)} + \sigma_y \left(\frac{\varepsilon^p}{A_y} \right)^{\frac{1}{n}} . \quad (2.22)$$

For the purpose of illustration some experimental results are shown in Fig. 4 to 7. Figs. 4+5 show dynamic stress-strain curves obtained by Maiden and Green [19] for titanium 6A-4V in compression tests. Note that here the total strain and total strain rate is used. Fig. 4 suggestively demonstrates that the dynamic stress-strain curves are approximately parallel for larger strains. According to the above theoretical model, the viscoplastic part of the curve should start off from Hooke's straight line at $\sigma = \sigma_y$. However, the static yield stress σ_y is difficult to infer from Fig. 4, since the curves are tangent to Hooke's straight line. One should realize of course, that the assumption of a static stress-strain curve or static yield surface is, on physical grounds, possibly not realistic.

The flow stresses at various strains are plotted in Fig. 5 as a function of the total strain rate; in this strain regime the total strain rate is essentially equal to the viscoplastic strain rate.

Hauser [20] has obtained flow stresses for stainless steel Type AISI 304 at room temperature as a function of the strain rate with the strain as a parameter, Fig. 6. Also included are proof stress $\sigma_{0,2}$ -values for AISI 304, solution annealed, measured by Steichen et al. [21-23, 24]. Note that again, to a first approximation, these semilogarithmic plots are parallel.

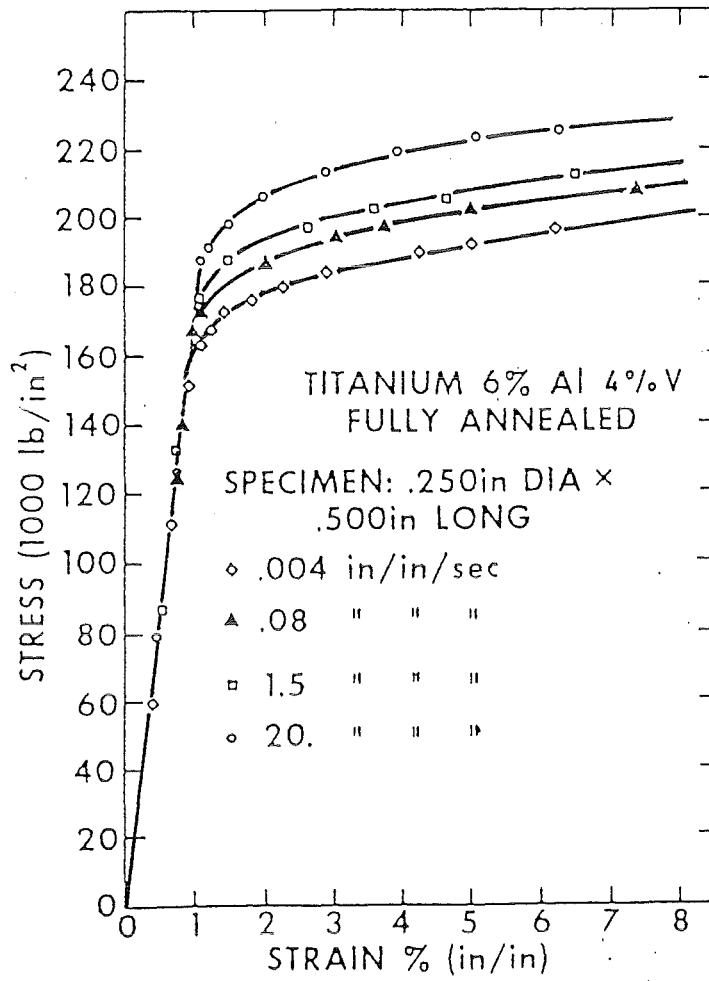


Fig. 4: Compression Tests on Titanium , from [19]

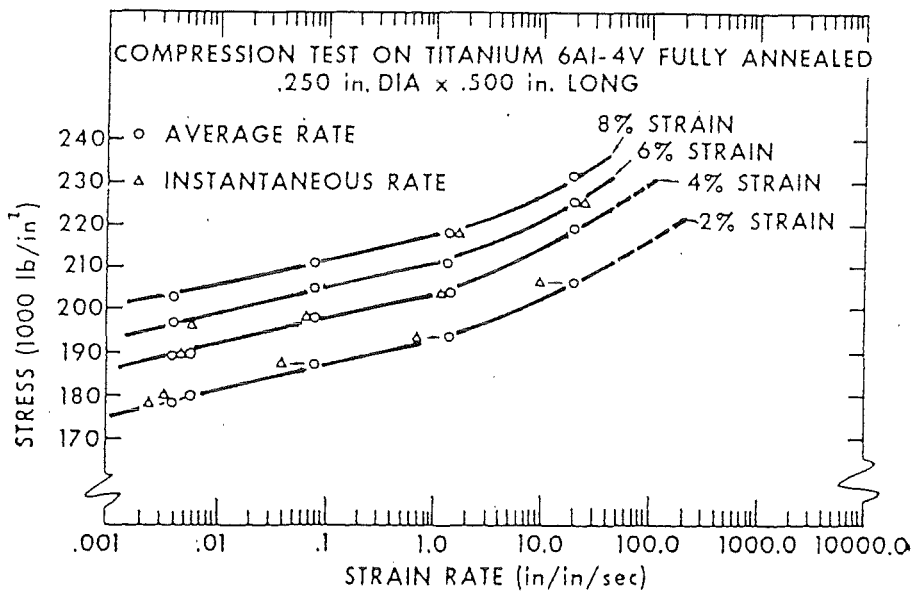


Fig. 5: Stress Versus Strain Rate for Compression Tests on Titanium, from [19]

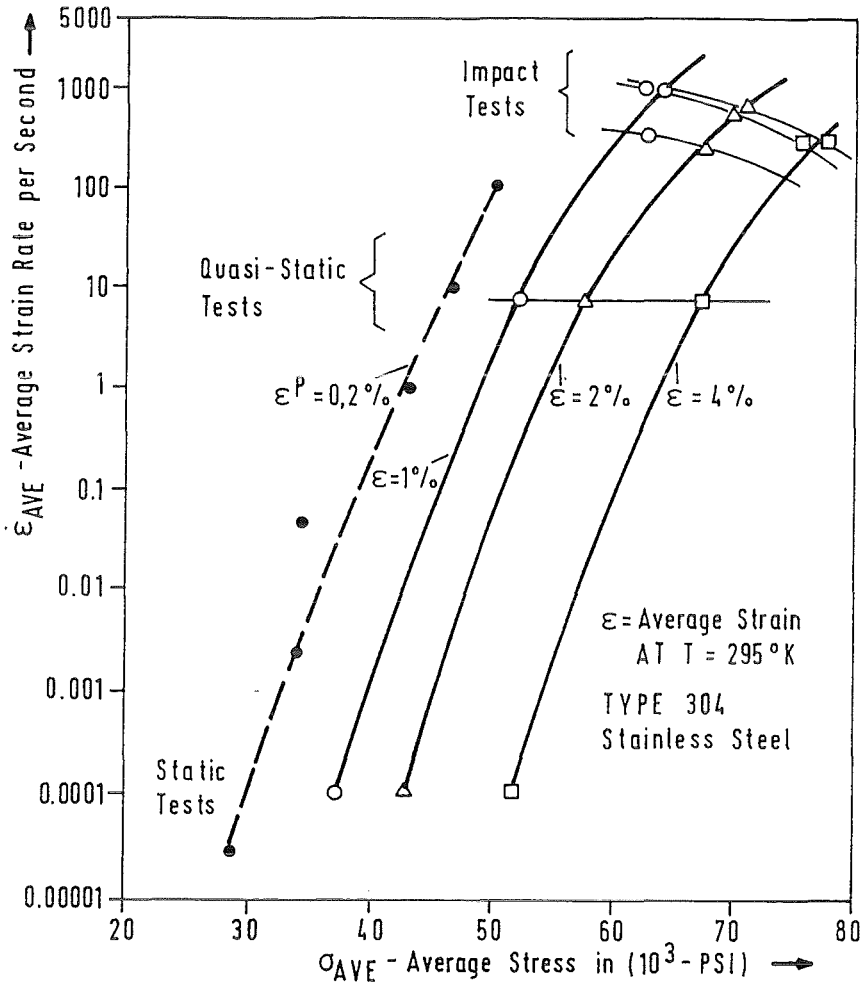


Fig. 6: Effect of Stress on Strain Rate at Constant Strain for Stainless Steel, Showing Sampling of Experimental Record, Based on [20]

The 0.2 % proof stress data for AISI 304 at room and elevated temperatures as well are presented in Fig. 7a. It is evident that the largest strain rate effect for the proof stress of AISI 304 (solution annealed) is present at room temperature. On the contrary, the ultimate stress, shown in Fig. 7b, is approximately rate insensitive in the range $2 \cdot 10^{-5} < \dot{\epsilon} < 10^2$ for temperatures between room temperature and $538^\circ C$. Beyond this temperature an increasing rate influence is observed. Fig. 7c illustrates the rate dependence of the uniform elongation at various temperature levels. At room temperature a significant decrease from a high level at small rates is observed with increasing strain rate down to a saturation level; in the range from $316^\circ C$ to $538^\circ C$ rate insensitivity is found, whereas above $538^\circ C$ an increase from a low level at small rates to a saturation level is seen.

Extensive dynamic tensile testing of several austenitic steels, especially AISI type 316, at different strain rates and temperatures has been performed by Albertini and Montagnani and collaborators (e.g. ref. [69] and references cited therein).

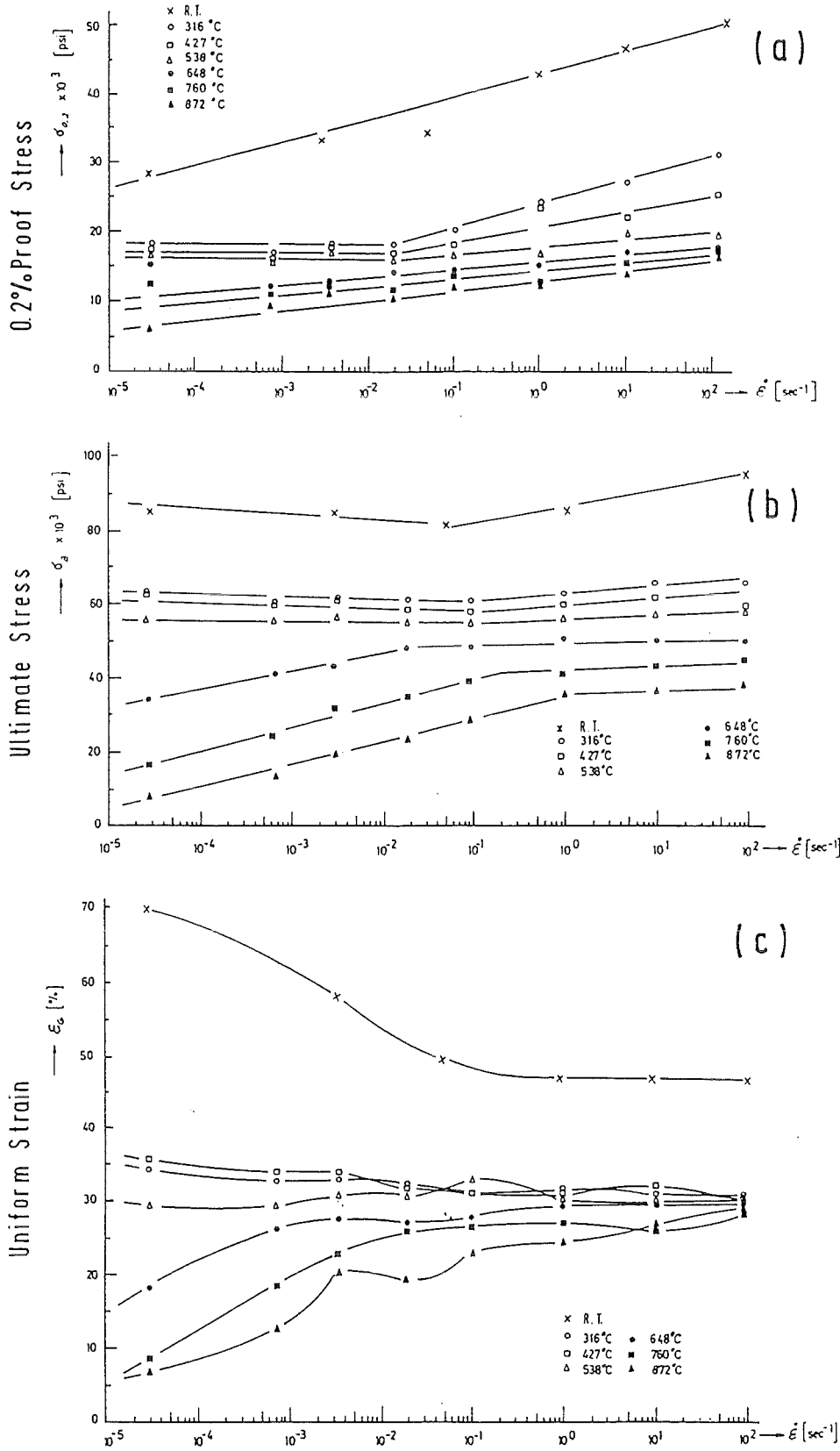


Fig. 7: Influence of Strain Rate $\dot{\epsilon}$ on Proof Stress, Ultimate Stress and Uniform Strain of Austenitic SS Type 304 (Annealed) at Different Temperatures; Based on [21 - 24]

This work includes also various damaging effects (creep, fatigue, irradiation) which are not considered here.

It appears that the simple model, equ. (2.22), which implies the additivity of the strain dependent hardening stress and the strain rate dependent viscous stress at any temperature level, cannot describe the measured dynamic stress-strain curve at all temperature levels. In any case the complex temperature influence must be accounted for if the prototype and the model operate at different temperature levels.

It should be pointed out that these data are not sufficient to identify uniquely the parameters of the above mathematical model, if not additional assumptions are made. At this place the question of the identification of the constitutive model will not be further discussed but in section 3.2.4 an identification for a simplified version will be done.

For a formally complete description the initial and boundary conditions are required. The usual boundary conditions are displacement and stress boundary conditions, i.e.

$$\begin{aligned} u_k &= U_k \text{ on } \partial B_u \\ \sigma_{kl} n_l &= T_k \text{ on } \partial B_\sigma \end{aligned} \quad \text{for all } t \quad (2.23)$$

where

$$\partial B = \partial B_u \cup \partial B_\sigma$$

is the boundary of the body and U_k and T_k are prescribed displacement and stress components at the corresponding parts of the boundary. The initial conditions are assumed to characterize the undeformed state of rest, i.e.,

$$\begin{aligned} u_k &= 0 \\ \frac{\partial u_k}{\partial t} &= 0 \end{aligned} \quad \text{for } t = 0 \text{ and all } x_k \in B. \quad (2.24)$$

3. Similarity Laws for the Deformation Behavior

3.1 Derivation of Similarity Laws

The basic quantities in mechanics and their appropriate dimensions are usually given by (e.g. [25])

length, time and mass.

The dimensions of all other quantities in mechanics can then be obtained from the definition of these quantities. Therefore, from a dimensional point of view it suffices to define a

$$\begin{aligned} \text{characteristic length} & l_R \\ \text{characteristic time} & t_R \\ \text{characteristic mass} & m_R \end{aligned} \quad (3.1)$$

for any system, be it the prototype or the model. However, for the present purpose it is convenient to use an alternative set of characteristic quantities, i.e., a

$$\begin{aligned} \text{characteristic length} & l_R \\ \text{characteristic velocity} & v_R \\ \text{characteristic density} & \rho_R \end{aligned} \quad (3.2)$$

Thus, if necessary, we get for the set (3.1)

$$t_R = l_R / v_R, \quad m_R = \rho_R l_R^3. \quad (3.3)$$

The "method of differential equations" requires the introduction of dimensionless independent and dependent variables. According to the equations in section 2.1, the following dimensionless variables are introduced:

Cartesian coordinates	$x'_k = x_k / l_R$	
displacements	$u'_k = u_k / l_R$	
time	$t' = t v_R / l_R$	
velocities	$v'_k = v_k / v_R$	
	$\frac{\partial u'_k}{\partial t'} = \frac{\partial u_k}{\partial t} \frac{1}{v_R}$	(3.4)
accelerations	$\frac{\partial^2 u'_k}{\partial t'^2} = \frac{\partial^2 u_k}{\partial t^2} l_R / v_R^2$	
strains	$\varepsilon'_{kl} = \varepsilon_{kl}$	
strain rates	$\frac{\partial \varepsilon'_{kl}}{\partial t'} = \frac{\partial \varepsilon_{kl}}{\partial t} l_R / v_R$	
stresses	$\sigma'_{kl} = \sigma_{kl} / (\rho_R v_R^2)$	
stress rates	$\frac{\partial \sigma'_{kl}}{\partial t'} = \frac{\partial \sigma_{kl}}{\partial t} l_R / (\rho_R v_R^3)$	

In dimensionless terms the basic equations take the following form:

Cauchy's first law of motion

$$\frac{\partial \sigma'_{kl}}{\partial x'_k} + \frac{\rho}{\rho_R} \left(\frac{l_R g}{v_R^2} a_l - \frac{\partial^2 u'_l}{\partial t'^2} \right) = 0 ; \quad (3.5)$$

the strain displacement relations and strain partitioning

$$\varepsilon'_{kl} = \frac{1}{2} \left(\frac{\partial u'_k}{\partial x'_l} + \frac{\partial u'_l}{\partial x'_k} \right) = \varepsilon_{kl} ; \quad (3.6)$$

$$\varepsilon'_{kl} = \varepsilon_{kl}^e + \varepsilon_{kl}^p$$

Hooke's law

$$\varepsilon_{kl}^{e'} = \varepsilon_{kl}^e = \frac{1+\nu}{E} \rho_R v_R^2 \sigma'_{kl} - \frac{\nu}{E} \rho_R v_R^2 \sigma'_{nn} \delta_{kl} ; \quad (3.7)$$

yield function

$$f' = \frac{f}{\rho_R v_R^2} = \sigma'_{equ} - (\sigma'_y + R') \quad (3.8)$$

where

$$\left. \begin{aligned} \sigma'_{equ} &= \frac{\sigma_{equ}}{\rho_R v_R^2} = \left(\frac{3}{2} \sigma'_{o,mn} \sigma'_{o,mn} \right)^{\frac{1}{2}} \\ \sigma'_y &= \frac{\sigma_y}{\rho_R v_R^2} \\ R' &= \hat{R}'(p') = \frac{R}{\rho_R v_R^2} = \frac{\hat{R}(p)}{\rho_R v_R^2} \\ p' &= p ; \end{aligned} \right\} \quad (3.9)$$

flow law for the time-independent plastic response with isotropic hardening

$$\frac{\partial \varepsilon_{kl}^{p'}}{\partial t'} = \begin{cases} \frac{1}{h'} \left(\frac{\partial f'}{\partial \sigma'_{mn}} \frac{\partial \sigma'_{mn}}{\partial t'} \right) \frac{\partial f'}{\partial \sigma'_{kl}} ; & f' = 0 \cap \frac{\partial f'}{\partial \sigma'_{mn}} \frac{\partial \sigma'_{mn}}{\partial t'} > 0 \\ 0 & ; f' < 0 \text{ or} \\ & f' = 0 \cap \frac{\partial f'}{\partial \sigma'_{mn}} \frac{\partial \sigma'_{mn}}{\partial t'} \leq 0 \end{cases} \quad (3.10)$$

where

$$h' = \frac{d}{dp'} \left(\frac{\hat{R}(p)}{\rho_R v_R^2} \right) ; \quad (3.11)$$

evolution law for the viscoplastic response

$$\frac{\partial \varepsilon_{kl}^p}{\partial t'} = \frac{l_R}{v_R} A \left(\frac{1}{\sigma_N / \rho_R v_R^2} \right)^n \langle f' \rangle^n \frac{\partial f'}{\partial \sigma_{kl}} \quad (3.12)$$

with the Macauley-brackets

$$\langle f' \rangle = \begin{cases} f' , & f' > 0 \\ 0 , & f' \leq 0 ; \end{cases} \quad (3.13)$$

boundary conditions

$$\begin{aligned} u'_k &= U'_k := u_k / l_R && \text{on } \partial B'_u \\ \sigma'_{kl} n_l &= T'_k := T_k / (\rho_R v_R^2) && \text{on } \partial B'_\sigma \end{aligned} \quad (3.14)$$

and the initial conditions

$$\begin{aligned} u'_k &= 0 \\ \frac{\partial u'_k}{\partial t} &= 0 \quad \text{for } t' = 0 \text{ and } x'_k \in B' . \end{aligned} \quad (3.15)$$

This completes the formulation of the dimensionless system of basic equations.

Geometrical and physical similarity between the prototype and the model requires that the *dimensionless solutions* of this system of equations, both obtained for the prototype and the model, *are identical*. This is assured if and only if the dimensionless parameters and the dimensionless externally applied forces and constraints are the same for prototype and model. Identifying quantities related to the prototype by the index "p" and those related to the model by the index "m", the similarity conditions for both constitutive models are listed in Tab. 1.

	Elastic-Viscoplastic Behavior	Elastic Time-Independent Plastic Behavior
A	$\left(\frac{l_R g}{v_R^2} \right)_p = \left(\frac{l_R g}{v_R^2} \right)_m$	– ditto –
B	$\left(\frac{\rho(x)}{\rho_R} \right)_p = \left(\frac{\rho(x)}{\rho_R} \right)_m, \forall x'$	– ditto –
C	$\left(\frac{1+\nu}{E} \rho_R v_R^2 \right)_p = \left(\frac{1+\nu}{E} \rho_R v_R^2 \right)_m$	– ditto –
D	$\left(\frac{\nu}{E} \rho_R v_R^2 \right)_p = \left(\frac{\nu}{E} \rho_R v_R^2 \right)_m$	– ditto –
E	$\left(\frac{\sigma_y}{\rho_R v_R^2} \right)_p = \left(\frac{\sigma_y}{\rho_R v_R^2} \right)_m$	– ditto –
		(3.16) ^l
F	$\left(\frac{\hat{R}(p)}{\rho_R v_R^2} \right)_p = \left(\frac{\hat{R}(p)}{\rho_R v_R^2} \right)_m, \forall p$	– ditto –
G	$\left(\frac{l_R}{v_R} A \left(\frac{\rho_R v_R^2}{\sigma_N} \right)^n \right)_p = \left(\frac{l_R}{v_R} A \left(\frac{\rho_R v_R^2}{\sigma_N} \right)^n \right)_m$	– not applicable –
H	$(n)_p = (n)_m$	– not applicable –
J	$\left(\frac{u_k}{l_R} \right)_p = \left(\frac{u_k}{l_R} \right)_m, \text{ on } \partial B'_u$	– ditto –
K	$\left(\frac{T_k}{\rho_R v_R^2} \right)_p = \left(\frac{T_k}{\rho_R v_R^2} \right)_m, \text{ on } \partial B'_\sigma$	– ditto –

Tab. 1: Primary List of Similarity Conditions

Some of these conditions can be related to well known dimensionless parameters.

Condition (A, Tab. 1) states that the *Froude number*

$$Fr := \frac{v_R^2}{l_R g} \quad (3.17)$$

is the same for prototype and model

$$(Fr)_p = (Fr)_m. \quad (3.18)$$

The conditions (C, Tab. 1) and (D, Tab. 1), which follow from Hooke's law, yield

$$\left(\frac{E}{\rho_R v_R^2} \right)_p = \left(\frac{E}{\rho_R v_R^2} \right)_m, \quad (v)_p = (v)_m. \quad (3.19)$$

Using the *Cauchy number*

$$Ca = \frac{v_R}{\sqrt{E/\rho_R}}, \quad (3.20)$$

condition (3.19)₁ is equivalent to

$$(Ca)_p = (Ca)_m. \quad (3.21)$$

Note that $\sqrt{E/\rho_R}$ is the propagation velocity of small elastic disturbances in long slender rods; thus the Cauchy number resembles the Mach number in fluid mechanics:

$$C_a = v_R/c. \quad (3.22)$$

Condition (G, Tab. 1) may be put in a form which resembles a more familiar dimensionless parameter. Introducing the material parameter

$$\eta_n := \frac{\sigma_N}{A^{1/n}}, \quad (3.23)$$

which has the dimension [stress/(strain rate)^{1/n}] and which is a measure of the quasi-viscosity of the material, a "generalized Reynolds number"

$$\text{Re}_n := \frac{l_R v_R^{2n-1}}{\left(\eta_n / \rho_R\right)^n} \quad (3.24)$$

may be defined; then condition (G, Tab. 1) yields

$$\left(\text{Re}_n\right)_p = \left(\text{Re}_n\right)_m. \quad (3.25)$$

Obviously, the generalized Reynolds number corresponds to the classical Reynolds number for $n = 1$; that is

$$n = 1: \text{Re}_n = \text{Re} = \frac{l_R v_R}{\eta_1 / \rho_R}.$$

With these definition the primary list Tab. 1 yields a secondary equivalent list of conditions, Tab. 2.

	Elastic-Viscoplastic Behavior	Elastic Time-Independent Plastic Behavior
A	$(Fr)_p = (Fr)_m$	– ditto –
B	$\left(\frac{\rho}{\rho_R}\right)_p = \left(\frac{\rho}{\rho_R}\right)_m, \forall x'$	– ditto –
C	$(Ca)_p = (Ca)_m$	– ditto –
D	$(\nu)_p = (\nu)_m$	– ditto –
E	$\left(\frac{\sigma_y}{\rho_R v_R^2}\right)_p = \left(\frac{\sigma_y}{\rho_R v_R^2}\right)_m$	– ditto –
		(3.16) ^{II}
F	$\left(\frac{\hat{R}(p)}{\rho_R v_R^2}\right)_p = \left(\frac{\hat{R}(p)}{\rho_R v_R^2}\right)_m, \forall p$	– ditto –
G	$\left(\frac{Re}{n}\right)_p = \left(\frac{Re}{n}\right)_m$	– inapplicable –
H	$(n)_p = (n)_m$	– inapplicable –
J	$\left(\frac{U_k}{l_R}\right)_p = \left(\frac{U_k}{l_R}\right)_m, \text{ on } \partial B'_u$	– ditto –
K	$\left(\frac{T_k}{\rho_R v_R^2}\right)_p = \left(\frac{T_k}{\rho_R v_R^2}\right)_m, \text{ on } \partial B'_\sigma$	– ditto –

Tab. 2: Secondary List of Similarity Conditions

Up to now the characteristic quantities l_R , v_R , ρ_R have not been definitely defined. Usually they will be directly related to corresponding quantities of the model and prototype, for example some actual length (e.g. diameter) or actual velocity (e.g. impact velocity of a striker). However, the characteristic quantities may also be related to non-material physical quantities. One example will be discussed here which will give an alternative list of similarity conditions. Assume the characteristic velocity to be defined by the sound velocity in long slender bars:

$$v_R = c = \sqrt{E/\rho} \text{ and } \rho = \rho_R ; \quad (3.26)$$

here the characteristic density should correspond at least to some part of the structure. Then

$$\rho_R v_R^2 = E \quad (3.27)$$

and the dimensionless quantity (3.24) takes the form

$$\text{Re}_n = \frac{l_R}{v_R} A \left(\frac{\rho_R v_R^2}{\sigma_N} \right)^n = \frac{l_R}{l_{in}} \quad (3.28)$$

with

$$l_{in} = \frac{c}{A} \left(\frac{\sigma_N}{E} \right)^n . \quad (3.29)$$

The length l_{in} is solely characterized by constitutive quantities and is therefore termed "internal constitutive length". It can be interpreted as follows. With (2.15) and (2.19) we have

$$\dot{p} = A \left(\frac{f}{\sigma_N} \right)^n . \quad (3.30)$$

If the "overstress"

$$f = \sigma_{equ} - \left(\sigma_y + \hat{R}(p) \right) \quad (3.31)$$

takes the value*

$$f = E, \quad (3.32)$$

then the corresponding accumulated viscoplastic strain rate is given by

$$\dot{\rho}_E = A \left(\frac{E}{\sigma_N} \right)^n. \quad (3.33)$$

The internal constitutive length (3.29) is then given by

$$l_{in} = \frac{c}{\dot{\rho}_E}$$

or

$$l_{in} \dot{\rho}_E = c. \quad (3.34)$$

Consequently, l_{in} corresponds to the length of a specimen whose speed of viscoplastic extension under the overstress $f = E$ equals the elastic sound speed c .

With (3.26) - (3.28) the secondary list takes the form given in Tab. 3. Note that condition (C, Tab. 3) is identically satisfied since the Cauchy number is equal to "one" for both the model and the prototype. On the first sight it appears that the list of conditions is reduced by one due to the specific choice (3.26). However, this is a premature conclusion. For example, if the dynamic elastic-plastic problem involves the impact velocity v_{imp} of a striker, then similarity requires the equality of the dimensionless striker velocities, i.e.,

$$\left(\frac{v_{imp}}{c} \right)_p = \left(\frac{v_{imp}}{c} \right)_m. \quad (3.35)$$

Thus, a Cauchy number pops up again.

Whatever choice of dimensionless parameters and functions is made, Tables 1 to 3 are accompanied by the similarity requirements for the initial conditions, equ. (3.15).

*) In reality this is purely fictitious since $f \ll E$

	Elastic-Viscoplastic Behavior	Elastic Time-Independent Plastic Behavior
A	$\left(\frac{c^2}{l_R g} \right)_p = \left(\frac{c^2}{l_R g} \right)_m$	– ditto –
B	$\left(\frac{\rho}{\rho_R} \right)_p = \left(\frac{\rho}{\rho_R} \right)_m, \forall x$	– ditto –
C	$(Ca)_p = 1, (Ca)_m = 1$ identically satisfied	– ditto –
D	$(\nu)_p = (\nu)_m$	– ditto –
E	$\left(\frac{\sigma_y}{E} \right)_p = \left(\frac{\sigma_y}{E} \right)_m$	– ditto –
F	$\left(\frac{\hat{R}(p)}{E} \right)_p = \left(\frac{\hat{R}(p)}{E} \right)_m, \forall p$	– ditto –
G	$\left(\frac{l_R}{l_{in}} \right)_p = \left(\frac{l_R}{l_{in}} \right)_m$	– inapplicable –
H	$(n)_p = (n)_m$	– inapplicable –
J	$\left(\frac{U_k}{l_R} \right)_p = \left(\frac{U_k}{l_R} \right)_m$	– ditto –
K	$\left(\frac{T_k}{E} \right)_p = \left(\frac{T_k}{E} \right)_m$	– ditto –

(3.16)^{III}

Tab. 3: Tertiary List of Similarity Conditions

3.2 Interpretations and Discussion

3.2.1 Modeling Similarity of Gravitational Forces

Since the gravitational acceleration g cannot be controlled and is approximately constant,

$$g_p = g_m \quad (3.36)$$

condition (A) yields

$$\left(\frac{v_{Rp}}{v_{Rm}} \right)^2 = \frac{l_{Rp}}{l_{Rm}} = \lambda \quad (3.37)$$

where λ is the ratio of the characteristic lengths

$$\lambda := \frac{l_{Rp}}{l_{Rm}} \geq 1; \quad (3.38)$$

note that the discussion will be restricted to cases where the model is always smaller than the prototype. Condition (3.37) shows that the choice of the characteristic lengths completely determines the ratio of the characteristic velocities and vice versa. Obviously, this reduces the flexibility of the small scale simulation considerably; for example, from (3.37) it follows that the sound velocities have to satisfy the condition

$$\frac{c_p}{c_m} = \frac{v_{Rp}}{v_{Rm}} = \sqrt{\lambda}. \quad (3.39)$$

According to condition (E & F) the initial yield stress σ_y and the hardening stress R have to satisfy

$$\frac{\sigma_{yp}}{\sigma_{ym}} = \frac{\rho_{Rp}}{\rho_{Rm}} \lambda, \quad \frac{\left(\hat{R}_{(p)} \right)_p}{\left(\hat{R}_{(p)} \right)_m} = \frac{\rho_{Rp}}{\rho_{Rm}} \lambda. \quad (3.40)$$

Of primary interest are steel structures and here the densities in model and prototype are approximately the same. Thus,

$$\frac{\sigma_{yp}}{\sigma_{ym}} \approx \lambda, \quad \frac{\left(\hat{R}_{(p)}\right)_p}{\left(\hat{R}_{(p)}\right)_m} \approx \lambda \quad (3.41)$$

and with (3.19) the ratio of Youngs moduli is approximately

$$\frac{E_p}{E_m} \approx \lambda. \quad (3.42)$$

If the viscoplastic response is important, then in addition (G) and (H) have to be observed. From (3.25) one gets with (3.39)

$$\frac{\left(\eta_n\right)_p}{\left(\eta_n\right)_m} \approx \lambda^{\frac{2n+1}{2}}. \quad (3.43)$$

In principle, these conditions can be satisfied, however, in practice it is rather difficult. For example, if the scaling factor λ is prescribed, e.g. $\lambda = 10$, then the yield stress in the model must be reduced by a factor 10. Alternatively, the ratio of the yield stresses etc. determine the geometric scale factor.

If the material of the model and the prototype is chosen to be the *same* (at the same temperature), then the conditions (A) to (G) can consistently be satisfied only if

$$\lambda = 1,$$

i.e. a small scale model test is not possible. This is true whether one accounts for viscoplasticity and plasticity or not.

Frequently, however, gravitational effects may be safely neglected. Then condition (A), i.e. the equality of the Froude numbers, can be deleted. As a consequence the geometric scale factor λ and the ratio of characteristic velocities v_{Rp}/v_{Rm} are uncoupled.

Throughout the following this assumption will be made.

3.2.2 Modeling the Density Distribution

The similarity condition (B) has a very simple interpretation: The density distributions of model and prototype must be the same, they differ only by a constant factor

$$\rho_m(x) = \frac{\rho_{Rm}}{\rho_{Rp}} \rho_p(x). \quad (3.44)$$

If the density is uniformly constant throughout the model and the prototype and if the characteristic density ρ_R is taken to be this material value ρ_0 , then condition (B) is identically satisfied.

3.2.3 Modeling the Constitutive Response

The conditions (C) to (H) are all related to the constitutive behavior: Conditions (C) and (D) concern the elastic response, conditions (E) and (F) the time independent plastic response, and conditions (G) and (H) the viscoplastic effects.

These requirements may be interpreted in terms of the empirical data which are used for the identification of the constitutive model. Here it is assumed that the elastic moduli have been determined in separate purely elastic experiments and are known in advance.

In dynamic plasticity [24, 26, 27] a basic experiment is the dynamic tensile test, i.e., a test at approximately constant engineering strain rate or constant cross head velocity. The outcome is a set of stress-total strain curves with the strain rate as a parameter. For the above elastic-viscoplastic model these curves can be obtained by integrating the differential constitutive relations

$$\begin{aligned} \dot{\varepsilon} &= \dot{\varepsilon}^e + \dot{\varepsilon}^p = \text{const.} \\ \dot{\varepsilon}^e &= \dot{\sigma}/E \\ \dot{\varepsilon}^p &= \begin{cases} A \left(f/\sigma_N \right)^n, & f > 0 \\ 0 & , f \leq 0 \end{cases} \\ f &= \sigma - \left(\sigma_y + \hat{R}_{(\varepsilon^p)} \right) \end{aligned} \quad (3.45)$$

which yields the stress as a function of time or total strain. The typical result is shown schematically in Fig. 8.

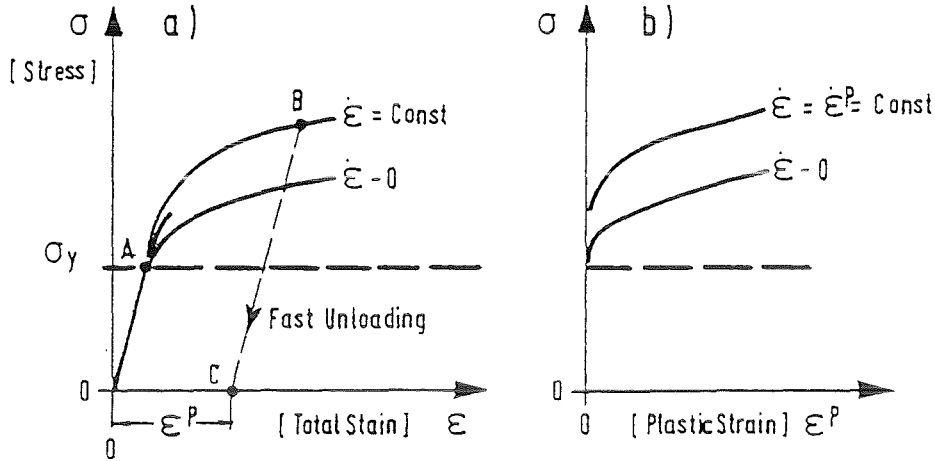


Fig. 8: Dynamic Stress-Strain Diagrams (Schematic)

The representation in Fig. 8a still contains the elastic strain $\epsilon^e = \sigma/E$. The plastic strain at B can be obtained in a fast unloading experiment which leads to point C. Note that during this *fast* unloading no further plastic strain is produced since the generation of viscoplastic strain is a time dependent process and the time interval is too short.

Thus, if experimental stress-total strain curves are given as shown in Fig. 8a, they also can be represented as stress-plastic strain curves (Fig. 8b). Of course, the curve parameter is still the total strain rate $\dot{\epsilon} = \dot{\epsilon}^e + \dot{\epsilon}^p$. For the initial part the elastic strain rate is the dominating contribution but for the later and largest part the viscoplastic strain rate is essential. Therefore, the curve parameter in Fig. 8 is considered to be approximately equal to the viscoplastic strain rate $\dot{\epsilon}^p$. The constitutive model under discussion yields a "dynamic stress - viscoplastic strain curve" at constant viscoplastic strain rate as given by equ. (2.22). In the uniaxial case this is

$$\sigma = \sigma_y + \hat{R}_{(\dot{\epsilon}^p)} + \sigma_y \left(\dot{\epsilon}^p / A_y \right)^{1/n} \quad (3.46)$$

Using the dimensionless variables (3.4), (3.9) and the generalized Reynolds number (3.24), equ. (3.46) takes the following dimensionless form

$$\sigma' = \frac{\sigma}{\rho_R v_R^2} = \frac{\sigma_y}{\rho_R v_R^2} + \frac{\hat{R}(\varepsilon^P)}{\rho_R v_R^2} + \left[\frac{1}{Re} \right]^{1/n} \left(\frac{d\varepsilon^P}{dt'} \right)^{1/n} \quad (3.47)$$

This expression contains the similarity terms (E to H, Tab. 2). Its structure leads to the following statement, which is alternative to the similarity conditions (E to H, Tab. 2):

Provided the viscoplastic responses of model and prototype can be described within the same class of constitutive models, i.e., equ. (2.7), (2.14), and (2.19), then physical similarity requires, among others,

- *equality* of the dimensionless "dynamic stress - viscoplastic strain curves" for the *same* dimensionless viscoplastic strain rates

$$\left(\frac{d\varepsilon^P}{dt'} \right)_p = \left(\frac{d\varepsilon^P}{dt'} \right)_m$$

or

$$\left(\frac{d\varepsilon^P}{dt} \right)_m = \left(\frac{d\varepsilon^P}{dt} \right)_p \lambda \frac{v_{Rm}}{v_{Rp}} \quad (3.48)$$

If only time-independent plasticity is considered, then the last term in (3.47) is to be deleted and (3.47) simplifies to

$$\sigma' = \frac{\sigma_y}{\rho_R v_R^2} + \frac{\hat{R}(\varepsilon^P)}{\rho_R v_R^2} =: \frac{\hat{\sigma}(\varepsilon^P)}{\rho_R v_R^2} ; \quad (3.49)$$

thus, similarity simply requires, among others,

- *equality* of the dimensionless "stress-plastic strain curves", i.e.

$$\left(\frac{\hat{\sigma}(\varepsilon^P)}{\rho_R v_R^2} \right)_p = \left(\frac{\hat{\sigma}(\varepsilon^P)}{\rho_R v_R^2} \right)_m, \quad \forall \varepsilon^P \quad (3.50)$$

One may raise the question whether this criterion applies also to the "experimental stress - total strain curves" in tension such that

$$\left(\frac{\dot{\sigma}(\varepsilon)}{\rho_R v_R^2} \right)_p = \left(\frac{\dot{\sigma}(\varepsilon)}{\rho_R v_R^2} \right)_m \quad (3.51)$$

Some reflection about the geometric construction of the curves $\dot{\sigma}(\varepsilon)$ from the knowledge of E and $\dot{\sigma}(\varepsilon p)$ and with the additivity of elastic and plastic strains confirms the validity of the similarity condition (3.51).

A statement equivalent to (3.51) can be made for the elastic-viscoplastic material behavior, however, the constant curve parameter is still the dimensionless viscoplastic strain rate (3.48)₁ and not the dimensionless *total* strain rate.

It should be noted that the dimensionless stress - strain curve can be obtained by choosing any "stress-related" normalizing quantity, for example, instead of $\rho_R v_R^2$, one can take Young's modulus E (see Table 3), the yield stress σ_y or the ultimate stress σ_u .

In general it is not a simple matter to find a material for the small scale model test which satisfies the similarity condition. In the following this and related questions are discussed separately for the time-independent plastic and the viscoplastic behavior.

Elastic - time independent plastic material

For the elastic-time independent plastic material response there is a chance to find a model material which satisfies the similarity condition approximately in some strain interval $0 \leq \varepsilon \leq \varepsilon_t$ of interest since only a single stress-strain curve has to be simulated. If such a material is found, then the similarity condition (E) yields

$$\frac{v_{Rm}}{v_{Rp}} = \sqrt{\frac{\rho_{Rp} \sigma_{ym}}{\rho_{Rm} \sigma_{yp}}} \approx \sqrt{\frac{\sigma_{ym}}{\sigma_{yp}}} = \sqrt{\frac{E_m}{E_p}} \quad (3.52)$$

Thus, the choice of the model material puts a constraint on the characteristic velocities, e.g., the impact velocities.

In particular the identification of a model material is required if the *model test cannot be performed at the same temperature level as the prototype*, e.g., the prototype is at elevated temperature (T) whereas the model operates at room temperature (R.T.). There is an exceptional situation where *the same material* can

be used for the model test. If the temperature affects the stress-strain curve uniformly such that

$$\frac{E_{(T)}}{E_{(RT)}} = \frac{\sigma_{y(T)}}{\sigma_{y(RT)}} = \frac{\hat{R}_{(\varepsilon^P, T)}}{\hat{R}_{(\varepsilon^P, RT)}} = \theta_{(T)}, \quad \forall \varepsilon^P, \quad (3.53)$$

then similarity of the stress-strain curves at the different temperatures is assured and the *same* material can be used for the room temperature model test. Of course, if the temperature is non-uniformly distributed in the prototype then the variation of the material properties in the structure and the effect of thermal stresses are not properly modeled. Disregarding these effects, the characteristic velocity ratio is then given by

$$\frac{v_{Rm}}{v_{Rp}} = \sqrt{\frac{\rho_{Rp}}{\rho_{Rm}} \frac{1}{\theta(T)}}. \quad (3.54)$$

In the following the condition (3.53) is checked for two austenitic stainless steels, AISI 347 and AISI 304. Both steels are important in nuclear engineering: They are used for the upper internal structures of Light Water Reactors or Fast Breeders. Fig. 7 shows that a change of the strain rate by one order of magnitude, e.g. from $\dot{\varepsilon} = 10^1$ to 10^2 , does not affect the 0.2 % proof stress, ultimate stress and the uniform elongation of AISI 304 (annealed) significantly at any temperature; the largest influence is seen at room temperature. Such an order of magnitude change in strain rate corresponds to the difference in strain rate if the small scale model and the large scale prototype are related by a scale factor $\lambda = 10$ and if the same impact velocity is used, equ. (3.48); thus

$$\dot{\varepsilon}_m = \dot{\varepsilon}_p \lambda.$$

The main influence comes from a change in temperature from an elevated level, say 400 - 700 °C, down to room temperature. Therefore, the material response for model and prototype may be considered as approximately rate insensitive* but temperature dependent. Fig. 9 shows the temperature dependence of the proof stress and the ultimate stress of the two austenitic steels [28, 29] obtained in *quasistatic tensile tests*.

* This assumption implies that the strain rate does not vary too much in the structure.

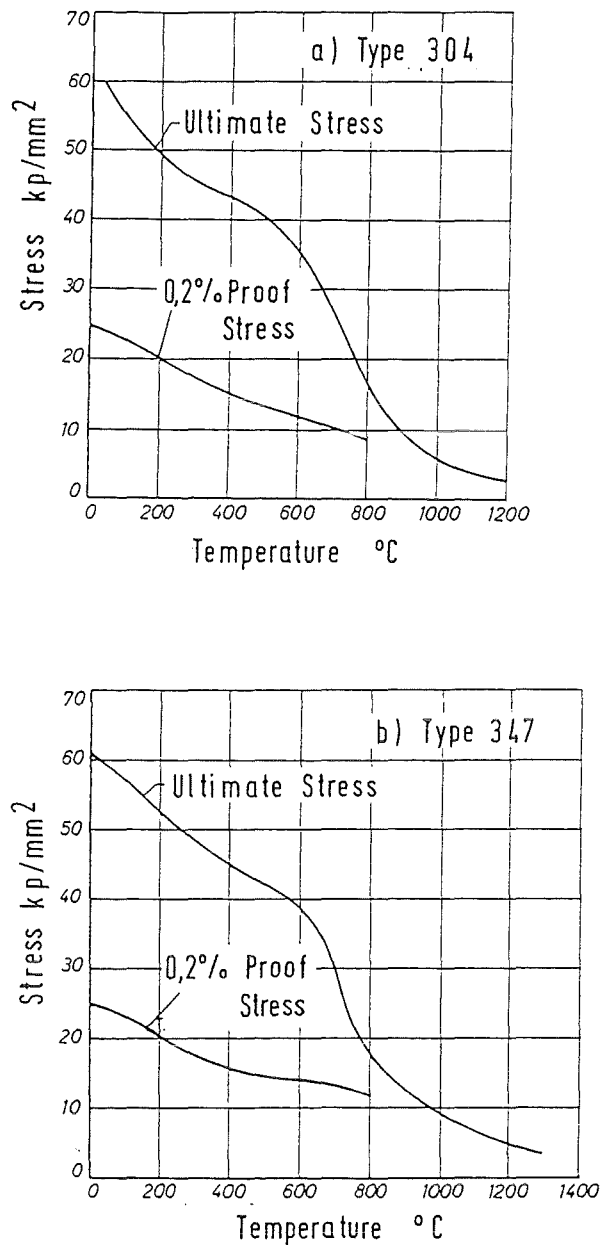


Fig. 9: Proof Stress and Ultimate Stress of AISI Type 304 and 347 Versus Temperature; from [28, 29]

Fig. 10 represents the temperature dependence of the ratios

$$\left[\frac{\sigma_{0,2}(T)}{\sigma_{0,2}(RT)} \right]_{\text{static}}, \left[\frac{\sigma_u(T)}{\sigma_u(RT)} \right]_{\text{static}}$$

in the interval $200^\circ\text{C} < T < 800^\circ\text{C}$. If perfect similarity of the stress strain curve at all temperatures with that at room temperature were found, then

- the two ratios should be the same at all temperatures, and
- the uniform elongations should be equal.

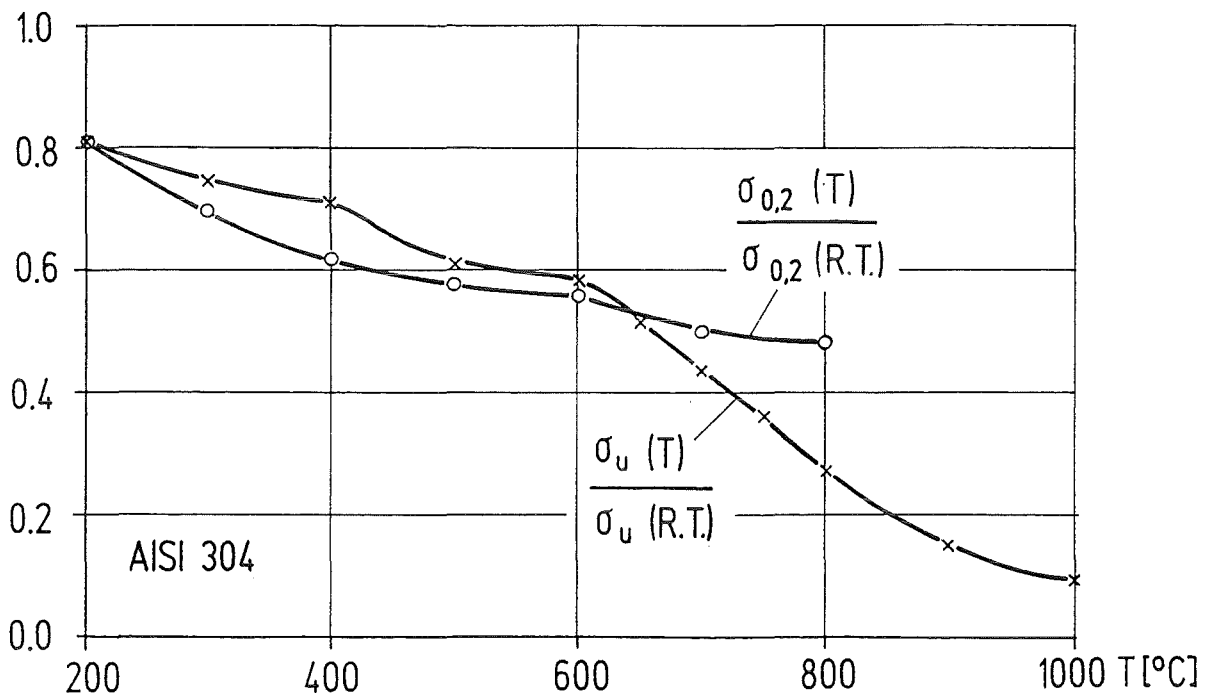
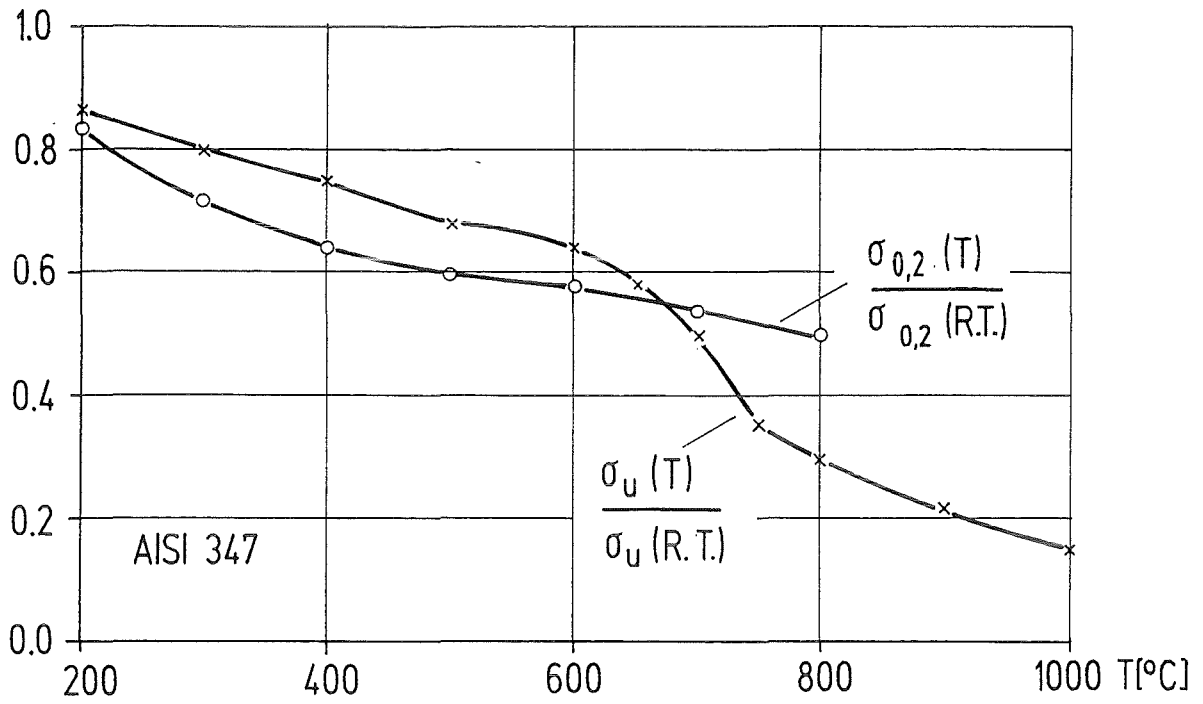


Fig. 10: Normalized Quasistatic 0.2 % Proof Stress and Ultimate Stress of AISI Type 304 and 347 Versus Temperature

Fig. 10 shows that the first requirement is not strictly satisfied, but the relative difference is not large between room temperature and 700 °C.

A more representative comparison is obtained if dynamic stress-strain data are used. Here the results of Steichen et al. [21] for AISI 304 (annealed) shown in Fig. 7 are used. The maximum strain rate is limited to $\dot{\epsilon} = 10^2 \text{ s}^{-1}$. Therefore, it is assumed that the prototype operates at $\dot{\epsilon}_p = 10 \text{ s}^{-1}$. Then for $\lambda = 10$ the model sees a strain rate of $\dot{\epsilon}_m = 10^2 \text{ s}^{-1}$. Therefore, the following ratios are determined:

$$\frac{\sigma_{0,2} (T, \dot{\epsilon} = 10)}{\sigma_{0,2} (RT, \dot{\epsilon} = 10^2)} \quad , \quad \frac{\sigma_u (T, \dot{\epsilon} = 10)}{\sigma_u (RT, \dot{\epsilon} = 10^2)}$$

as well as

$$\frac{\sigma_{0,2} (T, \dot{\epsilon} = 10^2)}{\sigma_{0,2} (RT, \dot{\epsilon} = 10^2)} \quad , \quad \frac{\sigma_u (T, \dot{\epsilon} = 10^2)}{\sigma_u (RT, \dot{\epsilon} = 10^2)}$$

It is found that

$$\frac{\sigma_{0,2} (T, \dot{\epsilon} = 10)}{\sigma_{0,2} (RT, \dot{\epsilon} = 10^2)} \approx \frac{\sigma_u (T, \dot{\epsilon} = 10)}{\sigma_u (RT, \dot{\epsilon} = 10^2)}$$

The first pair of ratios is the relevant one. Fig. 11a demonstrates that the relative difference in the ratios has increased. This is due to the fact that the temperature influence is different in quasistatic tensile tests compared to dynamic tensile tests.

Finally, in Fig. 11b the ratio of the uniform elongations

$$\frac{\epsilon_g (T, \dot{\epsilon} = 10)}{\epsilon_g (T, \dot{\epsilon} = 10^2)}$$

is plotted. Perfect similarity would require a ratio of 1. But unfortunately the uniform elongation $\epsilon_g (RT, \dot{\epsilon} = 10^2)$ in the fictitious model is clearly larger than that in the fictitious prototype. If the uniform elongation is taken as a failure limit, then the "ductility" of the model is definitely too large. These mismatched data prove that an other material choice for the model is required, if a size effect due to temperature differences is to be prevented.

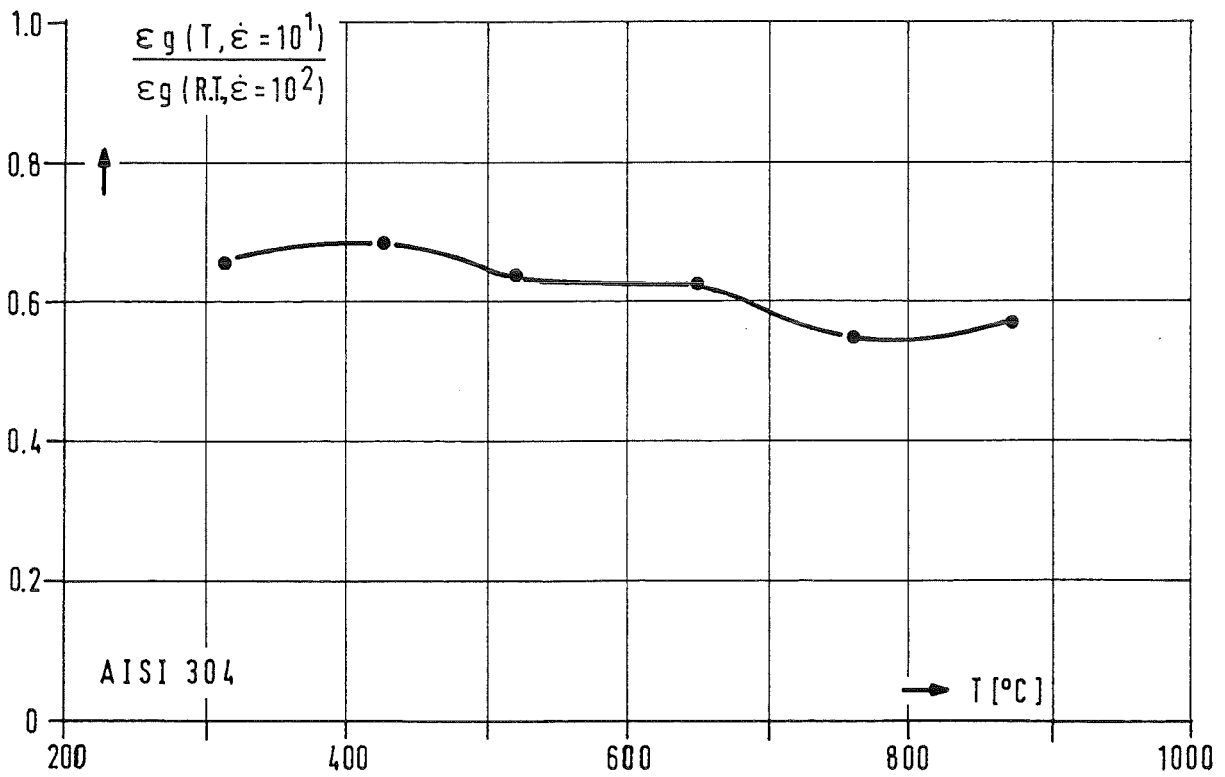
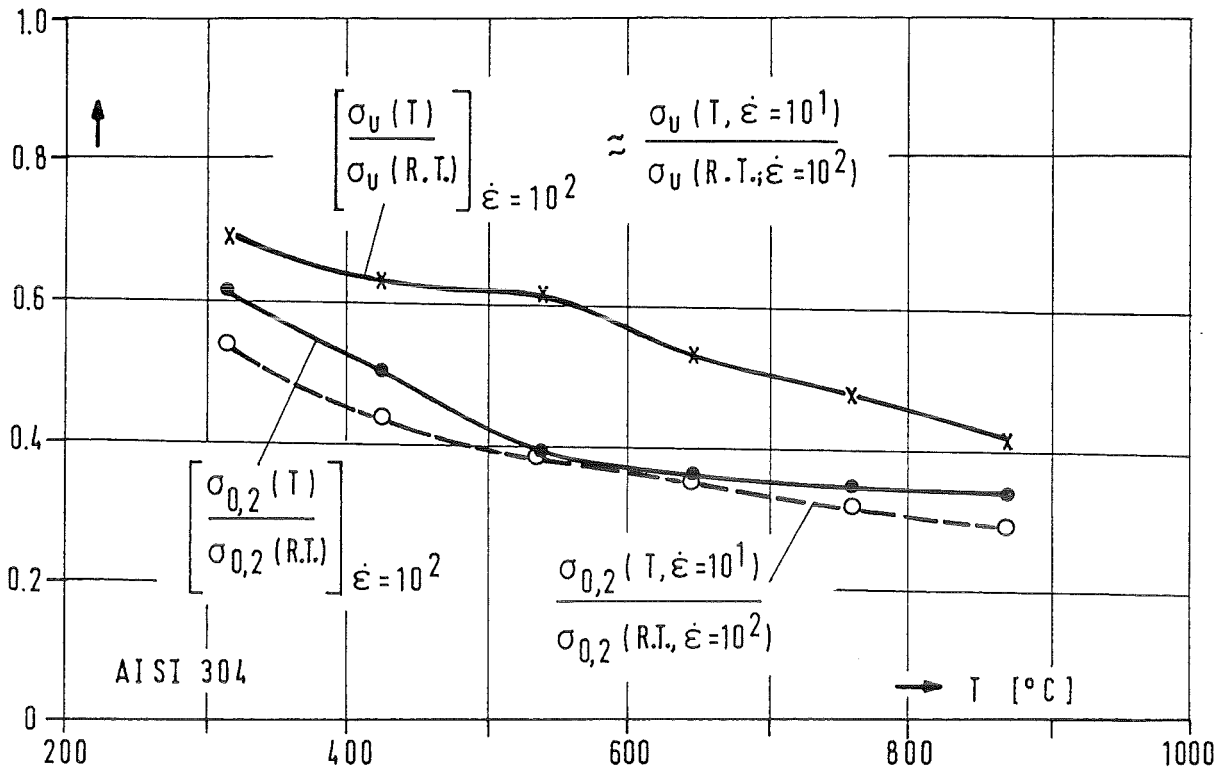


Fig. 11: Normalized Dynamic 0.2 % Proof Stress, Ultimate Stress and Normalized Uniform Elongation of AISI Type 304 Versus Temperature

A fortunate simulation is found if the model test can be performed at the *same* temperature as the prototype and the *same material* can be used (replica models). Assume that the material properties

$$E, \nu, \sigma_y, \hat{R}_{(\epsilon^p)}$$

do not depend on the scale factor λ , i.e., tensile tests of different size specimens taken from the same block of material yield the same stress-strain curve. Then the similarity conditions (C) and (E - G) (Tab. 2) are satisfied if and only if the characteristic velocities are the same

$$v_{Rm} = v_{Rp} \quad (3.55)$$

A restriction on the geometric scale factor λ does not exist since gravitational forces are assumed to be negligible.

Note that the conclusion (3.55) is obtained both for the purely elastic behavior (condition (C)) and the time independent plastic behavior (conditions (E) and (F)) (Tab. 2) independently.

A basic requirement for the validity of (3.55) is the *scale invariance* of the elastic-plastic material properties. This essential, presently taken for granted, will be discussed separately in section 3.2.5.

Elastic-viscoplastic material

For the elastic-viscoplastic material response it is more difficult to find a model material which satisfies the similarity conditions since not only a single stress-strain curve but a *set* of curves has to be simulated. If a wide range of strain rates has to be covered, this may be practically impossible.

If the small scale test is done at the same temperature as required in the full scale situation and the *same material* is used, then following conclusions are obtained (Tab. 2)

$$\begin{aligned} \text{(C)} \quad & \text{satisfied only iff} \quad v_{Rm} = v_{Rp} \\ \text{(E) \& (F)} \quad & \text{satisfied only iff} \quad v_{Rm} = v_{Rp} \end{aligned} \quad (3.56)$$

but then the contribution (G) on the generalized Reynolds number equ. (3.24) yields

$$\lambda = \frac{l_{Rp}}{l_{Rm}} = 1 ; \quad (3.57)$$

thus a small scale model test using the same material is not possible. Here again the scale invariance of basic material parameters and functions is tacitly assumed (see section 3.2.5).

In reality most structural steels are more or less strain rate sensitive and should be modeled by a viscoplastic material model. However, in some cases the sensitivity is moderate and one is tempted to ignore this effect. Thus, the material is simply considered to be time-independent plastic.

If the small scale model test is then done with the same material at the same temperature as used in the full scale situation, then the strict scaling laws are not satisfied and a *size effect* occurs. In the following section this size effect is treated to some extent for rather simple conditions.

3.2.4 Size Effect for Viscoplastic Material Response

3.2.4.1 Constant Flow Stress Assumption

To illustrate the size effect a simple impact problem is considered: A mass with a given kinetic energy impacts a moderately rate sensitive but massless strut in a compressive deformation mode (Fig. 12). Note that wave propagation and buck-

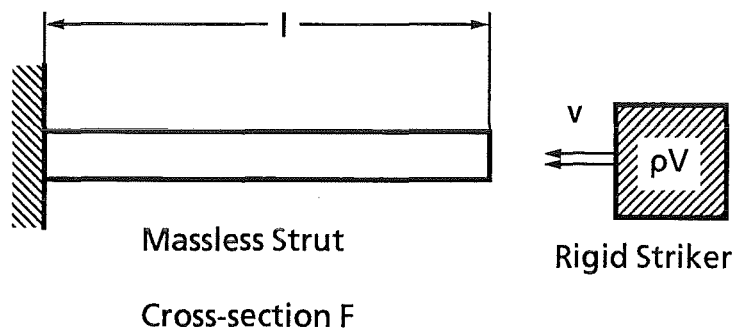


Fig. 12: Impact Problem (Schematic)

ling phenomena are not considered. The kinetic energy of the mass is

$$E_{kin} = \frac{1}{2} \rho v^2 V \quad (3.58)$$

$$\left. \begin{array}{l} \rho: \text{ density} \\ V: \text{ volume} \\ v: \text{ impact velocity} \end{array} \right\} \text{ of rigid striker .}$$

The material response is described by a simplified viscoplastic model: Elastic deformations are entirely ignored such that the total strain rate consists only of the viscoplastic part

$$\varepsilon = \varepsilon^p, \quad \dot{\varepsilon} = \dot{\varepsilon}^p ;$$

further the strain hardening term $\hat{R}_{(\varepsilon^p)}$ is neglected. Then equ. (3.46) simplifies to

$$\sigma = \sigma_y + \sigma_y \left(\frac{\dot{\varepsilon}}{A_y} \right)^{1/n}, \quad \sigma \geq \sigma_y . \quad (3.59)$$

The data of Steichen et al. [21-24] for stainless steel AISI 304 at room temperature (Fig. 7) may be used to determine the parameters of the above simple model, provided the measured 0.2 % proof stresses are interpreted as the dynamic yield stresses σ , equ. (3.59), at vanishing viscoplastic strain. Note that such an interpretation is conceptually not possible for the complete elastic-viscoplastic model described in section 2.

A proper identification approach would be to develop an optimized fit to all the measured data within a prescribed strain rate interval but this leads to a nonlinear system of algebraic equations for σ_y , A_y and n . Forrestal and Sagartz [31] have performed a fit to these data but the method they used is not readily available. They obtained [31]

$$\begin{aligned} \sigma_y &= 172.34 \text{ MPa} , \quad A_y = 100 \text{ s}^{-1} , \quad n = 10 \\ &= 25 \cdot 10^3 \text{ psi} \end{aligned} \quad (3.60)$$

and this fit is shown in Fig. 13.

It should be observed that the above data correspond to the following choice of the static yield

$$\sigma_y \approx \frac{1}{2} \sigma^{**} \quad (3.61)$$

where σ^{**} is the measured proof stress at a strain rate $\dot{\varepsilon}^{**} = 10^2 \text{ s}^{-1}$. If the measured data point $(\dot{\varepsilon}^{**}, \sigma^{**})$ is then exactly fitted by the relation (3.59), one finds

$$A_y = \dot{\epsilon}^{**} = 10^2 \text{ s}^{-1}. \quad (3.62)$$

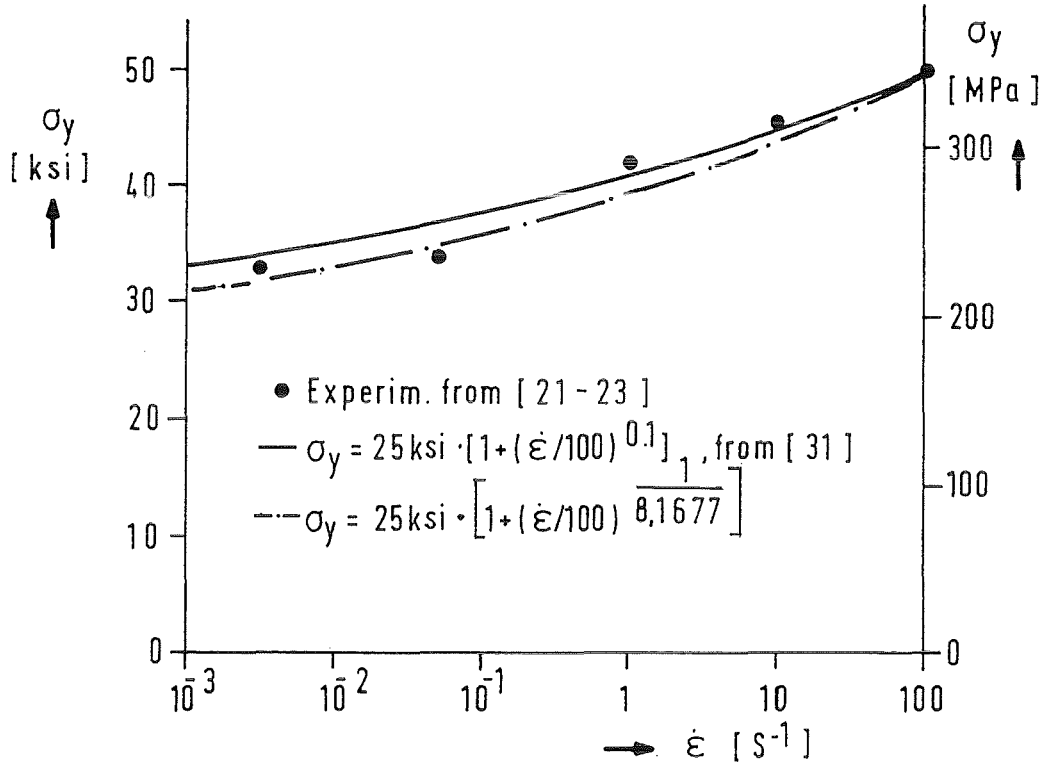


Fig. 13: 0.2 % Proof Stress Versus Strain Rate (Room Temperature), Based on [31]

The choice of the "static yield stress" equ. (3.61) can be interpreted as follows. The existence of a "static yield stress" is not evident from the data in Fig. 7. Therefore, a choice has to be made, for example the *smallest* measured dynamic proof stress or some value below this one. According to Fig. 7, the value of $\sigma_y = 25 \text{ ksi}$ corresponds to an extrapolated proof stress at about $\dot{\epsilon} \approx 10^{-5} \text{ s}^{-1}$.

In the following the same choice is made, i.e.

$$\begin{aligned} \sigma_y &= \frac{1}{2} \sigma^{**} = \frac{1}{2} 344.74 \text{ MPa} = 172.34 \text{ MPa} = 25 \cdot 10^3 \text{ psi} \\ A_y &= \dot{\epsilon}^{**} = 10^2 \text{ s}^{-1}. \end{aligned} \quad (3.63)$$

Then the exponent "n" is determined by a least square fit to the room temperature data of Fig. 7 in the range $10^{-5} < \dot{\epsilon} \leq 10^2$ as follows

$$\sum_{i=1}^6 \left[\ln \left(\frac{\sigma_i - \sigma_y}{\sigma_y} \right) - \frac{1}{n} \ln \left(\frac{\dot{\epsilon}_i}{A_y} \right) \right]^2 = \text{Min}$$

which yields

$$\frac{1}{n} = \frac{\sum_{i=1}^6 \ln \left(\frac{\sigma_i - \sigma_y}{\sigma_y} \right) \ln \left(\frac{\dot{\varepsilon}_i}{A_y} \right)}{\sum_{i=1}^6 \left[\ln \left(\frac{\dot{\varepsilon}_i}{A_y} \right) \right]^2} \quad (3.64)$$

where $(\dot{\varepsilon}_i, \sigma_i)$ are the measured data pairs. One obtains

$$n = 8.1177 . \quad (3.65)$$

The measured yield stresses and the fit are compared in Fig. 13. Note the difference of the exponents. This is partly due to the fact that in equ. (3.64) the data base is somewhat larger. This concludes the parameter identification.

If the small-scale model and the full-scale prototype are made from the same material and the impact velocities are the same

$$v_p = v_m = v, \quad (3.66)$$

then the kinetic energies scale according to

$$\frac{\left(E_{kin} \right)_p}{\left(E_{kin} \right)_m} = \left(\frac{v_p}{v_m} \right) = \lambda^3 . \quad (3.67)$$

For reasons of simplicity it is assumed that the flow stresses in the struts are constant or can be represented by some average value $\bar{\sigma}_p$ and $\bar{\sigma}_m$, respectively. Then the plastic work in the struts are

$$W_p = (\bar{\sigma} \varepsilon F)_p, \quad W_m = (\bar{\sigma} \varepsilon F)_m \quad (3.68)$$

where F is the cross section area of a strut. Assuming that the kinetic energy is completely dissipated by the plastic deformation, then

$$\left(E_{kin} \right)_p = W_p, \quad \left(E_{kin} \right)_m = W_m . \quad (3.69)$$

Thus,

$$\bar{\sigma}_m \varepsilon_m = \bar{\sigma}_p \varepsilon_p \quad (3.70)$$

i.e., the plastic work per unit volume are the same in the prototype and model. From (3.70) one gets

$$\frac{\varepsilon_m}{\varepsilon_p} = \frac{\bar{\sigma}_p}{\bar{\sigma}_m} . \quad (3.71)$$

The initial strain rates in the struts are

$$\left(\dot{\varepsilon}_o \right)_p = \frac{v}{l_p} , \quad \left(\dot{\varepsilon}_o \right)_m = \frac{v}{l_m} \quad (3.72)$$

and therefore

$$\left(\dot{\varepsilon}_o \right)_m = \lambda \left(\dot{\varepsilon}_o \right)_p ; \quad (3.73)$$

with $\lambda > 1$ the initial strain rate in the model is λ -times larger than in the prototype. Therefore, the initial flow stress in the model is larger than in the prototype. With

$$\frac{\varepsilon_m}{\varepsilon_p} = \frac{\bar{\sigma}_p}{\bar{\sigma}_m} < 1 \quad (3.74)$$

the final strain in the model is underestimated; this relative underestimation is inversely proportional to the relative increase in the average flow stress in the small-scale model.

In the following an estimation of the flow stress ratio $\bar{\sigma}_p/\bar{\sigma}_m$ is given. Initially the strain rate is

$$\dot{\varepsilon}_o = \frac{v}{l} .$$

After the first contact of the mass and the strut the velocity and thus the strain rate continuously decreases until the mass has come to a halt. Thus the strain rate varies in the interval

$$0 \leq \dot{\varepsilon} \leq \dot{\varepsilon}_o . \quad (3.75)$$

Accordingly, the flow stress σ is bounded by

$$\sigma_y \leq \sigma \leq \sigma_y \left(1 + \left(\frac{\dot{\varepsilon}_o}{A_y} \right)^{1/n} \right).$$

Using the lower bound as an estimate for $\bar{\sigma}$, one gets

$$\left(\frac{\varepsilon_m}{\varepsilon_p} \right)' = \frac{\bar{\sigma}_p}{\bar{\sigma}_m} = \frac{\sigma_y}{\sigma_y} = 1.$$

The upper bound yields

$$\left(\frac{\varepsilon_m}{\varepsilon_p} \right)'' = \frac{\sigma_y \left(1 + \left(\frac{\dot{\varepsilon}_{op}}{A_y} \right)^{1/n} \right)}{\sigma_y \left(1 + \left(\frac{\dot{\varepsilon}_{om}}{A_y} \right)^{1/n} \right)}; \quad (3.76)$$

with (3.73) one obtains

$$\left(\frac{\varepsilon_m}{\varepsilon_p} \right)'' = \frac{1 + \Delta''_{\sigma p}}{1 + \Delta''_{\sigma p} \lambda^{1/n}} \quad (3.77)$$

where

$$\Delta''_{\sigma p} := \left(\frac{\dot{\varepsilon}_{op}}{A_y} \right)^{1/n}, \quad \dot{\varepsilon}_{op} = \frac{v}{l_p}. \quad (3.78)$$

Consequently, the use of the lower bound amounts to ignoring the viscous effect such that similarity is obtained. The use of the upper bounds yields a dependence of $\varepsilon_m/\varepsilon_p$ on the geometric scale factor.

With $\lambda > 1$, formally equ. (3.77) may be simplified:

- (1) If the initial dynamic yield stress is very large compared to the static yield stress σ_y for the prototype, i.e. $\Delta''_{\sigma p} \gg 1$, then

$$\left(\frac{\varepsilon_m}{\varepsilon_p} \right)'' = \frac{1}{\lambda^{1/n}}.$$

- (2) If this is true only for the model, i.e. $\Delta''_{\sigma p} \lambda^{1/n} \gg 1$ only, then

$$\left(\frac{\varepsilon_m}{\varepsilon_p} \right)'' = \underbrace{\left(\frac{1 + \Delta''_{\sigma p}}{\Delta''_{\sigma p}} \right)}_{> 1} \frac{1}{\lambda^{1/n}}.$$

However, it appears that these simplified situations are difficult to obtain for real materials.

An improved estimation can be derived as follows. The equation of motion for the point mass is

$$\rho V \ddot{x} = -\sigma F. \quad (3.79)$$

With

$$\frac{u}{l} = \varepsilon \quad (3.80)$$

and (3.59) equ. (3.79) reads

$$\ddot{\varepsilon} = \frac{d\dot{\varepsilon}}{dt} = -\frac{1}{\rho l V} \frac{F}{\sigma_y} \left(1 + \left(\frac{\dot{\varepsilon}}{A_y} \right)^{1/n} \right). \quad (3.81)$$

Separation of variables yield as a first integral

$$\int_{\dot{\varepsilon}_0}^{\dot{\varepsilon}} \frac{d\dot{\varepsilon}}{\left[1 + \left(\frac{\dot{\varepsilon}}{A_y} \right)^{1/n} \right]} = -\frac{1}{\rho l V} \frac{F}{\sigma_y} t. \quad (3.82)$$

Unfortunately a closed form solution for the left hand side is not available. Therefore, it is reasonable to try an approximate solution of (3.81) by using an average value $\bar{\sigma}'''$ for the flow stress σ on the r.h.s. of (3.79) in the strain rate interval (3.75). Thus

$$\begin{aligned}\bar{\sigma}''' &= \frac{\sigma_y}{\dot{\epsilon}_o} \int_0^{\dot{\epsilon}_o} \left(1 + \left(\frac{\dot{\epsilon}}{A_y} \right)^{1/n} \right) d\dot{\epsilon} \\ &= \frac{\sigma_y}{\dot{\epsilon}_o} \left\{ \dot{\epsilon}_o + \frac{1}{A_y^{1/n}} \dot{\epsilon}_o^{\frac{1}{n}+1} \frac{n}{n+1} \right\} \\ &= \sigma_y \left\{ 1 + \left(\frac{\dot{\epsilon}_o}{A_y} \right)^{1/n} \frac{n}{n+1} \right\}.\end{aligned}\tag{3.83}$$

With this results integration of (3.79) yields

$$\left(\frac{\epsilon_m}{\epsilon_p} \right)''' = \frac{1 + \Delta_{\sigma p}'''}{1 + \Delta_{\sigma p}''' \lambda^{1/n}}\tag{3.84}$$

where

$$\Delta_{\sigma p}''' = \left(\frac{\dot{\epsilon}_{op}}{A_y} \right)^{1/n} \frac{n}{n+1} = \Delta_{\sigma p}'' \frac{n}{n+1}, \quad \dot{\epsilon}_o = \frac{v}{l_p}.\tag{3.85}$$

Clearly

$$0 < \Delta_{\sigma p}''' < \Delta_{\sigma p}''.\tag{3.86}$$

Note that for large values of the exponent n the factor $(n/(1+n))$ is close to 1. Thus

$$\Delta_{\sigma p}''' \approx \Delta_{\sigma p}'', \quad n \gg 1\tag{3.87}$$

and the upper bound estimate for $\bar{\sigma}$ is sufficiently accurate.

These results will be illustrated by some numerical data for the stainless steel model described above. From (3.85) it is evident that Δ'''_{op} depends on the initial strain rate in the prototype strut. For two initial strain rates $\dot{\epsilon}_{op}$ and different scale factors λ the corresponding ratios $(\epsilon_m/\epsilon_p)'''$ and Δ'''_{op} are listed in Tab. 4.

$\dot{\epsilon}_{op} (s^{-1})$	$\Delta'''_{op} (-)$	$(\epsilon_m/\epsilon_p)'''$		
		$\lambda = 2$	10	50
10 ⁻¹	0.4095	0.9748	0.913	0.8475
10 ²	0.890	0.9559	0.866	0.774

Tab. 4: Size Effect under Impact Conditions for Stainless Steel AISI 304 at Room Temperature

It is seen that the underestimation in the permanent strain of the model is always less than 14 % for scale factors $\lambda \leq 10$ and $\dot{\epsilon}_{op} \leq 10^2$.

3.2.4.2 Varying Viscous Stress

One should remember that the simple formular (3.84) is based on the assumption that the deformation is approximately uniform in the structure and a constant average flow stress is representative. For the above example the dynamic yield stress varies in the prototype by a factor of 2 between the "dynamic" value $\sim 347 \text{ N/mm}^2$ at an initial rate of $\dot{\epsilon}_{op} = 10^2 \text{ s}^{-1}$ and the "static" value $\sim 172 \text{ N/mm}^2$; this is a considerable margin and it is not clear whether an accountance for this decrease of the flow stress during the deformation, which is a kind of "viscous softening", would affect the ratio $(\epsilon_m/\epsilon_p)'''$.

Some orientation may be obtained from a numerical study on penetration and perforation dynamics. Anderson, Mullin and Kuhlmann [32] performed a computational study to quantify the effects of strain rate on replica-model experiments of penetration and perforation. The impact of a tungsten-alloy long rod projectile into an armor steel target at 1.5 km s^{-1} was investigated. The target considered was 4340 steel and its constitutive response was represented by the Johnson-Cook model [33]:

$$\sigma_{\text{eq}} = 792 \left[1 + 0.644 \varepsilon_{\text{eq}}^{0.26} \right] \left[1 + 0.014 \ln \dot{\varepsilon}_{\text{eq}}^* \right] \left[1 - T^{* 1.03} \right];$$

$$\dot{\varepsilon}_{\text{eq}}^* \geq 1$$

σ_{eq} : v. Mises effective flow stress (MPa)

ε_{eq} : equivalent plastic strain

$$\dot{\varepsilon}_{\text{eq}}^* = \dot{\varepsilon}_{\text{eq}} / \dot{\varepsilon}_0, \quad \dot{\varepsilon}_0 = 1 \text{ s}^{-1}$$

T^* : homologous temperature .

Fig 14 shows the stress-strain response under isothermal and adiabatic conditions (thermal softening).

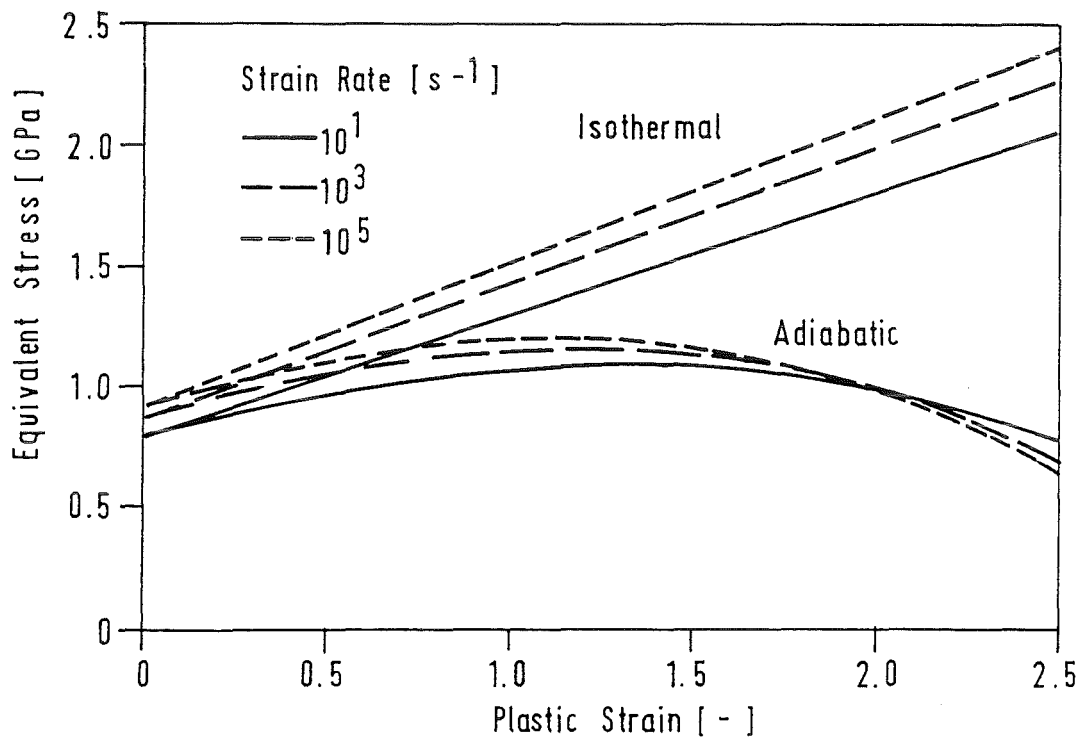


Fig. 14: Stress-Strain Diagram for 4340 Steel According to the Johnson-Cook Model for Different Strain Rates and Under Isothermal and Adiabatic Conditions, from [32]

The constitutive behavior of the tungsten alloy is described by

$$\sigma_{\text{eq}} = 1350 \left[1 + 0.06 \ln \dot{\epsilon}_{\text{eq}}^* \right].$$

The strain rate sensitivity of the target material for isothermal conditions is moderate: An increase of three orders of magnitude from $\dot{\epsilon}_{\text{eq}} = 1 \text{ s}^{-1}$ to 10^3 increases the flow stress by about 10 %. The sensitivity of the rod material is more pronounced: The increase in flow stress is about $0.06/0.014 = 4.25$ times larger, i.e. 43 %. In comparison the increase in flow stress for stainless steel AISI 304 is about 50 % over the same strain rate interval.

Anderson, Mullin and Kuhlmann did the analysis with a three-dimensional Eulerian wave propagation computer program; it includes, of course, a varying viscous stress and thermal softening. It was found that over a scale factor of 10, strain rate effects change the depth of penetration, for semi-infinite targets, and the residual velocity and length of the projectile, for finite thickness targets, by about 5 % only. Such a small effect is likely not separable from experimental scatter.

A more definite conclusion can be obtained by calculating some examples. If equation (3.81) or (3.82) were integrable analytically, the influence of the decrease of the viscous stress could easily be estimated. But a closed form integral of the left hand side of (3.82) does not exist. Therefore, modified rate models are considered. Instead of (3.59) the relation

$$\left. \begin{aligned} \sigma &= \bar{\sigma}_y \cdot \left(1 + \frac{\dot{\epsilon}}{\bar{A}_y} \right)^{1/\bar{n}}, \quad \bar{n} > 1 \\ \text{and the linear relation} \\ \sigma &= \bar{\sigma}_y \cdot \left(1 + \frac{\dot{\epsilon}}{\bar{A}_y} \right) \end{aligned} \right\} \quad (3.88)$$

are used. Then the appropriately changed left hand side of (3.82) yields

Nonlinear model:

$$\int_{\dot{\varepsilon}_o}^{\dot{\varepsilon}} \frac{d\gamma}{\left(1 + \frac{\gamma}{\bar{A}_y}\right)^{1/\bar{n}}} = \frac{\bar{A}_y}{1 - \frac{1}{\bar{n}}} \left[\left(1 + \frac{\dot{\varepsilon}}{\bar{A}_y}\right)^{\frac{\bar{n}-1}{\bar{n}}} - \left(1 + \frac{\dot{\varepsilon}_o}{\bar{A}_y}\right)^{\frac{\bar{n}-1}{\bar{n}}} \right]$$

Linear model:

$$\int_{\dot{\varepsilon}_o}^{\dot{\varepsilon}} \frac{d\gamma}{\left(1 + \frac{\gamma}{\bar{A}_y}\right)} = \bar{A}_y \ln \left(\frac{1 + \frac{\dot{\varepsilon}}{\bar{A}_y}}{1 + \frac{\dot{\varepsilon}_o}{\bar{A}_y}} \right)$$

(3.89)

Equ. (3.89) combined with the r.h.s. of (3.82) gives

Nonlinear model:

$$\dot{\varepsilon}(t) = -\bar{A}_y + \left[\left(\dot{\varepsilon}_o + \bar{A}_y\right)^{\frac{\bar{n}-1}{\bar{n}}} - \frac{1}{\bar{A}_y} \frac{1}{\rho l V} \frac{F}{\bar{\sigma}_y} \left(\frac{\bar{n}-1}{\bar{n}}\right) t \right]^{\frac{\bar{n}}{\bar{n}-1}}$$

Linear model:

$$\dot{\varepsilon}(t) = \bar{A}_y \left\{ \left(1 + \frac{\dot{\varepsilon}_o}{\bar{A}_y}\right) e^{-\frac{1}{\bar{A}_y} \frac{1}{\rho l V} \frac{F}{\bar{\sigma}_y} t} - 1 \right\}$$

(3.90)

The impacting mass comes to a halt when $\dot{\varepsilon} = 0$; thus

Nonlinear model:

$$t_f = \tilde{A}_y \rho l \frac{V}{F} \frac{1}{\tilde{\sigma}_y} \frac{\tilde{n}}{\tilde{n}-1} \left[\left(\dot{\varepsilon}_o + \tilde{A}_y \right)^{\frac{\tilde{n}}{\tilde{n}-1}} - \tilde{A}_y^{\frac{\tilde{n}}{\tilde{n}-1}} \right]$$

Linear model:

$$t_f = \tilde{A}_y \rho l \frac{V}{F} \frac{1}{\tilde{\sigma}_y} \ln \left(1 + \frac{\dot{\varepsilon}_o}{\tilde{A}_y} \right)$$

(3.91)

The integration of (3.90) yields with the initial condition

$$t = 0, \varepsilon = 0$$

Nonlinear model:

$$\varepsilon(t) = -\tilde{A}_y t - \tilde{A}_y \rho l \frac{V}{F} \frac{1}{\tilde{\sigma}_y} \frac{\tilde{n}}{(2\tilde{n}-1)}$$

$$\cdot \left\{ \left[\left(\dot{\varepsilon}_o + \tilde{A}_y \right)^{\frac{\tilde{n}-1}{\tilde{n}}} - \frac{1}{\tilde{A}_y} \frac{1}{\tilde{n}} \frac{1}{\rho l V} \frac{F}{\tilde{\sigma}_y} \left(\frac{\tilde{n}-1}{\tilde{n}} \right) t \right]^{\frac{2\tilde{n}-1}{\tilde{n}-1}} \right.$$

$$\left. - \left[\left(\dot{\varepsilon}_o + \tilde{A}_y \right)^{\frac{\tilde{n}-1}{\tilde{n}}} \right]^{\frac{2\tilde{n}-1}{\tilde{n}-1}} \right\}$$

(3.92)

Linear model:

$$\varepsilon(t) = \left(1 + \frac{\dot{\varepsilon}_o}{\tilde{A}_y} \right) \tilde{A}_y^2 \rho l \frac{V}{F} \frac{1}{\tilde{\sigma}_y} \left(1 - e^{-\frac{1}{\tilde{A}_y} \frac{1}{\rho l V} \frac{F}{\tilde{\sigma}_y} t} \right) - \tilde{A}_y t$$

Consequently, the final strains are

$$\left. \begin{aligned}
 & \text{Nonlinear model:} \\
 \varepsilon_f &= \tilde{A}_y^2 \rho l \frac{V}{F} \frac{1}{\tilde{\sigma}_y} \frac{\tilde{n}}{\tilde{n}-1} \cdot \\
 & \left\{ \frac{\tilde{n}-1}{2\tilde{n}-1} \left[\left(1 + \frac{\dot{\varepsilon}_o}{\tilde{A}_y} \right)^{\frac{2\tilde{n}-1}{\tilde{n}}} - 1 \right] - \left[\left(1 + \frac{\dot{\varepsilon}_o}{\tilde{A}_y} \right)^{\frac{2\tilde{n}-1}{\tilde{n}}} - 1 \right] \right\} \\
 & \text{Linear model:} \\
 \varepsilon_f &= \tilde{A}_y^2 \rho l \frac{V}{F} \frac{1}{\tilde{\sigma}_y} \left[\frac{\dot{\varepsilon}_o}{\tilde{A}_y} - \ln \left(1 + \frac{\dot{\varepsilon}_o}{\tilde{A}_y} \right) \right].
 \end{aligned} \right\} \quad (3.93)$$

With

$$\varepsilon_{om} = \frac{v}{l_m} = \frac{v}{l_p} \frac{l_p}{l_m} = \varepsilon_{op} \lambda \quad (3.94)$$

and

$$\frac{F_p}{F_m} \frac{V_m}{V_p} \frac{l_m}{l_p} = \frac{1}{\lambda^2}$$

the ratio of the final strains of the model and the prototype are

Nonlinear model:

$$\frac{\varepsilon_{fm}}{\varepsilon_{fp}} = \frac{1}{\lambda^2} \left\{ \frac{\bar{n}-1}{2\bar{n}-1} \left[\left(1 + \frac{\dot{\varepsilon}_{op}}{\bar{A}_y} \lambda \right)^{\frac{2\bar{n}-1}{\bar{n}} - 1} \right] \right.$$

$$\left. - \left[\left(1 + \frac{\dot{\varepsilon}_{op}}{\bar{A}_y} \lambda \right)^{\frac{\bar{n}-1}{\bar{n}} - 1} \right] \right\}.$$

$$\left\{ \frac{\bar{n}-1}{2\bar{n}-1} \left[\left(1 + \frac{\dot{\varepsilon}_{op}}{\bar{A}_y} \lambda \right)^{\frac{2\bar{n}-1}{\bar{n}} - 1} \right] \right.$$

$$\left. - \left[\left(1 + \frac{\dot{\varepsilon}_{op}}{\bar{A}_y} \lambda \right)^{\frac{\bar{n}-1}{\bar{n}} - 1} \right] \right\}^{-1}$$

(3.95)

Linear model:

$$\frac{\varepsilon_{fm}}{\varepsilon_{fp}} = \frac{1}{\lambda^2} \frac{\frac{\dot{\varepsilon}_{op}}{\bar{A}_y} \lambda - \ln \left(1 + \frac{\dot{\varepsilon}_{op}}{\bar{A}_y} \lambda \right)}{\frac{\dot{\varepsilon}_{op}}{\bar{A}_y} - \ln \left(1 + \frac{\dot{\varepsilon}_{op}}{\bar{A}_y} \right)}.$$

These results should be compared to the corresponding results obtained under the assumption of a constant viscous flow stress $\bar{\sigma}$. With (3.88) one gets

Nonlinear model:

$$\bar{\sigma} = \frac{1}{\dot{\epsilon}_o} \bar{\sigma}_y \int_0^{\dot{\epsilon}_o} \left(1 + \frac{\dot{\epsilon}}{\tilde{A}_y} \right)^{\frac{1}{\tilde{n}}} d\dot{\epsilon} = \frac{1}{\dot{\epsilon}_o} \bar{\sigma}_y \tilde{A}_y \frac{\tilde{n}}{\tilde{n}+1} \left[\left(1 + \frac{\dot{\epsilon}_o}{\tilde{A}_y} \right)^{\frac{\tilde{n}+1}{\tilde{n}}} - 1 \right]$$

Linear model:

$$\bar{\sigma} = \frac{1}{\dot{\epsilon}_o} \bar{\sigma}_y \int_0^{\dot{\epsilon}_o} \left(1 + \frac{\dot{\epsilon}}{\tilde{A}_y} \right) d\dot{\epsilon} = \bar{\sigma}_y \cdot \left[1 + \frac{\dot{\epsilon}_o}{2\tilde{A}_y} \right]$$

(3.96)

Observing (3.71) the strain ratios are

Nonlinear model:

$$\frac{\epsilon_m}{\epsilon_p} = \frac{\bar{\sigma}_p}{\bar{\sigma}_m} = \lambda \frac{\left[1 + \frac{\dot{\epsilon}_{op}}{\tilde{A}_y} \right]^{\frac{\tilde{n}+1}{\tilde{n}}} - 1}{\left[1 + \frac{\dot{\epsilon}_{op}}{\tilde{A}_y} \lambda \right]^{\frac{\tilde{n}+1}{\tilde{n}}} - 1}$$

Linear model:

$$\frac{\epsilon_m}{\epsilon_p} = \frac{\bar{\sigma}_p}{\bar{\sigma}_m} = \frac{1 + \frac{\dot{\epsilon}_o}{2\tilde{A}_y}}{1 + \frac{\dot{\epsilon}_o}{2\tilde{A}_y} \lambda}$$

(3.97)

For a quantitative comparison of the two ratios $\varepsilon_{fm}/\varepsilon_{fp}$ and $\varepsilon_m/\varepsilon_p$ it is necessary to choose the parameters $\tilde{\sigma}_y$, \tilde{A}_y and \tilde{n} of the two material models. Both models are defined in relation to the model equ. (3.59), i.e.,

$$\left. \begin{aligned} \sigma &= \sigma_y \left[1 + \left(\frac{\dot{\varepsilon}}{A_y} \right)^{\frac{1}{n}} \right] \\ \sigma_y &= 25 \text{ ksi}, \quad A_y = 100 \text{ s}^{-1}, \quad n = 8.1177. \end{aligned} \right\} \quad (3.98)$$

Equ. (3.98) represents a n th-order root parabola whose vertex is positioned on the ordinate at $\sigma/\sigma_y = 1$ (Fig. 15). The nonlinear relation (3.88)₁ may be written as

$$\frac{\sigma}{\tilde{\sigma}_y} = \left(1 + \frac{A_y}{\tilde{A}_y} \frac{\dot{\varepsilon}}{A_y} \right)^{\frac{1}{\tilde{n}}}. \quad (3.99)$$

It is an \tilde{n} th-order root parabola whose vertex is on the abscissa at $\dot{\varepsilon}/A_y = -\tilde{A}_y/A_y$ (Fig. 15).

This parabola is chosen such that it has two points in common with (3.98): The intersection on the ordinate such that

$$\tilde{\sigma}_y = \sigma_y \quad (3.100)$$

and the point

$$\left(\frac{\dot{\varepsilon}}{A_y} = 1, \frac{\sigma}{\sigma_y} = 2 \right).$$

Consequently

$$\frac{\sigma}{\sigma_y} = 2 = \left(1 + \frac{A_y}{\tilde{A}_y} \right)^{\frac{1}{\tilde{n}}}. \quad (3.101)$$

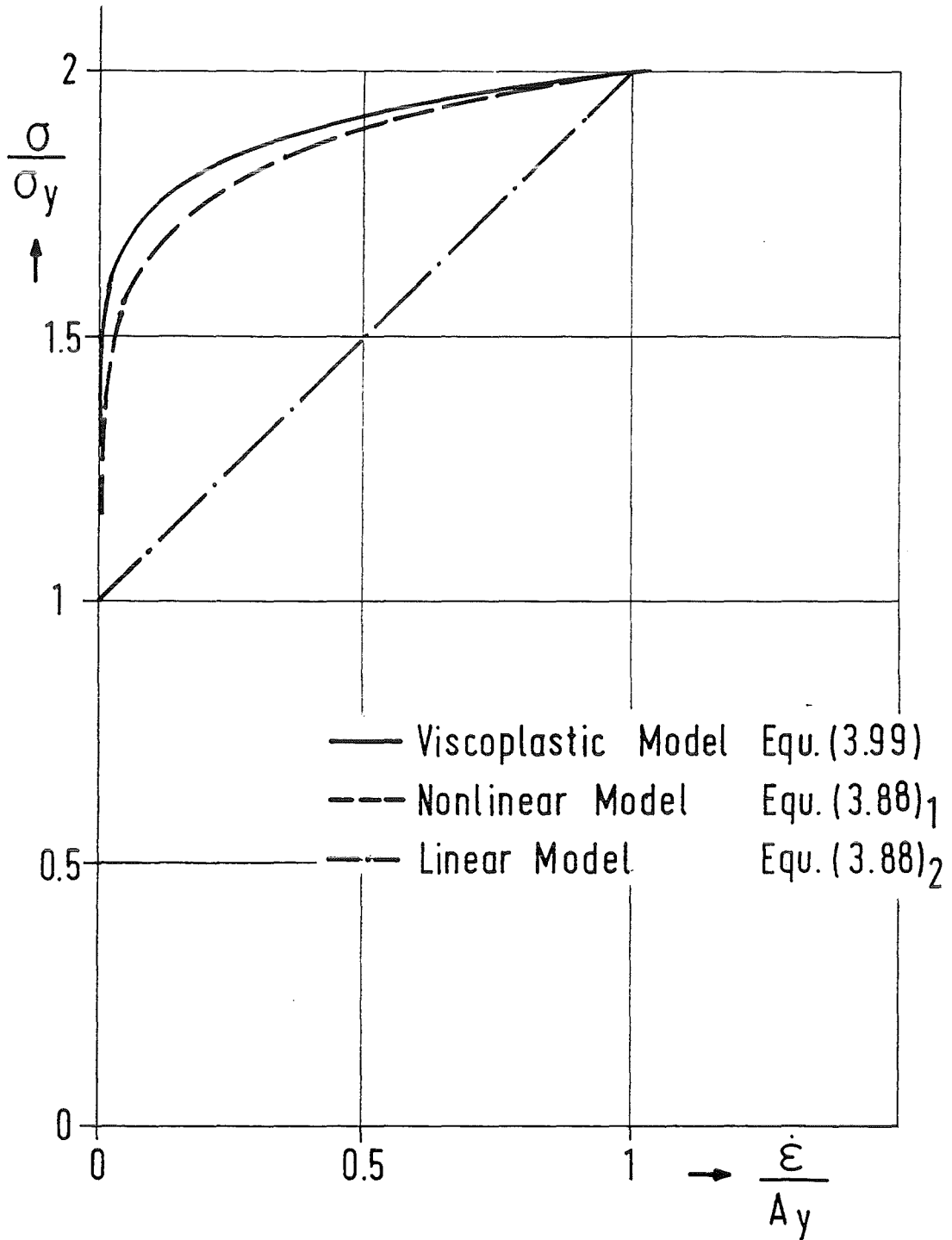


Fig. 15: Dynamic Yield Stress Versus Strain Rate for Three Different Constitutive Models

A third condition could be the least square fit of the two functions (3.98) and (3.99). However, this is a further non-linear condition. A more simpler but less accurate approach is as follows: It is required that the function (3.99) is just 5 % less than the value of (3.98) at $\dot{\epsilon}/A_y = 0.1$.*) Thus,

$$\left(1 + \frac{A_y}{\tilde{A}_y} 0.1 \right)^{\frac{1}{\tilde{n}}} = 0.95 \left(1 + (0.1)^{1/n} \right) = 1.665 . \quad (3.102)$$

From (3.101) and (3.102) one obtains

$$\frac{\ln \left(1 + \frac{A_y}{\tilde{A}_y} \right)}{\ln \left(1 + \frac{A_y}{\tilde{A}_y} 0.1 \right)} = \frac{\ln 2}{\ln 1.665\dots} = \beta = 1.359$$

and this yields

$$\left(1 + \frac{A_y}{\tilde{A}_y} 0.1 \right)^{\beta} = 1 + \frac{A_y}{\tilde{A}_y} . \quad (3.103)$$

A first estimate shows that $A_y/\tilde{A}_y \gg 1$. Therefore, (3.103) is approximated by

$$\left(\frac{A_y}{\tilde{A}_y} 0.1 \right)^{\beta} = \frac{A_y}{\tilde{A}_y} .$$

This yields as a first approximation

$$\frac{A_y}{\tilde{A}_y} = 0.1^{-\frac{\beta}{\beta-1}} = 6105.6 .$$

Further iterations yield

$$\frac{A_y}{\tilde{A}_y} = 6071 \quad (3.104)$$

* This choice was made to assure that (3.99) is a lower bound of (3.98) in the interval $0 < \dot{\epsilon}/A_y < 1$.

which is accurate up to the 4th digit. Thus

$$\left. \begin{aligned} \tilde{A}_y &= 1.647 \cdot 10^{-2} \\ \text{and} \\ \tilde{n} &= \frac{\ln \left(1 + \frac{A_y}{\tilde{A}_y} \right)}{\ln 2} = 12.568 . \end{aligned} \right\} \quad (3.105)$$

With these parameters the function (3.99) is shown in Fig. 15.

For the linear model the following choice is made

$$\tilde{\sigma}_y = \sigma_y , \quad \tilde{A}_y = A_y \quad (3.106)$$

and this relation is also plotted in Fig. 15. Thus, the nonlinear and linear model (3.88) are qualitatively rather different: The nonlinear model is similar to the original visco-plastic model (3.98) and over a large strain rate regime the flow stress varies only moderately; the linear model varies continuously.

The two approaches (3.95) and (3.97) are exercised for the selected values

$$\dot{\epsilon}_{op} = 10^2 \text{ s}^{-1} , \quad \lambda = 2, 10, 50$$

and the results are summarized in Tab. 5.

Tab. 5: Size Effect under Impact Conditions for a Nonlinear and Linear Constitutive Model with Different Assumptions about the Flow Stress

	$\frac{\epsilon_{fm}/\epsilon_{fp} \text{ (Varying Flow Stress)}}{\epsilon_m/\epsilon_p \text{ (Constant Flow Stress)}}$		
	$\lambda = 2$	$\lambda = 10$	$\lambda = 50$
Nonlinear Model	$\frac{0.94635}{0.94638}$	$\frac{0.83261}{0.83266}$	$\frac{0.73253}{0.73253}$
Linear Model	$\frac{0.734}{0.75}$	$\frac{0.2477}{0.25}$	$\frac{0.060}{0.058}$

For a very large scaling range $\lambda \leq 50$ it is seen the results of the approximate method yielding $\varepsilon_m/\varepsilon_p$ are quite sufficiently accurate not only for the nonlinear model but also for the linear model. This is understandable for the nonlinear model since the viscous stress varies moderately over one order of magnitude of strain rate.

It is also noted that the size effect of the nonlinear model is comparable to that of the original viscoplastic model (Tab. 4) and it is relatively moderate. However, the linear model shows a rather pronounced size effect.

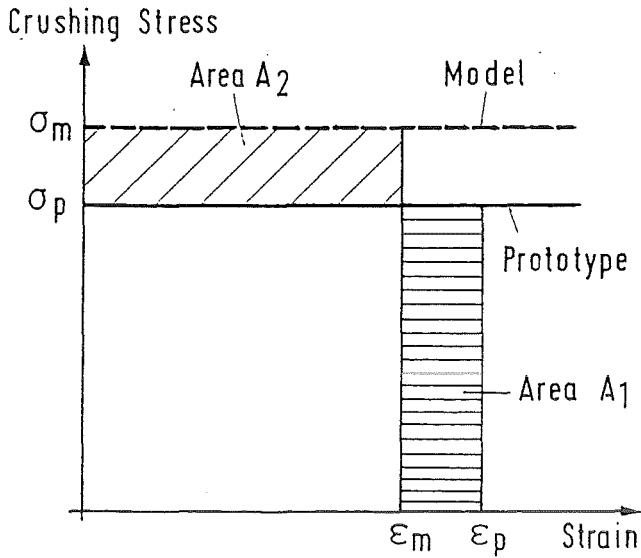
3.2.4.3 Enhancement of the Strain Rate Effect Due to Strain- or Deformation-Softening

In connection with interpretations of discrepancies between impact experiments of replica models and linear scaling theory [34] Calladine [35] pointed out that in structures with a falling load-deflection characteristic an increase in the flow stress in the small scale model due to a strain rate effect causes a proportionally much larger decrease in the final deformation than in structures with a constant load-deflection characteristic. A falling load-deflection characteristic is not so much a constitutive property but a property of the structure and is related to a crushing or buckling phenomenon. Qualitatively this effect may be explained as shown in Fig. 16. It is valid for the case the *specific* kinetic energy of the impacting mass is the same for both the model and the prototype and is completely dissipated by plastic work; also a strain rate sensitive material is used. Fig. 16a shows the simple case with a constant crushing force as treated in section 3.2.4.1 which yields

$$\frac{\varepsilon_m}{\varepsilon_p} = \frac{\bar{\sigma}_p}{\bar{\sigma}_m} \quad (3.107)$$

Fig. 16b demonstrates a falling crushing stress which is proportionally enhanced in the model due to the strain rate effect. The equality of corresponding plastic work areas implies

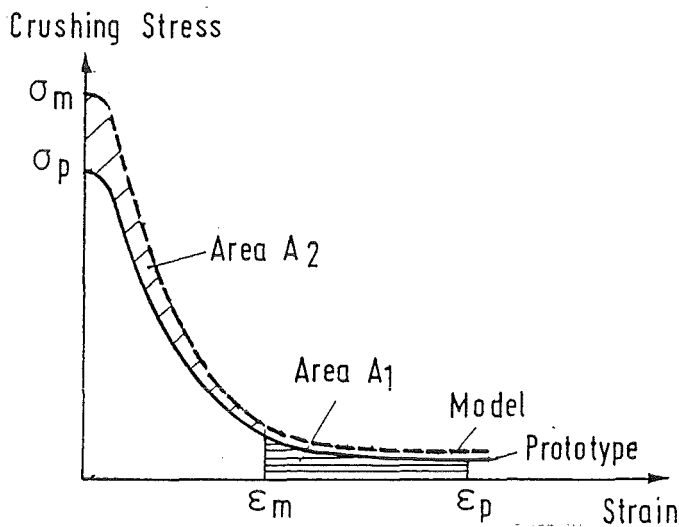
$$\frac{\varepsilon_m}{\varepsilon_p} < \frac{\sigma_p}{\sigma_m} = \text{const.} \quad (3.108)$$



a) Constant Crushing Stress

ϵ_m = final strain, model
 ϵ_p = final strain, prototype
 Area under graph \propto energy of plastic deformation per unit volume.
 Total energy absorbed per unit volume is the same for model and prototype, since impact energy is proportional to specimen volume

Hence $A_1 = A_2$ and $\frac{\epsilon_p}{\epsilon_m} = \frac{\sigma_m}{\sigma_p}$



b) Falling Crushing Stress

From the previous argument $A_1 = A_2$

Hence, by inspection $\frac{\epsilon_p}{\epsilon_m} > \frac{\sigma_m}{\sigma_p}$

Fig. 16: Enhancement of Size Effect in Viscoplasticity Due To Strain-Softening, from [35]

Calladine [35] has performed a simple analysis but this needs correction and supplementation.

In the following a visco-plastic model with a strain softening behavior is considered:

$$\sigma = \underbrace{\left(\sigma_0 + \sigma_1 e^{-\alpha \epsilon^r} \right)}_{\text{strain softening}} \underbrace{\left(1 + \left(\frac{\dot{\epsilon}}{A_y} \right)^{1/n} \right)}_{\text{strain rate sensitivity}} \quad (3.109)$$

and it is assumed that all parameters are scale invariant. Fig. 16b gives a qualitative impression of the stress-strain response at constant strain rate. It should be noted that this is a mathematical construct and the parameters σ_0 , σ_1 , α , and $r > 1$ are not related to physical data of a real structure. For the impact problem considered the strain rate influence is approximated as before by the mean value

$$\frac{1}{\dot{\epsilon}_0} \int_0^{\dot{\epsilon}_0} \left(1 + \left(\frac{\dot{\epsilon}}{A_y} \right)^{1/n} \right) d\dot{\epsilon} = 1 + \left(\frac{\dot{\epsilon}_0}{A_y} \right)^{1/n} \frac{n}{n+1}$$

in the rate interval $0 \leq \dot{\epsilon} \leq \dot{\epsilon}_0$ where

$$\dot{\epsilon}_0 = \frac{v}{l}$$

is the initial strain rate. Thus

$$\sigma \approx \sigma_0 \left(1 + \frac{\sigma_1}{\sigma_0} e^{-\alpha \epsilon^r} \right) \left(1 + \left(\frac{\dot{\epsilon}_0}{A_y} \right)^{1/n} \frac{n}{n+1} \right). \quad (3.110)$$

With this simplification the stress work is

$$\int_0^\epsilon \sigma d\epsilon = \sigma_0 \left(1 + \left(\frac{\dot{\epsilon}_0}{A_y} \right)^{1/n} \frac{n}{n+1} \right) \int_0^\epsilon \left(1 + \frac{\sigma_1}{\sigma_0} e^{-\alpha \epsilon^r} \right) d\epsilon. \quad (3.111)$$

Substituting

$$\epsilon^* = \alpha^{1/r} \epsilon \quad (3.112)$$

the last integral in (3.111) is

$$\int_0^{\varepsilon} \left(1 + \frac{\sigma_1}{\sigma_0} e^{-\alpha \varepsilon^r} \right) d\varepsilon = \frac{1}{\alpha^{1/r}} \left[\varepsilon^* + \frac{\sigma_1}{\sigma_0} \int_0^{\varepsilon^*} e^{-\varepsilon^{*r}} d\varepsilon^* \right] \quad (3.113)$$

$$= \frac{1}{\alpha^{1/r}} \left[\varepsilon^* + \frac{\sigma_1}{\sigma_0} \frac{1}{r!} E_r (\varepsilon^*) \right].$$

Here E_r is defined by

$$E_r (x) = r! \int_0^x e^{-t^r} dt \quad (3.114)$$

and shown in Fig. 17. The function $E_r(x)$ is the error integral.

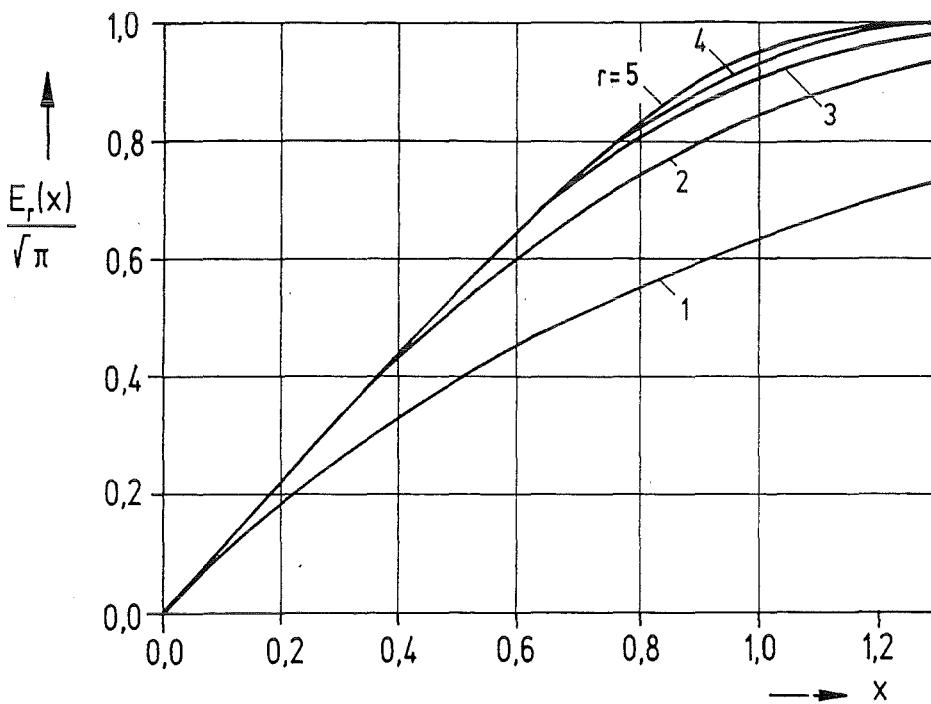


Fig. 17: Error Integral and Related Functions [36]

Consequently,

$$\int_0^\varepsilon \sigma d\varepsilon = \sigma_0 \left[1 + \left(\frac{\dot{\varepsilon}_0}{A_y} \right)^{1/n} \frac{n}{n+1} \right] \cdot \left[\varepsilon + \frac{1}{\alpha^{1/r}} \frac{\sigma_1}{\sigma_0} \frac{1}{r!} E_r (\varepsilon^*) \right]. \quad (3.115)$$

Following energetic arguments (section 3.2.4.1), the stress work for the small scale model equals that of the full scale prototype

$$\left(\int_0^\varepsilon \sigma d\varepsilon \right)_m = \left(\int_0^\varepsilon \sigma d\varepsilon \right)_p. \quad (3.116)$$

Thus

$$\frac{\varepsilon_m + \frac{1}{\alpha^{1/r}} \frac{\sigma_1}{\sigma_0} \frac{1}{r!} E_r (\varepsilon_m^*)}{\varepsilon_p + \frac{1}{\alpha^{1/r}} \frac{\sigma_1}{\sigma_0} \frac{1}{r!} E_r (\varepsilon_p^*)} = \frac{1 + \left(\frac{\dot{\varepsilon}_{0p}}{A_y} \right)^{1/n} \frac{n}{n+1}}{1 + \left(\frac{\dot{\varepsilon}_{0m}}{A_y} \right)^{1/n} \frac{n}{n+1}} = \left(\frac{\varepsilon_m}{\varepsilon_p} \right)'''; \quad (3.117)$$

here equ. (3.84) is observed. A further simplification is necessary to obtain a usable result. Assume that the residual stress σ_0 at large strains is small or vanishing, then (3.117) simplifies

$$\frac{E_r (\varepsilon_m^*)}{E_r (\varepsilon_p^*)} = \frac{1 + \left(\frac{\dot{\varepsilon}_{0p}}{A_y} \right)^{1/n} \frac{n}{n+1}}{1 + \left(\frac{\dot{\varepsilon}_{0m}}{A_y} \right)^{1/n} \frac{n}{n+1}} < 1. \quad (3.118)$$

For small values of

$$\varepsilon_p^* = \frac{1}{\alpha^{1/r}} \varepsilon_p$$

the function E_r is approximately linear and therefore

$$\frac{E_r (\varepsilon_m^*)}{E_r (\varepsilon_p^*)} \approx \frac{\varepsilon_m^*}{\varepsilon_p^*} = \frac{\varepsilon_m}{\varepsilon_p} = \left(\frac{\varepsilon_m}{\varepsilon_p} \right)'''. \quad (3.119)$$

Thus, the deformation softening has no effect. For large values of ε^* the function $E_r/\sqrt{\pi}$ may be approximated by a power function in some interval. For example, with $r=2$

$$\frac{E_2(\varepsilon^*)}{\sqrt{\pi}} \approx A \cdot (\varepsilon^*)^c \quad (3.120)$$

where

$$\begin{aligned} A = 0.8427, \quad c = 0.6951, \quad 0.5 \leq \varepsilon^* \leq 1.0 \\ A = 0.9427, \quad c = 0.3370, \quad 1.0 \leq \varepsilon^* \leq 1.5 \end{aligned} \quad (3.121)$$

These parameters have been found by fitting the power function to the values of $E_2/\sqrt{\pi}$ at the end-points of the intervals. The power function underestimates $E_2/\sqrt{\pi}$ in the middle of the intervals by less than 3 %. Then the l.h.s. of (3.118) is approximated by

$$\frac{E_2\left(\varepsilon_m^*\right)}{E_2\left(\varepsilon_p^*\right)} \approx \left(\frac{\varepsilon_m^*}{\varepsilon_p^*}\right)^c = \left(\frac{\varepsilon_m}{\varepsilon_p}\right)^c \quad (3.122)$$

Here, of course, it is assumed that both values ε_m^* and ε_p^* are within the same interval.

These approximations finally yield, observing (3.84),

$$\frac{\varepsilon_m}{\varepsilon_p} = \left(\frac{1 + \Delta_{\sigma p}'''}{1 + \Delta_{\sigma p}''' \lambda^{1/n}}\right)^{1/c} = \left(\frac{\varepsilon_m}{\varepsilon_p}\right)'''^{1/c} \quad (3.123)$$

Since $c < 1$, the deformation softening further decreases the final strain in the model beyond the decrease due to the strain rate sensitivity. For example, with $\lambda = 10$ and $\dot{\varepsilon}_{op} = 10^2 \text{ s}^{-1}$, one gets from Tab. 5

$$\left(\frac{\varepsilon_m}{\varepsilon_p}\right)'''' = \frac{1 + \Delta_{\sigma p}'''}{1 + \Delta_{\sigma p}''' \lambda^{1/n}} = 0.866$$

and thus

$$\frac{\varepsilon_m}{\varepsilon_p} = \begin{cases} 0.812 & \text{if } 0.5 \leq \alpha^{1/2} \varepsilon < 1.0 \\ 0.650 & \text{if } 1.0 \leq \alpha^{1/2} \varepsilon < 1.5 \end{cases} \quad (3.124)$$

where ε represents ε_m and ε_p . In the first case the effect of deformation softening is less than 10 % and in second it amounts about 25 %.

It should be realized that these sample calculations were done to illustrate the general qualitative trend; quantitatively they are not related to a precise mechanical model.

3.2.5 Scale Invariance of Material Data

A fundamental requirement for similarity experiments with replica models, i.e. small scale models made from - nominally - the "same material" as the large prototype, is the *scale invariance* of the basic material data and functions as assumed in the theory. The realization of this requirement has technological as well as physical limitations [37].

The technological size effect observed for material data obtained in small and large size specimens is due to different fabrications, e.g. casting, cold working or forging conditions, heat treatment, and mechanical treatment (turning, grinding). However, this effect can be limited or even eliminated by keeping treatments for the different size specimens the "same". Beyond that one should take care of the fact that the different size specimens are taken from the same position of the raw material to eliminate gross inhomogeneities.

In spite of such precautions size effects on material data have been found.

Faulhaber et al. [38] supposedly state that for *homogeneous states* of tensile and compressive stresses similarity laws are sufficiently accurate such that the yield stress and the ultimate stress are size invariant. This is demonstrated in Fig. 18 which shows, among others, the upper tensile yield stress of a plain carbon steel obtained by Morrison [39]; a scale factor of $1 \leq \lambda \leq 3.55$ is covered. In Fig. 20 the ultimate tensile stress for 7075-T6 aluminium is plotted as a function of specimen size with $1 \leq \lambda \leq 8.2$ and Fig. 21a presents the ultimate tensile strength of AISI H-11-steel which corresponds to 1.3343 (X38 Cr Mo V51) [40].

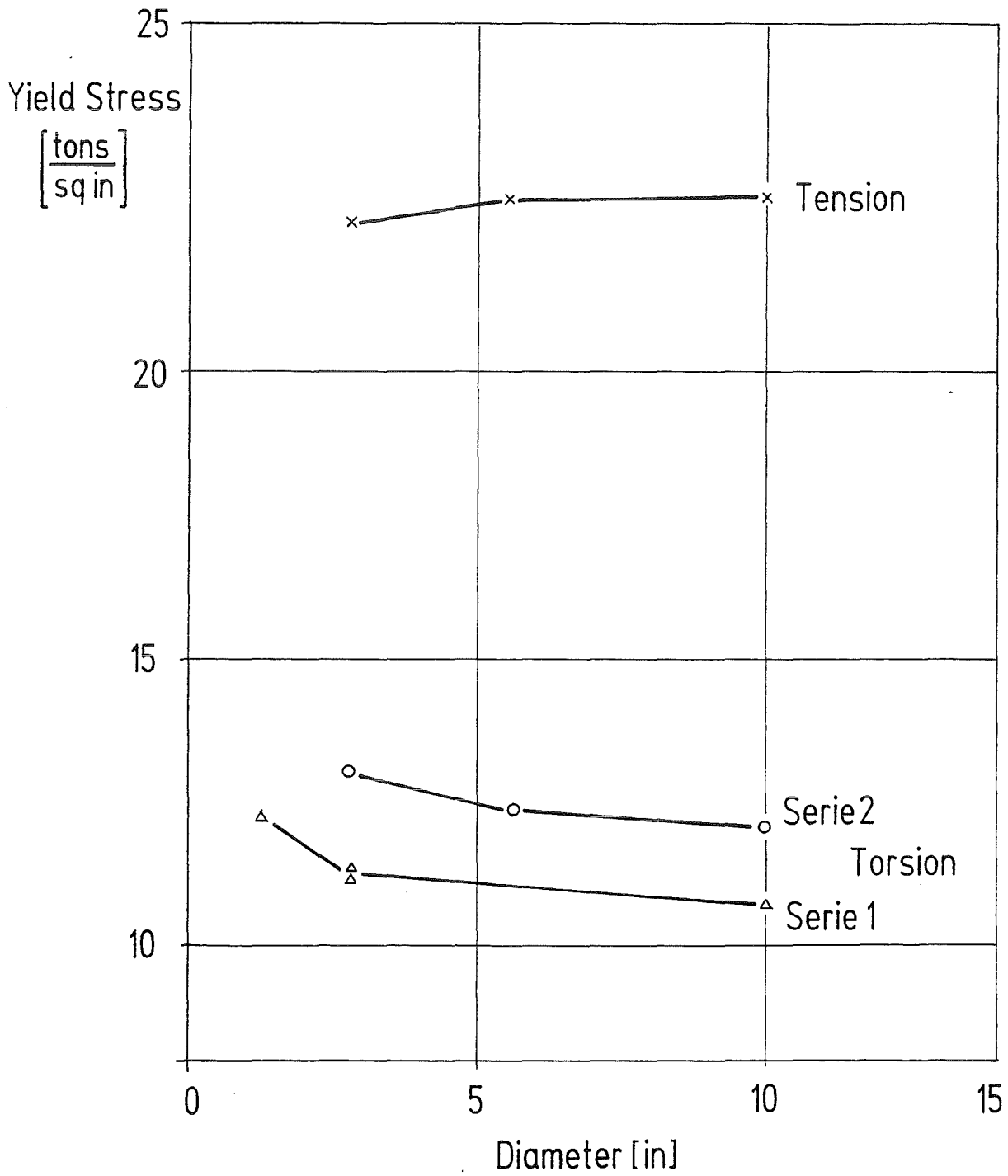


Fig. 18: Size Dependence of the Apparent Yield Stress of a Carbon Steel; from [39]

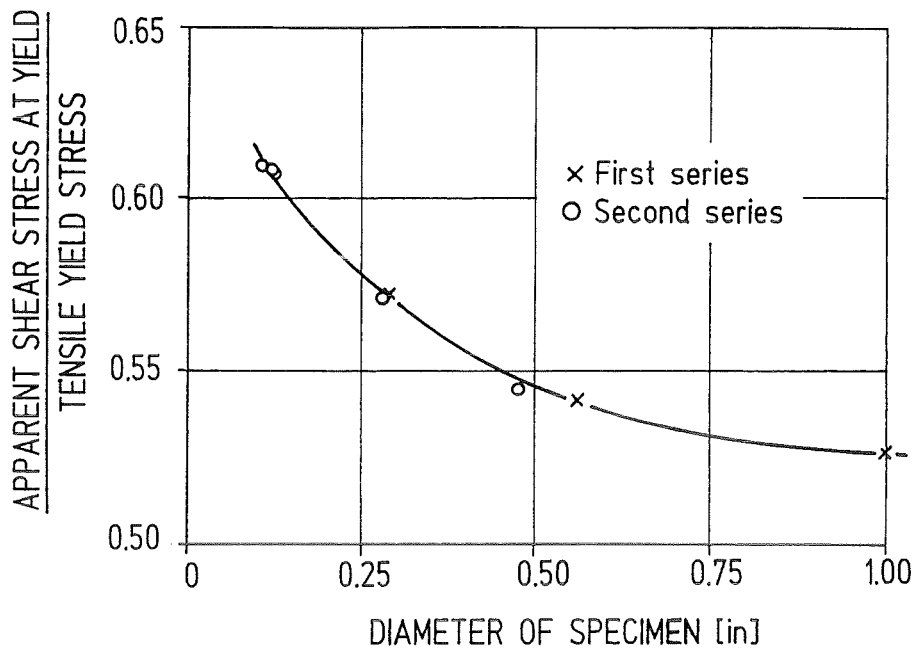


Fig. 19: Size Effect of the Apparent Yield Stress in Torsion, from [39]

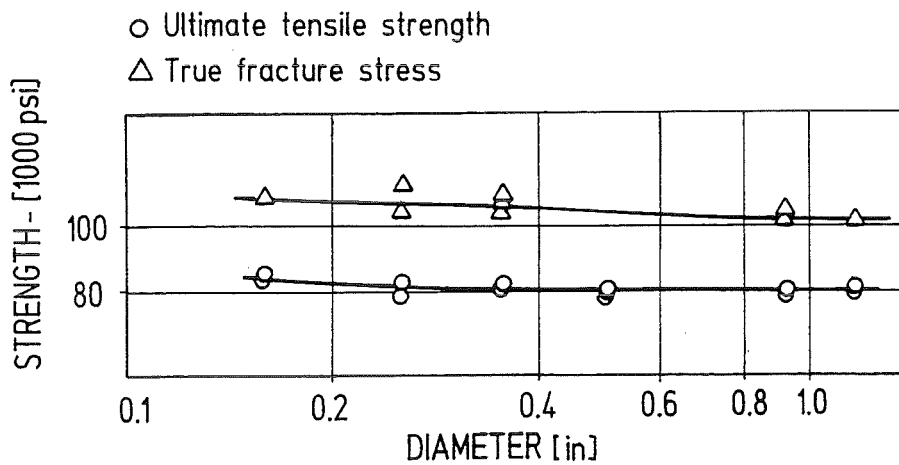


Fig. 20: Effect of Section Size on the Tensile Strength of 7075-T6 Aluminium; from [40]

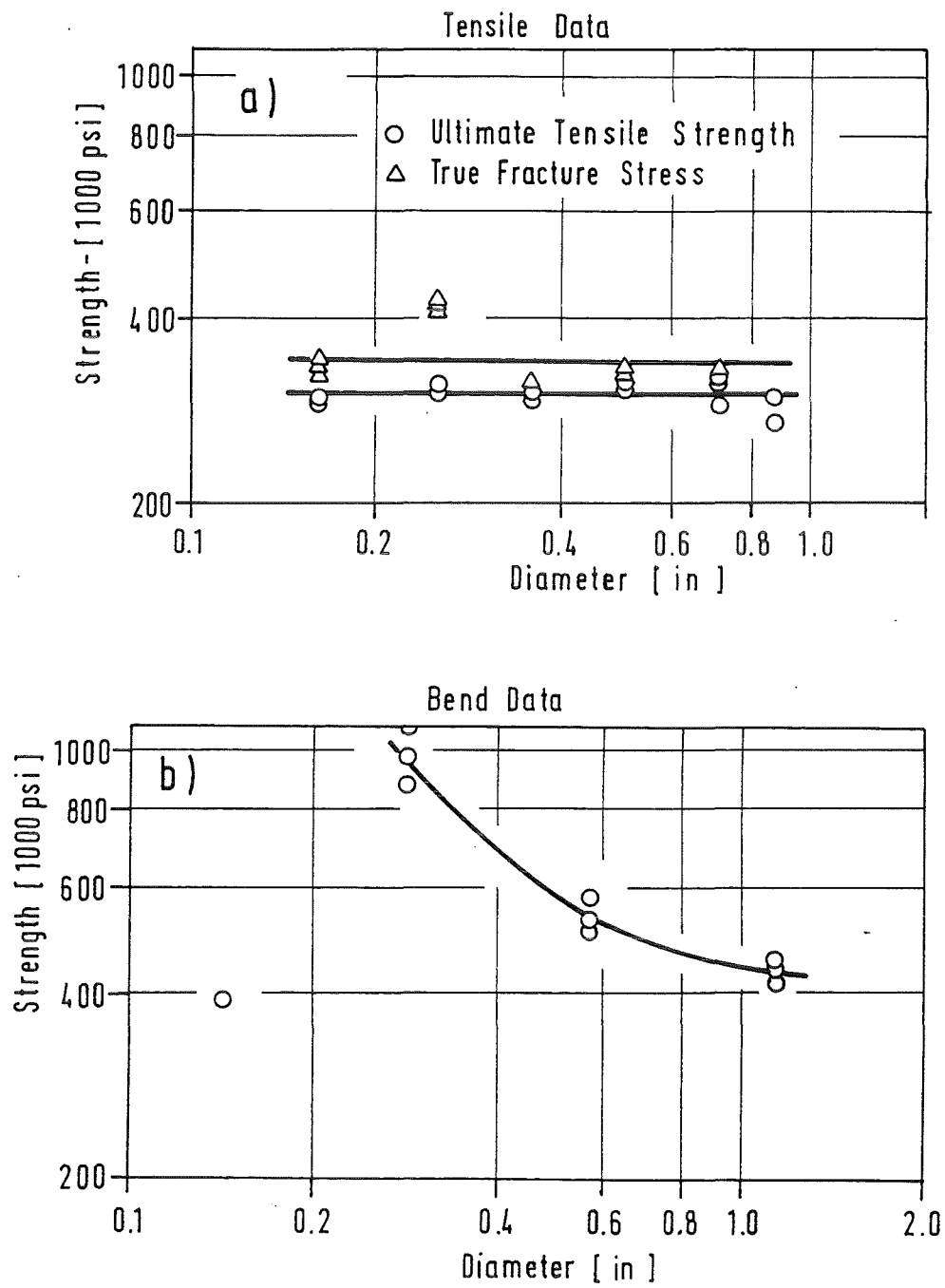


Fig. 21: Effect of Section Size on the Tensile and Bend Strength of H-11-Steel; from [40]

Thorton [41] performed tensile tests of annealed samples of a ground-to-thickness low carbon steel sheet and obtained values for the quasi-static lower yield stress, ultimate stress, and elongation (Tab. 6).

Tab. 6: Mechanical Properties of Low Carbon Steel Sheets (annealed 1 hr at 500 °C, air cooled), from [41]

Scale factor λ	Thickness mm	0.2 % Proof Stress MPa	Ultimate Stress MPa	% Elongation 2 in. (5.08 cm)
1	3.25	248	311	35
1.33	2.44	249	314	33
2	1.64	261	319	29
2.66	1.22	264	318	28
4	0.83	266	322	29

Over the range of scale factors $1 \leq \lambda \leq 4$ the lower yield stress increases moderately by about 7 % whereas the elongation reduces by 17 %.

Shearin, Ruark and Trimble [42] reported that true size effects in ordinary tensile tests of ductile engineering materials are so small that they are difficult to detect and still more difficult to measure. They found a small size effect in the maximum true stress and in the breaking stress of a nickel-chromium steel; however, errors were large enough to mask the effect and make their reality uncertain. However, an unmistakable size effect was found in the reduction of area.

If *inhomogeneous stress distributions* are present, for example such simple cases as pure bending or torsion, the situation is complex; of course inhomogeneous stress distributions are also generated by corners, notches or cracks but these are not considered here. Thum and Wunderlich [43] observed an increase in the yield stress in case of bending of about 40 - 60 % compared with the yield in tension. Also the height, width or length of the specimen had no sensible effect, results which may suggest that there is no size effect. However, the specimen had no geometric similarity. It was also found that the form of the cross section relative to the plane of bending has an important effect on the magnitude of the yield stress: The more material is concentrated around the neutral axes, the higher is the yield stress in bending.

Thum and Wunderlich proposed a qualitative explanation for this effect: Steel and probably also other metals yield in *finite thickness layers* if some layer has reached the yield stress found in a tensile test, then this layer gives suddenly way

to the loading. This formulation is still rather vague; in the later discussion an interpretation will be given which allows a quantitative analysis.

The results of Thum and Wunderlich, however, are subject to doubts since the specimens were not sufficiently homogeneous: It is stated in [43] that nearly all steels were segregated; therefore, the yield strength in the boundary layer was smaller than in the core region.

Morrison [39] has performed a series of careful tension, torsion and bending tests as well as combined tests on the (upper) yield of plain carbon steel with particular reference to the effect of size of the specimens. The tension tests (Fig. 18) were already mentioned above. The torsion (Fig. 18) and bending tests (Fig. 21b) yielded an increase in the apparent stress at yield with decreasing specimen size. Fig. 18 shows the results for two series of torsion tests differing in the heat treatment. In Fig. 19 these torsion test results are normalized with respect to the tensile yield stress and are combined. If the one inch-diameter specimen is the prototype, then these tests cover a scale factor up to $\lambda=8.67$ and the ratio of the apparent shear stress at yield is

$$\left(\frac{\tau_m}{\tau_p} \right)_{\lambda=8.67} = 1.155 \quad (3.125)$$

where the subscript "m" refers to the "model" and "p" to the "prototype".

For the the bending test (Fig. 22) there is no sudden change in the slope of the curves as the moment is increased; it is therefore impossible to tabulate a value of the stress at which yield occurred on the bases of these curves alone. But it is apparent that the shape of the curves are affected by the size of the specimen. These bending experiments cover a range of $1 \leq \lambda \leq 5.2$ and the maximum value increases by about 8 % when the size is decreased from the largest to the smallest specimen.

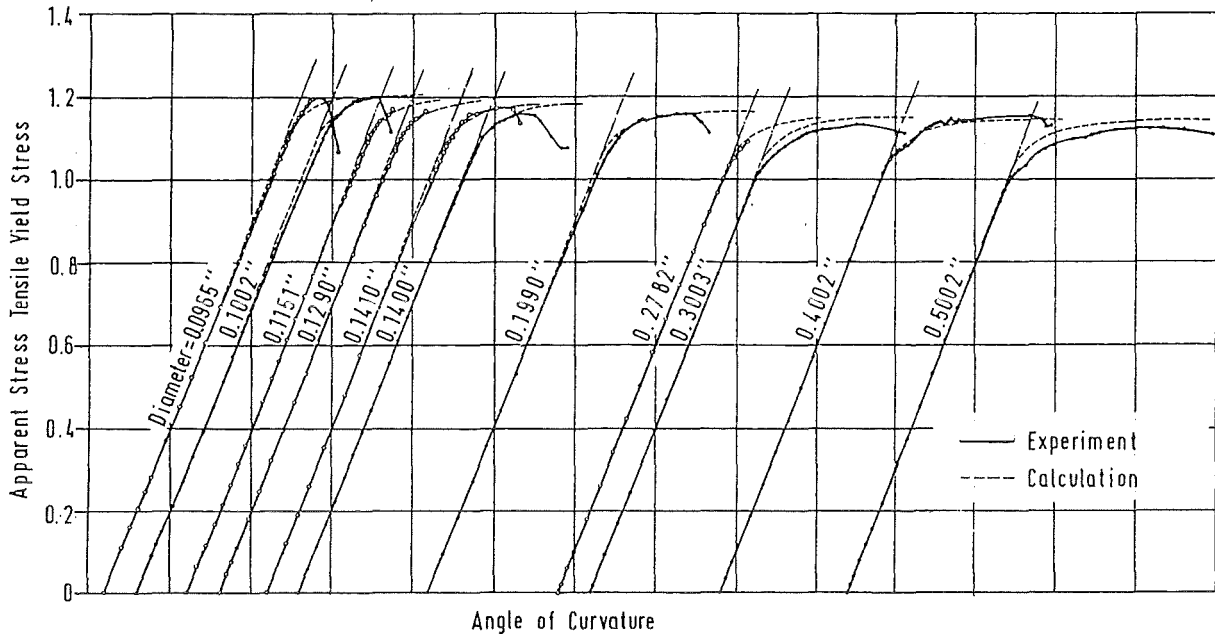


Fig. 22: Size Effect in Flexure: Moment-Angle Curves; from [39]

Morrison discussed the effect of inhomogeneous stress distribution in relation to the crystal structure. He stated that "yield cannot occur in an individual crystal surrounded by unyielding material but only in a number of crystals which occupy a sufficient thickness to permit of the complicated readjustment which must take place before movement can occur, it is unreasonable to expect to find yield before a stress equal to the yield stress in uniform tension is applied to a depth of this magnitude. It seems reasonable to suppose that the depth might be of a few crystal diameters." Morrison [39] proposed a model simulating the drop in yield stress (upper and lower yield stress) and which involves a single length parameter. Fitting this parameter to the experimental results, the dotted curves in Fig. 22 are obtained.

Weiss and Yukawa [40] have published strength data for bending specimens (Fig. 21 b) made from AISI H-11. Here again a size effect with the same trend is present and is very pronounced over a scale range of $1 \leq \lambda < 4.8$. Unfortunately, the precise meaning of the strength data is not given in [40] and also other details of the experiments are missing.

The present data for monotonous quasistatic loading support the opinion that the yield stress and ultimate stress for *homogeneous stress fields* are scale invari-

ant or only moderately depending on scale, provided technological variability is excluded and the specimens are taken from a very homogeneous material; also the specimen should not be too small so that they lose their polycrystalline character. Shearin et al. [42] state that $50 \div 100$ grains should be present across a diameter.

Whether the uniform elongation, the strain associated to the ultimate stress and indicating the initiation of necking, is also scale invariant, is presently not known to the author.

Further, there is experimental evidence that the *classical local yield criteria* - where local values of the stress etc. define the initiation of yielding - *are not valid for inhomogeneous stress field*; i.e., when a stress gradient is present (e.g. bending and torsion). Deviations of about 15 % in the yield have been found for a scale factor of $\lambda \approx 10$ [39]. Much larger deviations have also been observed [38, 40]. Clearly, this problem needs further attention.

A fairly general and qualitative explanation is as follows. A material, which is homogeneous from a macroscopic point of view, is structured on a microscopic level due to the grain structure, micro-inhomogenities and defects. Therefore, the material data obtained in a usual tensile test with nominally homogeneous state of stress represent *average values over some finite area or volume*.

If stresses in a structure do not change appreciably across spatial regimes, then it may suffice to compare a *local stress* value with the corresponding characteristic material value obtained in a tensile test. However, if large *stress gradients* are present due to bending or torsion in smooth structures or due to corners, notches and cracks with stress singularities, the comparison of a local stress value with characteristic *average* material data is not appropriate. Rather some averaging procedure or integral measures*) must be used [44 - 46]. It is also noted that the stress gradient, e.g. $\partial\sigma/\partial z$ in the case of bending of a beam, depends on the geometric scale factor λ if the "same materials" are used in the model and prototype:

$$\left(\frac{\partial\sigma}{\partial z} \right)_m = \lambda \left(\frac{\partial\sigma}{\partial z} \right)_p, \quad \sigma_p = \sigma_m, \quad z_p = \lambda z_m$$

*) Such measures were taken especially to cope with stress singularities [45, 46], e.g. the concept of "Mikrostützwirkung" (micro-supporting effect) of Neuber [46].

i.e. the stress gradient is λ -times larger in the small scale model than in the large scale prototype. Therefore, the microstructural variations have a more pronounced effect for smaller models. This implies a size effect.

If the yield condition should reflect scale dependence as observed in the experiments, then phenomenological approaches are conceivable to describe this size effect; for example:

- an *integral yield condition* which involves the stress (or strain) distribution in a finite region of the body
- or a *local condition* which involves not only the *stress (or strain)* but also *stress gradients (or strain gradients)*.

Such conditions automatically involve a length scale.

The second approach, e.g. the inclusion of first or higher-order spatial gradients of the plastic strain in the yield condition, was used by various authors (Fleck et al [48], Zbib [49] and Mühlhaus and Aifantis [50], Zbib and Aifantis [51, 52]) to explain or describe several observed plasticity phenomena which display a size effect such as the increase of hardening with a greater imposed strain gradient or the modeling of shear banding.

In the following the first approach is illustrated by a simple example for the case of pure bending and torsion. This choice is motivated by the suggestion of Thum and Wunderlich [43] as well as Morrison [39]. It is noted that similar approaches are used to characterize the size dependence of the fatigue limit [44, 47]; this is partly based on statistical concepts.

Pure Bending:

The following model describes the initiation of yielding in a finite thickness boundary region of a beam with rectangular cross section (Fig. 23). It is assumed that, considering a standard tensile test, a single value σ_0 defines the initiation of yielding*), i.e. the existence of an upper *and* lower yield stress is excluded. It is assumed that the average stress in a boundary layer of thickness d^* , section area $A^* = Bd^*$ and volume $V^* = A^*L$, where B is the width and L is the length of the beam, must attain the uniform tensile yield stress σ_0 to initiate "yielding in this

*) A precise operational definition of "yielding" is not given here; in the experiments different concepts are used.

layer". In addition it is necessary to make an assumption which of the three geometric quantities d^* , A^* and possibly V^* should be viewed as a *scale invariant material property*; this choice is postponed.

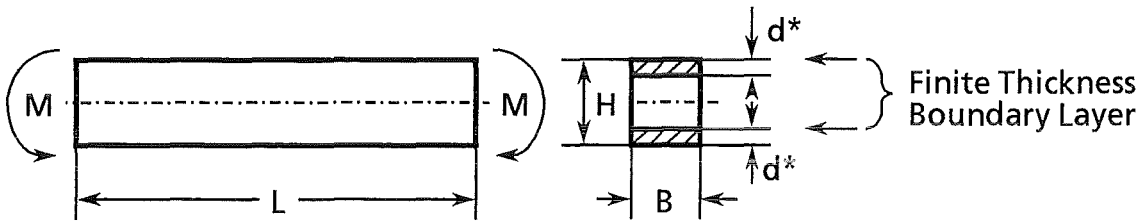


Fig. 23: Pure Bending of a Beam with a "Micro-Supporting Effect" in a Finite Thickness Boundary Layer

If H is the height of the cross section, then the integral yield condition is

$$\frac{1}{A^*} \int_{H/2-d^*}^{H/2} \sigma B dz = \frac{1}{d^*} \int_{H/2-d^*}^{H/2} \sigma dz = \sigma_o, \quad A^* = d^* B. \quad (3.126)$$

As long as the condition (3.126) is not satisfied the stress distribution is entirely elastic

$$\sigma(z) = \frac{M}{J} z, \quad \begin{array}{l} M \quad : \text{bending moment} \\ J = \frac{BH^3}{12} \quad : \text{moment of inertia} \end{array}$$

Integration of the left hand side of (3.126) yields

$$\frac{1}{d^*} \int_{H/2-d^*}^{H/2} \sigma dz = \frac{1}{d^*} \frac{M}{J} \left(\frac{H}{2} \right)^2 \frac{1}{2} \left[1 - \left(1 - \frac{d^*}{H/2} \right)^2 \right].$$

With

$$\sigma_{\max} = \frac{M H}{J 2},$$

which is the maximum elastic bending stress at $z=H/2$, one gets for the initiation of yielding

$$\sigma_{\max} = \sigma_o \frac{d^*}{H/2} \frac{2}{\left[1 - \left(1 - \frac{d^*}{H/2} \right)^2 \right]}; \quad (3.127)$$

of course, this is only valid if $d^* / (H/2) \leq 1$.

It is convenient to introduce the area (or volume) ratio

$$a^* = \frac{A^*}{BH/2} = \frac{d^*}{H/2} \quad (3.128)$$

where $BH/2$ is the cross section area in tension (or compression) and A^* is the yielding section in tension (or compression). Then (3.127) takes the form

$$\frac{\sigma_{\max}}{\sigma_o} = a^* \frac{2}{\left[1 - (1 - a^*)^2\right]} \quad (3.129)$$

For $a^* \rightarrow 0$ one derives (applying l'Hospitals rule)

$$\lim_{a^* \rightarrow 0} \frac{\sigma_{\max}}{\sigma_o} = 1 \quad (3.130)$$

and with $a^* \rightarrow 1$ one gets

$$\lim_{a^* \rightarrow 1} \frac{\sigma_{\max}}{\sigma_o} = 2. \quad (3.131)$$

Fig. 24 shows the apparent yield stress σ_{\max} in bending as a function of $1/a^* \geq 1$. This curve reflects the size dependence of the apparent yield stress in different ways, depending on the hypotheses used:

- (α) If the thickness d^* of the yielding layer is a *scale invariant material property*, which corresponds to the number of grains across the layer, then

$$\frac{1}{a^*} = \frac{H/2}{d^*}$$

and the abscissa in Fig. 24 is proportional to the size of the specimens with rectangular cross section (case A).

- (β) If the area A^* is a scale invariant material property, then $1/a^* = (BH/2) / A^*$ which is proportional to the square of the length scale. Especially, if the cross section is quadratic, one gets

$$\frac{1}{a^*} = \frac{H^2/2}{A^*}$$

- (γ) Provided $V^* = A^* \cdot L$ is a scale invariant material property, then

$$\frac{1}{a^*} = \frac{LBH/2}{V^*}$$

is proportional to the cube of the length scale. However, since there is no stress gradient along the length of the beam, this choice is not physically plausible.

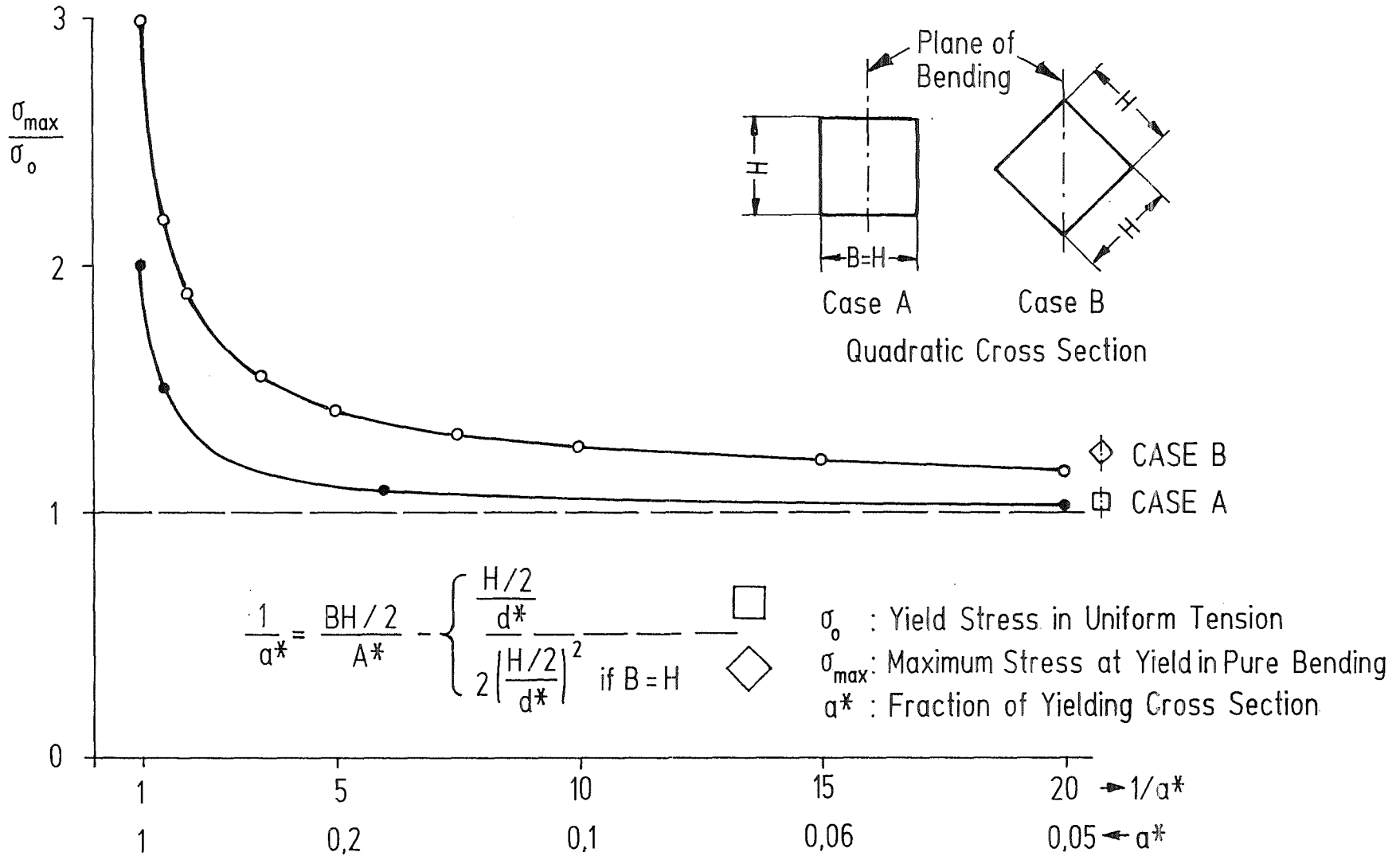


Fig. 24: Size Effect on the Yield Stress in Bending due to an Integral Yield Condition

In any case for $1/a^*$ close to 1, i.e. for "small" specimens, the increase of the apparent yield stress in bending above the uniform tension yields stress σ_0 is considerable. However, for $1/a^* > 5$ the size effect is less than 10 %.

For the purpose of illustration it is shown that the integral yield condition (3.127) can also be formulated in a *local form involving a stress gradient*. For the case of *pure bending* (case A) the bending stress distribution may be represented by

$$\sigma(z) = \sigma_{(z=H/2)} + \left(\frac{d\sigma}{dz} \right)_{z=H/2} (z - H/2) .$$

Inserting this in (3.126) and integration yields

$$\begin{aligned} \frac{1}{d^*} \int_{H/2-d^*}^{H/2} \left[\sigma_{(z=H/2)} - \left(\frac{d\sigma}{dz} \right)_{H/2} (z - H/2) \right] dz = \\ = \sigma_{\max} + \left(\frac{d\sigma}{dz} \right)_{H/2} \frac{H}{2} \frac{1}{2} \left[1 - \frac{d^*}{H/2} \right] . \end{aligned}$$

Thus, instead of (3.126) one has

$$\sigma + \left(\frac{d\sigma}{dz} \right) \frac{H}{2} f(a^*) \leq \sigma_0 , \quad f(a^*) = \frac{1}{2} (1 - a^*) \tag{3.132}$$

=====

where the underlined term represents the influence of the stress gradient on the yielding. Note that (3.132) is a derived condition and not an a priori postulate as (3.126).

One should recall the experimental results of Thum and Wunderlich [43]: The more material is concentrated around the neutral axes, the higher is the yield stress in bending. In the following this effect is illustrated for the integral yield condition (3.126). Instead of a rectangular cross section used above (Case A), a quadratic cross section is considered with two opposite corners in the plane of bending (Case B), Fig. 25.

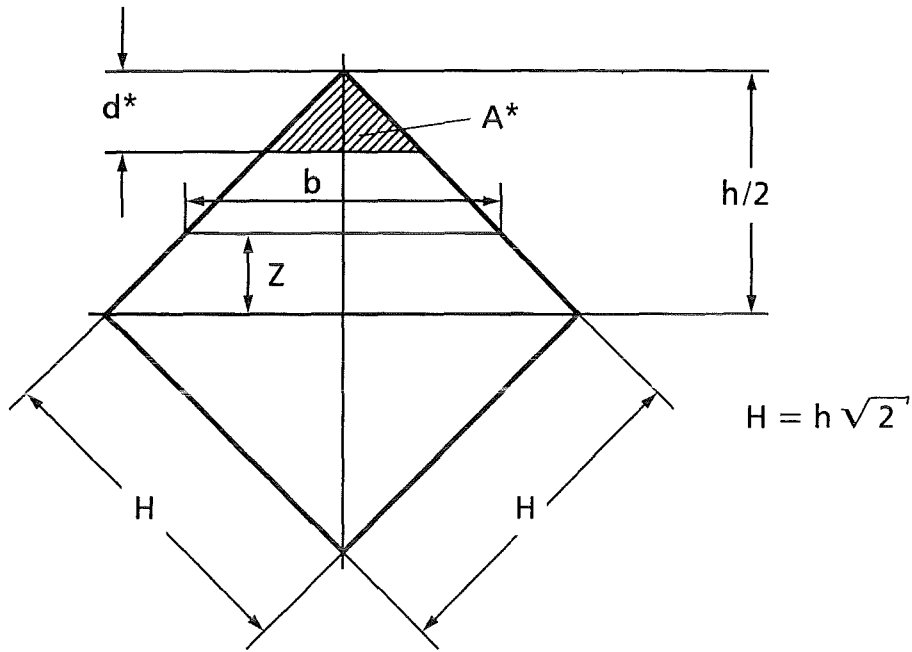


Fig. 25: Cross Section of Bend Specimen

The integral yield condition takes the form

$$\frac{1}{A^*} \int_{h/2-d^*}^{h/2} \sigma b(z) dz \leq \sigma_0 \quad (3.133)$$

with

$$A^* = d^{*2}, \quad b = h - 2z, \quad \sigma = \frac{M}{J} z \quad (3.134)$$

and integration yields

$$\frac{1}{A^*} \int_{h/2-d^*}^{h/2} \sigma b(z) dz = \frac{1}{A^*} \frac{M}{J} \left(\frac{h}{2} \right)^3 \left[\frac{1}{3} \left(1 - \frac{d^*}{h/2} \right)^2 + \frac{2}{3} \left(1 - \frac{d^*}{h/2} \right)^3 \right].$$

Since

$$\sigma_{\max} = \frac{M h}{J 2}$$

one finds

$$\sigma_{\max} = \sigma_0 \left(\frac{d^*}{h/2} \right)^2 \frac{3}{1 - 3 \left(1 - \frac{d^*}{h/2} \right)^2 + 2 \left(1 - \frac{d^*}{h/2} \right)^3}. \quad (3.135)$$

Introducing the yielding fraction of the cross section in tension (or compression)

$$a^* = \frac{A^*}{H^2/2} = \frac{1}{2} \left(\frac{d^*}{H/2} \right)^2 = \left(\frac{d^*}{h/2} \right)^2, \quad (3.136)$$

equ. (3.135) may be written as

$$\frac{\sigma_{\max}}{\sigma_0} = a^* \frac{3}{1 - 3 \left(1 - \sqrt{a^*} \right)^2 + 2 \left(1 - \sqrt{a^*} \right)^3}. \quad (3.137)$$

One obtains

$$\left. \begin{aligned} \lim_{a^* \rightarrow 0} \frac{\sigma_{\max}}{\sigma_0} &= 1 \\ \text{and} \\ \lim_{a^* \rightarrow 1} \frac{\sigma_{\max}}{\sigma_0} &= 3. \end{aligned} \right\} \quad (3.138)$$

The relation (3.137) is also plotted in Fig. 24 (case B). It reflects a size dependence according to the hypotheses used:

- (α) Using the thickness d^* (Fig. 25) as a scale invariant material parameter, then

$$\frac{1}{a^*} = 2 \left(\frac{H/2}{d^*} \right)^2$$

for a quadratic cross section. Thus $1/a^*$ is proportional to the square of the length scale which is in contrast to case A. Therefore, for constant values H (and d^* , of course) the two curves in Fig. 24 are not directly comparable; a change of the scale of the abscissa is necessary. Also it is felt that d^* of case B is not physically equivalent to the thickness value d^* of case A: The width of the yielding region in case B is varying between $2d^*$ and zero.

(β) If the area A^* is a material property, then

$$\frac{1}{a^*} = \frac{A^*}{H^2/2}$$

which is proportional to the square of the length scale. Thus, the results of case A and B in Fig. 24 can be directly compared if the cross sections are quadratic, i.e. $B=H$. Then it is seen that the orientation of the cross section with respect to the plane of bending has a significant effect on the apparent yield stress: The more material is surrounded around the neutral axes, the larger is the apparent yield stress σ_{\max} . This is in qualitative agreement with the experimental data [43].

Torsion of a Circular Cross Section:

The integral yield condition takes the following form (Fig. 26)

$$\frac{1}{A^*} \int_{R-d^*}^R \tau 2\pi r dr \leq \tau_o \quad (3.139)$$

where τ_o is the uniform shear stress at yield. According to the von Mises or Tresca yield condition for homogeneous states of stress, the yield stress in shear is related to the yield stress in tension by

$$\tau_o = \begin{cases} \frac{1}{\sqrt{3}} \sigma_o = 0.5774 \sigma_o & \text{v. Mises} \\ \frac{1}{2} \sigma_o = 0.5 \sigma_o & \text{Tresca} \end{cases} \quad (3.140)$$

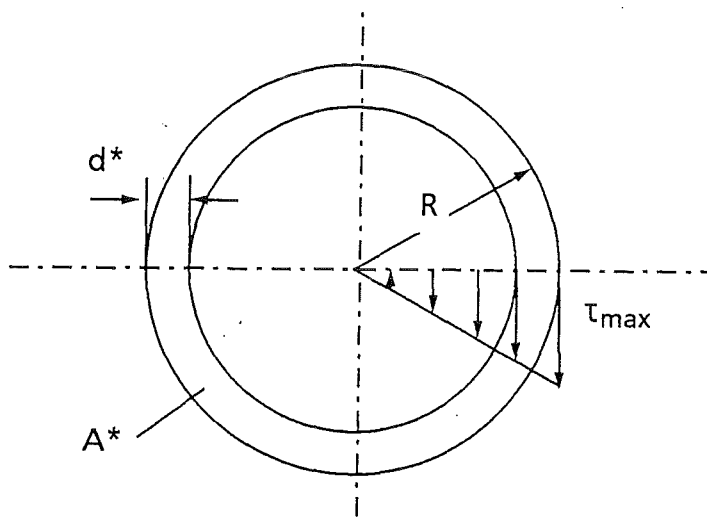


Fig. 26: Cross Section of Torsion Specimen

The elastic shear stress distribution is

$$\tau = \tau_{\max} r/R .$$

Integration of the left hand side of (3.139) gives

$$\frac{1}{A^*} \int_{R-d^*}^R \tau 2\pi r dr = \tau_{\max} \frac{\pi R^2}{A^*} \frac{2}{3} \left[1 - \left(1 - \frac{d^*}{R} \right)^3 \right] .$$

Thus the apparent shear stress at yield τ_{\max} is given by

$$\frac{\tau_{\max}}{\tau_o} = a^* \frac{3/2}{1 - \left(1 - \frac{d^*}{R} \right)^3} \quad (3.141)$$

where

$$a^* = \frac{A^*}{\pi R^2} \quad (3.142)$$

is the fractional part at yield of the cross sectional area πR^2 . With

$$A^* = \pi R^2 \left[1 - \left(1 - \frac{d^*}{R} \right)^2 \right] \quad (3.143)$$

one gets

$$\left. \begin{aligned} a^* &= 1 - \left(1 - \frac{d^*}{R} \right)^2 \\ \text{or} \quad \frac{d^*}{R} &= 1 - (1 - a^*)^{1/2} . \end{aligned} \right\} \quad (3.144)$$

Observing (3.144)₁ and (3.140)₁, equ. (3.141) reads

$$\frac{\tau_{\max}}{\sigma_o} = \frac{3}{2} \frac{\tau_o}{\sigma_o} \frac{a^*}{1 - (1 - a^*)^{3/2}} \quad (3.145)$$

where

$$\frac{3}{2} \frac{\tau_o}{\sigma_o} = \left\{ \begin{array}{l} \frac{\sqrt{3}}{2} = 0.8660 \quad \text{v. Mises} \\ \frac{3}{4} = 0.75 \quad \text{Tresca} \end{array} \right\} . \quad (3.146)$$

Special values are

$$\lim_{a^* \rightarrow 0} \frac{\tau_{\max}}{\sigma_o} = \frac{\tau_o}{\sigma_o} = \left\{ \begin{array}{l} \frac{1}{\sqrt{3}} = 0.5774 \quad \text{v. Mises} \\ \frac{1}{2} = 0.5 \quad \text{Tresca} \end{array} \right\} \quad (3.147)$$

which corresponds to the classical local yield condition and

$$\lim_{a^* \rightarrow 1} \frac{\tau_{\max}}{\sigma_o} = \frac{3}{2} \frac{\tau_o}{\sigma_o} = \left\{ \begin{array}{l} \frac{\sqrt{3}}{2} = 0.8660 \quad \text{v. Mises} \\ \frac{3}{4} = 0.75 \quad \text{Tresca} \end{array} \right\} . \quad (3.148)$$

Thus the maximum size effect is

$$\frac{\left(\tau_{\max} \right)_{a^* = 1}}{\left(\tau_{\max} \right)_{a^* = 0}} = \frac{3}{2} .$$

The simple theory of yielding presented here which involves only two scalar material parameters, i.e., σ_o and A^* or d^* , should be compared to the experimental results. Unfortunately, the data for the case of bending are insufficient, however, the combined torsional data of Morrison [39] can be used. These data are presented in Fig. 19 in a form which does not require the determination of σ_o , the tensile yield stress for homogeneous states of stress. Considering A^* as a material parameter, A^* was determined by trial and error in such a way that the theoretical value τ_{\max}/σ_o , equ. (3.145), agrees with the experimental value for the smallest specimen, i.e. for $2 \cdot R_{\min} = 0.1154$ in, and assuming either the von Mises or the Tresca stress ratio τ_o/σ_o , equ. (3.146).

This yields

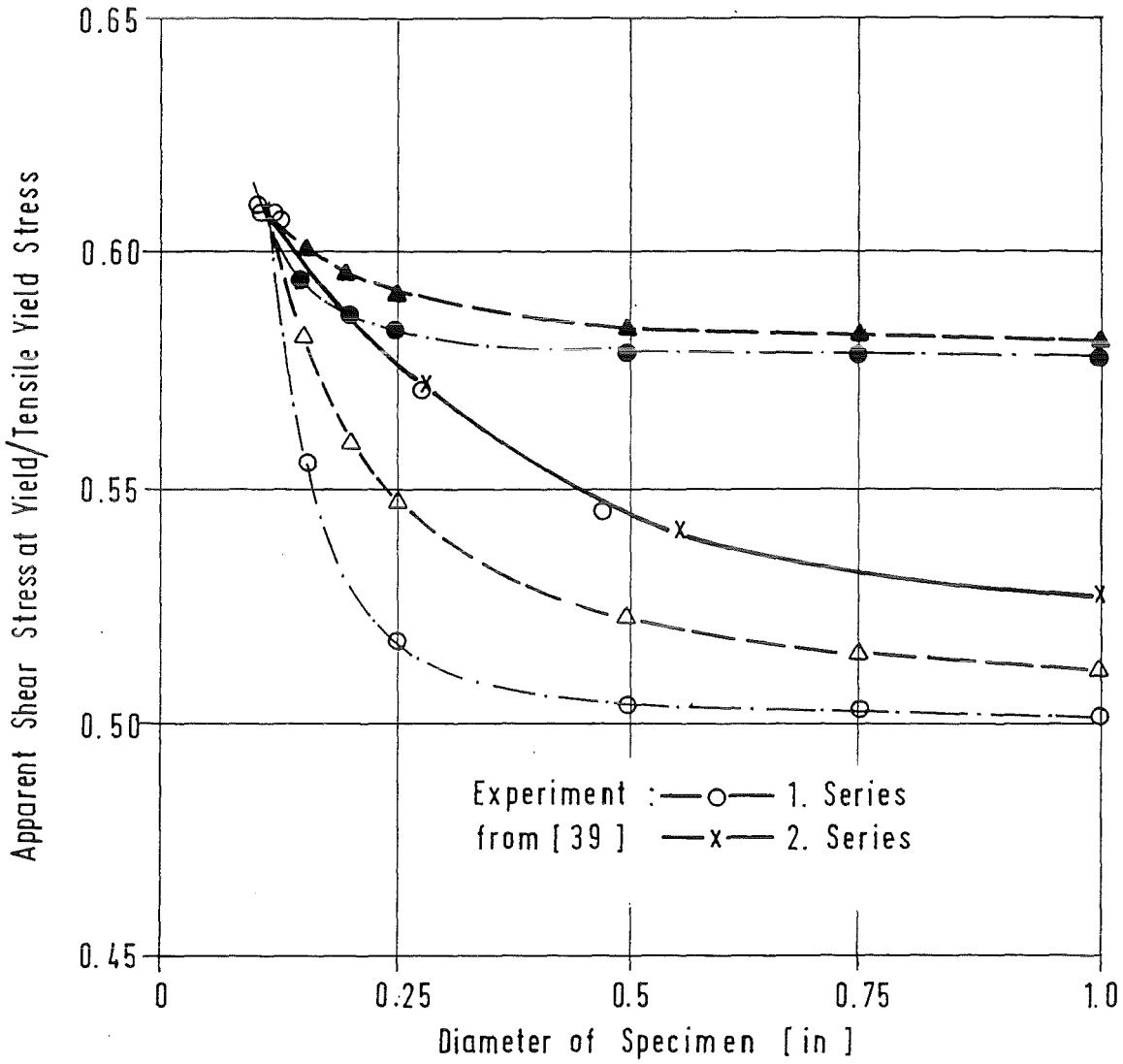
$$A^* = \begin{cases} 2.0253 \cdot 10^{-3} \text{ [in}^2\text{]} & \text{v. Mises} \\ 6.5083 \cdot 10^{-3} \text{ [in}^2\text{]} & \text{Tresca .} \end{cases} \quad (3.149)$$

Instead of A^* , also the yield thickness d^* was considered to be a size independent material parameter, and the fit procedure was repeated. One obtains

$$d^* = \begin{cases} 5.8868 \cdot 10^{-3} \text{ [in]} & \text{v. Mises} \\ 6.5083 \cdot 10^{-3} \text{ [in]} & \text{Tresca .} \end{cases} \quad (3.150)$$

The corresponding normalized shear stresses at yield and their size dependence according to equ. (3.145) are shown in Fig. 27. The largest discrepancies are found when the von Mises stress ratio $\tau_o/\sigma_o = 1/\sqrt{3}$ is used, independent of the choice of A^* or d^* as a constant material parameter. The best agreement is found when the Tresca stress ratio $\tau_o/\sigma_o = 1/2$ is applied and d^* is used as a material constant. It is interesting to note that the slope of this curve agrees approximately for diameters larger than 0.35 in. For smaller specimens the size sensitivity is still too large. It is clear that this choice of size effect parameter d^* is physically reasonable for the case of torsion; however, for more complex geometries and states of stress this concept is not readily realizable.

The experimental findings reported here and the above theoretical considerations suggest that it would be rather worthwhile to perform a comprehensive literature survey on this subject.



Theory	$A^* = \text{const}[\text{in}^2]$	$d^* = \text{const}[\text{in}]$
v. Mises $\frac{\tau_0}{\sigma_0} = \frac{1}{\sqrt{3}}$	$2.0253 \cdot 10^{-3}$ —●—	$5.8868 \cdot 10^{-3}$ —▲—
Tresca $\frac{\tau_0}{\sigma_0} = \frac{1}{2}$	$6.5085 \cdot 10^{-3}$ —○—	$2.2237 \cdot 10^{-3}$ —△—

Fig. 27: Size Effect in Torsion: Experiment and Theory

3.3 Scale Factors

The experimental results of a model test can be transferred to the full scale prototype situation if similarity holds. Here scale factors are required which allow to relate corresponding quantities of the model and the prototype. In the following, scale factors are defined and their interrelations are evaluated.

With the index notation

index "p" = prototype

index "m" = model

the following scale factors are introduced with respect to variables

$$\left. \begin{array}{ll}
 \text{coordinates} & \left(x_k \right)_p = M_l \left(x_k \right)_m \\
 \text{displacements} & \left(u_k \right)_p = M_u \left(u_k \right)_m \\
 \text{time} & (t)_p = M_t (t)_m \\
 \text{velocities} & \left(\dot{u}_k \right)_p = M_v \left(\dot{u}_k \right)_m \\
 \text{accelerations} & \left(\ddot{u}_k \right)_p = M_a \left(\ddot{u}_k \right)_m \\
 \text{strains} & \left(\varepsilon_{kl} \right)_p = M_\varepsilon \left(\varepsilon_{kl} \right)_m \\
 \text{strain rates} & \left(\dot{\varepsilon}_{kl} \right)_p = M_{\dot{\varepsilon}} \left(\dot{\varepsilon}_{kl} \right)_m \\
 \text{stresses} & \left(\sigma_{kl} \right)_p = M_\sigma \left(\sigma_{kl} \right)_m \\
 \text{single or resulting force} & (F)_p = M_F (F)_m
 \end{array} \right\} \quad (3.151)$$

and others as required.

Scale factors related to geometry and material data are

$$\left. \begin{aligned}
 \text{length, distance} \quad (l)_p &= M_l (l)_m \\
 \text{density} \quad (\rho_o)_p &= M_\rho (\rho_o)_m \\
 \text{Youngs modulus} \quad (E)_p &= M_E (E)_m \\
 \text{yield stress} \quad (\sigma_y)_p &= M_y (\sigma_y)_m \\
 \text{hardening stress} \quad (\hat{R}_{(p)})_p &= M_R (\hat{R}_{(p)})_m \\
 \text{relaxation parameter} \quad (A)_p &= M_A (A)_m
 \end{aligned} \right\} \quad (3.152)$$

Note that scale factors for the dimensionless material parameters ν and n are not required; similarity demands that their scale factors are equal to unity.

Similarity implies the equality of the dimensionless variables (3.4) for model and prototype. Observing (3.152) this yields

$$\begin{aligned}
 x'_k &= \left(\frac{x_k}{l_R} \right)_p = \left(\frac{x_k}{l_R} \right)_m \Rightarrow M_l = \frac{(l_R)_p}{(l_R)_m} =: \lambda \\
 u'_k &= \left(\frac{u_k}{l_R} \right)_p = \left(\frac{u_k}{l_R} \right)_m \Rightarrow M_u = M_l =: \lambda \\
 t' &= \left(\frac{t v_R}{l_R} \right)_p = \left(\frac{t v_R}{l_R} \right)_m \Rightarrow M_t = \left(\frac{v_R}{l_R} \right)_m \left(\frac{l_R}{v_R} \right)_p \\
 &= \frac{v_{Rm}}{v_{Rp}} \frac{l_{Rp}}{l_{Rm}} = \frac{v_{Rm}}{v_{Rp}} \cdot \lambda \quad \cdot \\
 & \quad \cdot \\
 & \quad \cdot
 \end{aligned} \quad (3.153)$$

$$\begin{aligned}
 \frac{\partial u_k'}{\partial t'} &= \left(\frac{\partial u_k}{\partial t} \frac{1}{v_R} \right)_p = \left(\frac{\partial u_k}{\partial t} \frac{1}{v_R} \right)_m \Rightarrow M_v = \frac{v_{Rp}}{v_{Rm}} & \dots \\
 \frac{\partial^2 u_k'}{\partial t'^2} &= \left(\frac{\partial^2 u_k}{\partial t^2} \frac{l_2}{v_R^2} \right)_p = \left(\frac{\partial^2 u_k}{\partial t^2} \frac{l_R}{v_R^2} \right)_m \Rightarrow M_a = \left(\frac{v_{Rp}}{v_{Rm}} \right)^2 \frac{l_{Rm}}{l_{Rp}} & \dots \\
 &= M_v^2 \frac{1}{\lambda} & \dots \\
 \varepsilon_{kl}' &= \left(\varepsilon_{kl} \right)_p = \left(\varepsilon_{kl} \right)_m \Rightarrow M_\varepsilon = 1 & \dots \\
 \frac{\partial \varepsilon_{kl}'}{\partial t'} &= \left(\frac{\partial \varepsilon_{kl}}{\partial t} \frac{l_R}{v_R} \right)_p = \left(\frac{\partial \varepsilon_{kl}}{\partial t} \frac{l_R}{v_R} \right)_m \Rightarrow M_{\dot{\varepsilon}} = \frac{v_{Rp}}{v_{Rm}} \frac{l_{Rm}}{l_{Rp}} = M_v \cdot \frac{1}{\lambda} & \dots \\
 \sigma_{kl}' &= \left(\frac{\sigma_{kl}}{\rho_R v_R^2} \right)_p = \left(\frac{\sigma_{kl}}{\rho_R v_R^2} \right)_m \Rightarrow M_\sigma = \left(\frac{v_{Rp}}{v_{Rm}} \right)^2 \frac{\rho_{Rp}}{\rho_{Rm}} & \dots \\
 &= M_v^2 M_\rho & \dots
 \end{aligned} \tag{3.153}$$

and

$$M_F = M_\sigma \lambda^2 = M_v^2 M_\rho \lambda^2 .$$

If the scale factors $M_l \equiv \lambda$, M_v and M_ρ are given, then the rest of the above factors are uniquely defined.

Provided gravitational forces are ignored, the similarity conditions (Tab. 1) imply the following relations for an elastic-viscoplastic material

$$M_E \frac{1}{M_\rho M_v^2} = 1, \quad M_y \frac{1}{M_\rho M_v^2} = 1, \quad M_R \frac{1}{M_\rho M_v^2} = 1$$

or

$$M_E = M_y = M_R = M_\rho M_v^2 \tag{3.154}$$

and

$$\lambda \frac{1}{M_V} M_A \left(M_\rho M_V^2 \frac{\left(\sigma_N \right)_m}{\left(\sigma_N \right)_p} \right)^n = 1; \quad (3.155)$$

here the choices of the normalizing stresses $(\sigma_N)_p$ and $(\sigma_N)_m$ are still arbitrary. If an elastic-time independent plastic material model is appropriate, then condition (3.155) drops out.

For replica models one obtains

$$M_\rho = 1, \quad M_E = M_y = M_R = 1, \quad M_A = 1;$$

thus, equ. (3.154) yields

$$M_V = 1$$

and this implies

$$M_t = \lambda, \quad M_a = \frac{1}{\lambda}, \quad M_{\dot{\epsilon}} = \frac{1}{\lambda}$$

and

$$M_\sigma = 1, \quad M_F = \lambda^2.$$

This applies to an elastic-time independent material behavior. For the viscoplastic response condition (3.155) is to be observed also and this yields

$$\lambda = 1,$$

a result already known: A small scale model test, obeying the similarity laws strictly, is not possible. This concludes the discussion of scale factors.

3.4 Summary and Conclusions

For future pressurized water reactors investigations are required to demonstrate that a core melt-down and a subsequent steam explosion does not endanger the integrity of the pressure vessel head and its bolting since a failure would impair the reactor containment. It was reasoned that an experimental approach, using a scaled down model of the upper part of the pressure vessel (scale 1:10) subjected to the impact of a liquid metal slug, is appropriate and similarity laws for fluid and solid continua should allow the transfer of the experimental results to the actual 1:1 configuration.

A survey of existing literature revealed that detailed systematic treatments of elastic-plastic or even elastic-viscoplastic deformation behavior and of failure or fracture rules under the aspect of similarity have found limited attention only. This situation initiated the present work which is documented in a two-part report. Here the emphasis is on aspects of similitude theory for solid continua and structures.

In Part I at hand the analysis is restricted solely to the *deformation behavior* of continua. In Part II, still under preparation, progressive damage processes and fracture are considered.

Similarity laws are derived and size effects are studied for two relatively simple constitutive models which allow to describe the multiaxial response under monotonous radial loading for two important phenomena:

- The motion and deformation of an elastic-viscoplastic continuum with isotropic hardening which allows to describe the strain-rate dependent yielding in dynamic plasticity; a power law influence of the strain rate on the flow stress is assumed.
- The motion and deformation of an elastic-time independent plastic continuum with isotropic hardening.

Both constitutive models are isothermal. The influence of temperature can be accounted for by adjusting the material parameters and functions to different isothermal tests. Here it must be considered that dynamic tensile tests at high rates are almost adiabatic and the plastic work dissipation may raise the temperature during the test. For some steels at a high temperature level a small temperature rise has a significant effect on the material data (thermal softening).

The simplicity of these models implies that uniaxial static and dynamic tensile tests suffice to identify the material parameters and functions.

The analysis is based on the assumption of infinitesimal strains and rotations such that the kinematics is linear. This has no consequences for the similarity laws as already noted by Goodier [53] and Langhaar [3]. Further, gravitational forces are discussed and assumed to be negligible.

The "method of differential equations" is applied to the balance equations, constitutive relations and initial and boundary conditions to derive the similarity conditions, for *structures with perfect geometric similarity*.* The reference values chosen for the model and the prototype are

l_R : reference length

v_R : reference velocity, e.g. impact velocity

ρ_R : reference density .

The geometric scale factor λ is defined by

$$\lambda = \frac{l_{Rp}}{l_{Rm}}$$

where the subscripts "p" and "m" refer to prototype and model, respectively. The "method of differential equations" requires to put the governing equations in a dimensionless form which automatically yields a set of dimensionless parameters as well as functions. Similarity of the small scale model and the large scale prototype implies the equality of the dimensionless solutions of the general initial-boundary value problem at homologous points and scaled times. For example, the implications for the stress and strain fields, σ_{kl} and ε_{kl} , are

* Of course, this is an idealized situation which cannot be perfectly realized. There are practical limitations on the construction of very small models [6]: For example, the wall thickness limitations due to a minimum number of grains across the thickness, manufacturing problems due to the required decrease of allowable tolerances, access to the interior of small models, difficulties and costs to duplicate all structural details. These aspects may dictate a deviation from similarity.

$$\left. \begin{aligned} \left(\frac{\sigma_{kl}}{\rho_R v_R^2} \right)_m &= \left(\frac{\sigma_{kl}}{\rho_R v_R^2} \right)_p \\ \left(\varepsilon_{kl} \right)_m &= \left(\varepsilon_{kl} \right)_p \end{aligned} \right\} \text{for all } \begin{aligned} \left(\frac{x_k}{l_R} \right)_m &= \left(\frac{x_k}{l_R} \right)_p \\ \left(t \frac{v_R}{l_R} \right)_m &= \left(t \frac{v_R}{l_R} \right)_p \end{aligned} .$$

Instead of $\rho_R v_R^2$ any other stress like normalizing quantity can be used.

The necessary and sufficient similarity conditions for the two constitutive models may be stated in alternative but equivalent formulations as indicated in Tab. 1-3 and in the associated text (section 3.1). They can be interpreted as follows:

General requirements are:

1. The density distribution in the model and in the prototype must be similar.
2. The boundary conditions (surface tractions and kinematic constraints) must be similar at homologous points and at scaled times.
3. The initial conditions must be similar at homologous points.

With respect to the constitutive behavior one has to distinguish between the two constitutive models and whether the test model is made of the same material as the prototype and is operated at the same temperature. The basic results are shown in Table 7 and are commented as follows.

Provided the material behavior of both the prototype and the model is described by the same class of *rate or time independent elasto-plasticity* but a different material is used for the model, then similarity of the deformation behavior requires the similarity of the stress-strain curves. This is a very well known fact and has been noted by Murphy [10], Goodier [53], and Langhaar [3]. The theoretical considerations give no restrictions for the geometric scale factor λ . However, the velocity scale factor

$$M_v = \frac{v_{Rp}}{v_{Rm}} ,$$

Tab. 7: Requirements on the Constitutive Relations for Similarity of the Deformation Behavior

Elastic-Time Independent Plastic Material Behavior	Elastic-Viscoplastic Material Behavior
Different Materials or Equal Materials but Different Temperatures	
<p>Equality of the dimensionless stress-strain curves</p> <p>Geometric scale factor λ arbitrary Velocity scale factor M_v restricted by</p> $M_v := \frac{v_{Rp}}{v_{Rm}} = \sqrt{\frac{\rho_{Rm} \sigma_{yp}}{\rho_{Rp} \sigma_{ym}}}$ <p>Difficult to realize</p>	<p>Equality of the dimensionless static and dynamic stress-strain curves for corresponding equal dimensionless viscoplastic strain rates, i.e.</p> $\dot{\epsilon}_m^P = \dot{\epsilon}_P^P \frac{\lambda}{M_v}$ <p>Geometric scale factor λ arbitrary Velocity scale factor M_v restricted by</p> $M_v = \frac{v_{Rp}}{v_{Rm}} = \sqrt{\frac{\rho_{Rm} \sigma_{yp}}{\rho_{Rp} \sigma_{ym}}}$ <p>Even more difficult to realize</p>
Equal Materials and Equal Temperatures	
<p>Geometrical scale factor λ arbitrary Velocity scale factor M_v restricted by</p> $M_v = \frac{v_{Rp}}{v_{Rm}} = 1$ <p>i.e. equal impact velocities</p>	<p>A model experiment with $\lambda \neq 1$, satisfying strictly the similarity laws, is not possible. Due to the visco-plasticity a size effect is present.</p>

given, e.g., by the ratio of the impact velocities, is determined by the ratio of Youngs moduli or the yield stresses or other stress quantities characteristic for the stress-strain curve:

$$M_V = \frac{v_{Rp}}{v_{Rm}} = \sqrt{\frac{\rho_{Rm} E_p}{\rho_{Rp} E_m}} = \sqrt{\frac{\rho_{Rm} \sigma_{yp}}{\rho_{Rp} \sigma_{ym}}} = \sqrt{\frac{M_\sigma}{M_\rho}}$$

Note that the ratio of the characteristic densities is close to one if both model and prototype are made from steel. In practice the identification of a suitable material for the model is not an easy matter, especially if similarity is required over a large strain range.

The use of a different rate-independent material for the model may be required if the model test has to be performed at a different temperature level than the prototype. This is due to the possible dissimilarity of the stress-strain curves of a material at different temperatures. If the same material is used for the model and the prototype but temperatures are not the same, this dissimilarity yields a "size effect". Whether or not it is tolerable or causes misleading conclusions needs analysis.

A fortunate situation is given when the same rate-independent material at the same temperature level can be used for the small scale model. Then similarity is trivially satisfied if, among others, the impact velocities are the same, a condition which can easily be realized. From the literature it appears that most model tests are of this nature.

Under these conditions not only the strains but also the stresses are the same in the model and the prototype at homologous points and scaled times.

The situation is rather different when *viscoplasticity is important for the material response*. If different materials or if equal materials but different temperatures are used for the model test, then, from a theoretical point of view, similarity requires that the dimensionless stress-strain curves of the model and the prototype are congruent for all corresponding dimensionless viscoplastic strain rates, i.e.

$$\left(\frac{\partial \varepsilon^p}{\partial t'} \right)_m = \left(\frac{\partial \varepsilon^p}{\partial t'} \right)_p, \quad t' = t \frac{v_R}{l_R}$$

or

$$\left(\dot{\epsilon}^p \right)_m = \left(\dot{\epsilon}^p \right)_p \frac{\lambda}{M_v} .$$

In terms of the constitutive model analyzed in section 3.1 - power law relation between the overstress and the viscoplastic strain rate - this is equivalent to the statement that the

- dimensionless static stress-strain curves are congruent
- the "generalized Reynolds numbers" $\frac{Re}{n}$ are the same and
- the exponents n , controlling the nonlinearity of the strain rate influence, are the same.

No restriction is found for the geometric scale factor λ but the velocity scale factor M_v is restricted as above by the scale factors for the stress and density.

The realization of these conditions is much more difficult compared to the rate independent constitutive model, since similarity of *two sets of dynamic stress-strain curves* is required. In practice this can hardly be achieved. Therefore, sometimes experimenters restrict their attention to a *single dynamic stress-strain curve* corresponding to a representative strain rate (e.g. Florence et al. [64], Romander [66]). This reduced similarity imposes a distortion on the results of the model test. If the model test is done with the same material at the same temperature as the prototype, similarity cannot be achieved. Any test of this kind will yield distorted results. This is a well known fact (e.g. Soper [55], Jones [14]). However, whether or not this size effect is tolerable depends on the strain rate sensitivity of the material.

The trend to be expected is as follows. Usually an increase of the strain rate in a tensile test yields an increase of the flow stress. Assume that a model test with the same viscoplastic material at the same temperature as the prototype is done and the same impact velocity is used. Then an increased strain rate is observed for the model, i.e. $\dot{\epsilon}_m = \dot{\epsilon}_p \lambda$, provided $\lambda > 1$. Thus the flow stress in the model is larger than in the prototype. Since the specific dissipated plastic work is the same in the model and the prototype, the strains will be underestimated in the model. Thus the result is non-conservative. Therefore, it is necessary to estimate this discrepancy. In section 3.2. a simple one degree of freedom model

- straight strut under compressive loading due to the impact of a mass at one end

is used to obtain a quantitative estimate. The material chosen is stainless steel AISI 304 at room temperature which is moderately strain rate sensitive: An increase of the strain rate by one order of magnitude from 10 to 10^2 s^{-1} yields an increase of the 0.2 % proof stress of about 10 %. The experimental data of Steichen [21-23] are interpolated by a power law relation between the plastic strain rate and the overstress, ignoring strain hardening and elasticity. Permanent strains for the model and the prototype are determined using the assumption of constant average flow stress during the deformation process. It is shown that the underestimation of the strain in the model increases nonlinearly with the scale factor λ and the initial strain rate of the prototype. However, the effect is moderate: For example, for a rather high initial strain rate of the prototype of 10^2 s^{-1} and a very large scale factor of 50 the underestimation is about 23 % (Tab. 4). The validity of the constant flow stress assumption has been checked using a modified but similar constitutive model. In this context it was found that the influence of the scale factor λ on the underestimate (the "size effect") is much larger for a linear stress-strain rate relation than for the non-linear one.

Of course, the present analysis does not account for any thermal softening effect; but at room temperature it is expected to be small. The "size effect" due to strain rate sensitivity (i.e. viscoplasticity) may be amplified due to strain or deformation softening: Calladine [35] had pointed out that in structures with a falling load-deflection characteristic an increase in the flow stress in the small scale model due to a strain rate effect causes a proportionally much larger decrease in the final deformation than in structures with a constant load-deflection characteristic. This enhanced size effect is qualitatively demonstrated using a fictitious strain softening model and avoiding some unrealistic premises in Calladine's work. However, for a realistic quantitative estimate of this effect a mechanical model must be defined.

In summary, apparently only one testing situation is unproblematic from a theoretical point of view: Models made from the same rate-insensitive material as the prototype and tested at the same temperature level (replica models).

However, an important premise for the validity of the derived similarity laws for replica models is the scale invariance of the basic material data and functions like Young's modulus E , Poisson's number ν , yield stress σ_y , and hardening stress $\hat{R}(\epsilon_p)$.

Published data indicate - technological variability excluded as far as possible - that a size dependence is present, its significance depending on the homogeneity

of the stress or strain distribution: It appears that the yield stress and the ultimate stress obtained in a tensile test (homogeneous state of stress) are approximately scale invariant. Whether the uniform elongation, also an important quantity characterizing the stress-strain curve and commonly not given, is also scale invariant, is presently not known to the author. This appears to be an important gap, especially if large deformations and failure are important.

On the other hand there is experimental evidence that the initiation of yielding is depending on the presence of a stress (or strain) gradient and this appears to be related to the microstructure of the material. It turns out that a size effect will be present yielding a higher flow resistance for small specimens. This also implies that the classical local yield criteria, characterized only by the local state of stress and strain, are insufficient. A simple non-local yield condition has been applied to illustrate this effect. Clearly, the study of the scale invariance of material data for homogeneous and especially inhomogeneous states of stress should be continued and extended.

Part I of this report closes with a derivation of the appropriate scale factors which is a trivial matter when the mechanical model is known.

Within the context of the similarity theory for the deformation behavior of solid materials and structures several aspects need further study or have not been discussed in this study at all and require attention:

- Quantitative determination of size effects due to inadequate material choice for the model. A special case of interest is the use of the same material for the model as used for the prototype but performing the model test at a different temperature.
- Scale invariance of material data under homogeneous and non-homogeneous states of stress and analysis of non-local plasticity theories.
- Collection of systematic scaled model tests from the literature and a quantitative comparison with the similarity laws. Some information may be obtained from the cited literature. It is the author's impression that it is sometimes difficult to understand the stated "agreement"; such judgements depend strongly on the intended application of the small scale model experiments and the assumed tolerance margin.

As stated above the important question of progressive damage and its influence on the deformation behavior as well as failure and fracture will be the subject of Part II of this report which is still in preparation.

References

- [1] R. Krieg, T. Malmberg, G. Messemer, T. Stach, E. Stratmanns: Slug Impact on the Vessel Head during a Postulated In-Vessel Steam Explosion in Pressurized Water Reactors; Assessments and Discussion of the Investigation Strategy. Accepted for publication in Nuclear Technology, 1995
- [2] R. Krieg, E. Wolf: Unpublished Report, Kernforschungszentrum Karlsruhe, Dez. 1990
- [3] H.L. Langhaar: Dimensional Analysis and Theory of Models, J. Wiley & Sons, London, 1957
- [4] J. Zierep: Ähnlichkeitsgesetze und Modellregeln der Strömungslehre, G. Braun, Karlsruhe, 1982
- [5] A.A. Gukhman: Introduction to the Theory of Similarity, Academic Press, New York - London, 1965
- [6] W.E. Baker, P.S. Westine, F.T. Dodge: Similarity Methods in Engineering Dynamics (Theory and Practice of Scale Modeling), Rev. Ed., Elsevier, Amsterdam - Oxford - New York - Tokyo, 1991
- [7] L.I. Sedov: Similarity and Dimensional Methods in Mechanics, 10th Ed., CRC Press, 1993
- [8] A.G. Hansen: Similarity Analyses of Boundary Value Problems in Engineering, Prentice-Hall, 1964
- [9] S.J. Kline: Similitude and Approximation Theory, Mc Graw-Hill Co., 1975
- [10] G. Murphy: Similitude in Engineering, Ronald Press N.Y., 1950
- [11] D.J. Schuring: Scale Models in Engineering, Fundamentals and Applications, Pergamon Press, 1977
- [12] E. Sjñecs: Similitude and Modeling, Elsevier Scientific Publ. Co., 1980
- [13] N. Jones: Similarity principles in structural mechanics, Int. J. Mech. Eng. Education 2,2, pp. 1- 10, 1974

- [14] N. Jones: Scaling of Inelastic Structures Loaded Dynamically, from: Struct. Impact and Crashworthiness, vol 1, Keynote Lectures, G.A.O. Davis Ed., Elsevier Appl. Sc. Pub., pp. 45-74, 1984
- [15] N. Jones: Structural Impact, Cambridge Univ. Press, New York - Port Chester - Melbourne - Sydney, 1989
- [16] T. Malmberg: Unpublished Report, Kernforschungszentrum Karlsruhe, 1992
- [17] J. Lemaitre, J.L. Chaboche: Mechanics of Solid Materials, Cambridge Univ. Press, New York - New Rochelle - Melbourne - Sydney, 1990
- [18] P. Perzyna: Fundamental Problems in Viscoplasticity, from "Advances in Appl. Mech", vol 9, Ed.: G.G. Chernyi et al., Academic Press, New York - London, pp. 243-377, 1966
- [19] C.J. Maiden, S.J. Green: Compressive Strain-Rate Tests on Six Selected Materials at Strain Rates from 10^{-3} to 10^4 In/In/Sec, Trans. ASME, J. Appl. Mech., pp. 496-504, Sept. 1966
- [20] F.E. Hauser: Techniques for Measuring Stress-Strain Relations at High Strain Rates, Experim. Mechanics, pp. 395-402, Aug. 1966
- [21] J.M. Steichen, M.M. Paxton: The Effect of Strain Rate on the Mechanical Properties of Austenitic Stainless Steel, HEDL-TME-71-56, May 1971
- [22] J.M. Steichen: High Strain Rate Mechanical Properties of Type 304 Stainless Steel and Nickel 200, HEDL-TME-71-145, Sept. 1971
- [23] J.M. Steichen: High Strain Rate Mechanical Properties of Type 304 and 316 Stainless Steel, HEDL-TME-71-164, Nov. 1971
- [24] T. Malmberg: Dynamisch plastisches Verhalten von Metallen, KfK 2023, Kernforschungszentrum Karlsruhe, Sept. 1974
- [25] W.H. Westphal: Physik, Springer Verlag, Berlin - Göttingen - Heidelberg, 1963
- [26] N. Cristescu: Dynamic Plasticity, North-Holland Publ. Comp., Amsterdam, 1967

- [27] N. Cristescu, I. Suliciu: Viscoplasticity, Martinus Nijhoff Publ., The Hague - Boston - London, 1982
- [28] Anonymus: Mechanische und physikalische Eigenschaften der austenitischen Chrom-Nickel-Stähle bei hohen Temperaturen, INCO Europe Limited, 2. Ed., 1977
- [29] Anonymus: Mechanische und physikalische Eigenschaften der austenitischen Chrom-Nickel-Stähle bei Raumtemperatur, INCO Europe Limited, 2. Ed., 1977
- [30] T.D. Parker: Strength of Stainless Steels at Elevated Temperature, from "Source Book on Materials for Elevated Temperature Applications", E.F. Bradley Ed., Am. Soc. for Metals 1979
- [31] M.J. Forrestal, M.J. Sagartz: Elastic-Plastic Response of 304 Stainless Steel Beams to Impulse Loads, Trans. ASME, J. Appl. Mech., vol 45, pp. 685-687, 1978
- [32] C.E. Anderson, S.A. Mullin, C.J. Kuhlman: Computer Simulation of Strain-Rate Effects in Replica Scale Model Penetration Experiments, Int. J. Impact Engng. 13, 1, pp. 35-52, 1993
- [33] G.R. Johnson, W.H. Cook: Fracture Characteristic of Three Metals Subjected to Various Strains, Strain Rates, Temperatures and Pressures, Engng. Fract. Mech. 21, 1, pp. 31-48, 1985
- [34] E. Booth, D. Collier, J. Miles: Impact Scaling of Plated Steel Structures, from: Structural Crashworthiness, N. Jones, T. Wierzbicki Ed., pp. 136-174, Butterworths 1983
- [35] C.R. Calladine: An Investigation of Impact Scaling Theory, Appendix 6.III to [34]
- [36] E. Jahnke, F. Emde: Table of Functions, 4. Ed., Dover Publ., New York, 1945
- [37] E. Siebel: Handbuch der Werkstoffprüfung, 2. Bd. Prüfung metallischer Werkstoffe. Springer Verlag, 1955

- [38] R. Faulhaber, H. Buchholtz, E.H. Schulz: Einfluß des Probendurchmessers auf die Biegeschwingungsfestigkeit von Stahl, *Stahl und Eisen*, 53 Jahrg. Nr. 43, pp. 1106-1108, 1933
- [39] J.L.M. Morrison: The Yield of Mild Steel with Particular Reference of the Effect of Size of Specimen, *Proc. of the Inst. of Mech. Eng.* 142, 1, pp. 193-223, 1939
- [40] V. Weiss, S. Yukawa: Critical Appraisal of Fracture Mechanics, from: Fracture Toughness Testing and its Applications, 67. Annual ASTM Meeting Chicago, June 21-26, 1964, ASTM STP No 381, pp. 1-22, 1965
- [41] P.H. Thornton: Static and Dynamic Characteristics of Scale Model Corrugated Tubular Sections, *Trans. ASME, J. Eng. Math. & Tech.*, pp. 357-362, Oct. 1975
- [42] P.E. Shearin, A.E. Ruark, R.M. Trimble: Size Effects in Steels and other Metals from Slow Notch Bend Tests, *Fracturing of Metals*, pp. 167-188, A.S.M. Cleveland, 1948
- [43] A. Thum, F. Wunderlich: Die Fließgrenze bei behinderter Formänderung (Ihre Bedeutung für das Dauerfestigkeits-Schaubild), *Forschung auf dem Gebiete des Ingenieurwesens* 3, 6, pp. 261-270, 1932
- [44] S. Sähn, H. Göldner: Bruch- und Beurteilungskriterien in der Festigkeitslehre, Fachbuchverlag Leipzig, Köln, 1993
- [45] K. Wieghardt: Über das Spalten und Zerreißen elastischer Körper, *Zeitschrift für Mathematik und Physik* 55, pp. 60-103, 1907
- [46] H. Neuber: Kerbspannungslehre, Springer Verlag, 1985
- [47] D. Radaj: Ermüdungsfestigkeit, Springer Verlag, 1995
- [48] N.A. Fleck, G.M. Muller, M.F. Ashley, J.W. Hutchinson: Strain Gradient Plasticity: Theory and Experiment, *Acta Metall. Mater.* 42, 2, pp. 475-487, 1994
- [49] H.M. Zbib: Strain Gradients and Size Effects in Nonhomogeneous Plastic Deformation, *Scripta Metall. & Mater.* 30, 9, pp. 1223-1226, 1994
- [50] H.B. Mühlhaus, E.C. Aifantis: A Variational Principle for Gradient Plasticity, *Int. J. Sol. & Struct.* 28, 7, pp. 845-857, 1991

- [51] H.M. Zbib, E.C. Aifantis: On The Structures and Width of Shear Bands, *Scripta Metallurgica* 22, pp. 703-708, 1988
- [52] H.M. Zbib, E.C. Aifantis: A Gradient-Dependent Model for the Portevin-le Chatelier Effect, *Scripta Metallurgica* 22, pp. 1331-1336, 1988
- [53] J.N. Goodier: Dimensional Analysis, from [54]
- [54] M. Hetenyi Ed.: *Handbook of Experimental Mechanics*, J. Wiley & Sons, New York, 1950
- [55] W.G. Soper: Scale Modeling, *Int. Sci. and Techn.*, pp. 60-69, Feb. 1967
- [56] D.F. Young: Basic Principles and Concepts of Model Analysis, *Experim. Mech.* 11, pp. 325-336, July 1971
- [57] G. Murphy: Scaling and Modeling for Experiment, *Shock and Vibration Bulletin* 10, 1, pp. 5-13, 1978
- [58] A.A. Ezra, F.A. Penning: Development of Scaling Laws for Explosive Forming, *Experimental Mech.*, pp. 234-239, Aug. 1962
- [59] T.A. Duffey: Scaling Laws for Fuel Capsules Subjected to Blast, Impact and Thermal Loading, Report No. SC-RR-70-134, Sandia Lab., Albuquerque, May 1970
- [60] W.T. Lowe, St.S. Al Hassani, W. Johnson: Impact Behavior of Small Scale Model Motor Coaches, *Proc. of Inst. of Mech. Eng.* 186, pp. 409-419, 1972
- [61] R.I. Emari: Scale Models of Automobile Collision with Breakaway Obstacles, *Experim. Mech.*, pp. 64-69, Feb. 1973
- [62] S. Holmes, G.E. Sleiter: Methods, Application and Cost Effectiveness of Scale Model Studies of Automobile Impacts, Contract No. DOT-HS-199-3-732, PB-237-553, US Dept. of Transportations, 1974
- [63] M. Huerta: Analysis, Scale Modeling and Full Scale Tests of a Truck Spent-Nuclear Fuel Shipping System in High Velocity Impact Against a Rigid Barrier, SAND 77-0270, Sandia Lab., Albuquerque, April 1978

- [64] A.L. Florence, G.R. Abrahamson, D.J. Cagliostro: Hypothetical Core Disruptive Accident Experiments on Simple Fast Test Reactor Models, Nucl. Eng. & Design 38, 95-108, 1976
- [65] A. Takei, M. Matsumara, O. Kawguchi, K. Okabayashi, Y. Ando, S. Kondo: Structural Shock Tests of Prototype "Monju" Scale Models, Nucl. Eng. & Design 38, pp. 109-129, 1976
- [66] C.M. Romander: Structural Response of 1/20 Scale Models of Above Core Structures to Increasingly Energetic Hypothetical Core Disruptive Accidents, Techn. Rep. 71, SAN-0115-T8, Stanford Research Inst. International, Menlo Park, Ca, July 1979
- [67] A.G. Atkins, Y.W. Mai: Elastic and Plastic Fracture, Ellis Horwood Lim., Chichester, Reprint 1988
- [68] J. Lubliner: Plasticity Theory, Macmillan Publishing Comp., New York, 1990
- [69] C. Albertini, K. Iida, A. Del Grande, M. Forlani, A. Pachera, M. Montagnani: Residual Tensile Properties at Low and High Strain Rates of AISI 316 H Predamaged by Creep, Low Cycle Fatigue, and Irradiation to 2 dpa, ASTM, STP 1046 V. II, pp. 387-403, 1990